1-1-2000

Analysis of the flow properties, crystallinity and processability of polymer bonded magnets

Peter Christopher Guschl
Iowa State University

Analysis of the flow properties, crystallinity and processability of polymer bonded magnets

by

Peter Christopher Guschl

A thesis submitted to the graduate faculty
in partial fulfillment of the requirement for the degree of
MASTER OF SCIENCE

Major: Chemical Engineering
Major Professor: Joshua U. Otaigbe

Iowa State University
Ames, Iowa
2000

Graduate College

Iowa State University

This is to certify that the Master's thesis of

Peter Christopher Guschl

has met the thesis requirements of Iowa State University

Signatures have been redacted for privacy

TABLE OF CONTENTS

CHAPTER 1. GENERAL INTRODUCTION

Thesis organization

This thesis includes four chapters. Chapter 1 is a summary of the material considerations of the constituent materials and production methods of polymer bonded magnets, the problems in their applications and processing, and, finally, the purpose of the extended research. Chapter 2 is a manuscript that discusses the effect of a liquid crystalline polymer and various Nd-Fe-B filler particle sizes and distributions on the rheological properties of a high temperature thermoplastic, poly (phenylene sulfide) (PPS). Chapter 3 encompasses the information of a paper that describes the polymer matrix crystallization enhancement due to the presence of the filler and a silane-coupling agent coated to the filler particles. Chapter 4 discusses the long range rheological effects and the yield behavior that the Nd-Fe-B particles have on the PPS binder. The general conclusion section is contained in Chapter 5.

Introduction

Industry has been avidly pursuing an alternative to purely metal magnets over the past couple of decades. Magnets are needed in various automotive and other electromechanical applications. Wherever a magnetic field is desired in order to convert magnetic energy to electrical energy, magnets are needed (i.e. Faraday's law - the motion of a magnetic field near a conductive surface will produce an electrical current or potential). Disadvantages, such as, high melting temperatures, heavy weight, and high oxidation potential of these purely metallic magnets (which can affect the magnetic properties of the magnet) have led researchers to investigate more efficient alternatives. Due to their versatile nature and ease of

processing, polymers, specifically thermoplastics and elastomers are being incorporated into the new solution. Polymer bonded magnets (PBM) utilize the concept of mixing a magnetic powder (filler) into a polymer matrix (binder). The resultant composite represents a lightweight material with a higher resistance to oxidation (although oxidation does still occur) and a much lower processing temperature range to work under [*e.g.* metals such as iron melt around 1535°C, whereas most thermoplastics melt in the range of 130°C (polyethylene) up to over 400°C (certain liquid crystal polymers)]. These PBM are to be used in aggressive thermal environments (~100°C or higher) and require thermal stability around those temperatures.

The research performed has investigated the industrial processing characteristics as well as ways to improve upon the material as a whole. The role of rheology of concentrated polymer systems is quite significant in today's industrial products, because it determines the processability of these materials under practical conditions. Polymer-bonded magnets (PBM) composed of polymer matrices and special rare earth magnetic alloys (e.g. Nd-Fe-B alloy) represent an important class of engineering materials used in electromechanical applications in automotive and non-automotive areas, where energy efficiency is a prime concern (1-5). The advantages of PBM over their metallic and ceramic counterparts include, as mentioned, low weight, resistance to corrosion, ease of machining and forming, and capability for high production rates. One drawback with the PBM is the slightly reduced magnetic properties, i.e. smaller B-H hysteresis loop due to reduced coercivity, in comparison to the pure metal equivalent. Comparable maximum energy products to the traditional metal magnet are only attained at extremely high volume fractions of the magnetic powder. The rheology of

concentrated filler/polymer systems such as the PBMs of this study is important because it underscores the processability of these materials under practical conditions.

The optimization of magnetic properties is a main objective of the project, however, issues arise that cause processability properties to be unfortunately compromised. In order to obtain this objective composites are required to be of high filler concentration (>50% by volume). Although, rheological studies of dilute and some concentrated suspensions have been previously reported for model monodisperse systems (6-15), it is widely recognized that rheological characterization and control of the viscosity of useful concentrated, non-spherical (anisotropic), polydisperse filler/polymer suspensions (e.g., PBM) is an inexact science due to the lack of theoretical models and experimental devices that can accurately define the complex flow behavior of such materials as a function of different physical and chemical parameters of the system. Further, systematic studies on rheological behavior of well-characterized, concentrated, polydisperse filler/polymer systems such as the PBMs of this study are very few (4).

In addition to this dilemma, processing at elevated temperatures in air, under melt rheological characterization experiments and aggressive environment applications, leads to thermal instability effects that increase composite viscosity by way of crosslinking the polymer chains and oxidation of the fine metallic powders. Interest in coupling agents, specifically silane coupling agents, arose as a remedy to this problem. The concept involves the theory of chemical bonding of the polymer chains to the surface of the filler particle, allowing better wetting or adhesion between the filler and binder. An important observation regarding the coupling agent is the increased stiffness (also referred to as modulus) and tensile strength of the final composite, because of this adhesion and improved crystallization

of the polymer on the surface of the filler. This coating has been observed to improve corrosion/oxidation resistance significantly. Other benefits of the agent include steric segregation between the particles. The coating acts as a dispersion agent, reducing the chances of aggregation and strong microstructural creation between the particles. Ultimately this aggregation will be a problem when dealing with external magnetic fields during flow (magnetorheology) of concentrated systems. Further improvement of the composites is seen in a slight reduction of viscosity when the coupling agent is used. It is the steric layer surrounding the filler that prevents particles from clustering and allows flow of the polymer melt around the particles.

Although PPS possesses advantages, the flow characteristics of highly filled PPS composites limit the application of common industrial injection molding. The use of functional additives within the PPS matrix has been previously reported to alleviate the aforementioned problems (4, 5, 16). The addition of a small amount of thermotropic liquid crystal polymer can lower the viscosity at low shear rates as well as enhance the modulus and strength of the PBM. This observation can be attributed primarily to the orientation of the liquid crystal polymer chains in the direction of the shear, allowing fewer entanglements to form and a lower resistance to flow. It has been suggested that the liquid crystal polymer's unique rheological behavior is attributed to its flexible and rigid rod-like chains (17). Vectra A950 was the liquid crystal polymer of choice blended in the PPS for the experiments described in this paper. Vectra A950 was chosen as a suitable additive because its flow behavior is similar, in some respects, to that of flexible thermoplastics (in this case its melting temperature is comparable to that of PPS used in the present study). Due to its random sequencing of the aromatic units, this copolyester molecule is relatively linear and

rigid. Additionally, its superior chemical and thermal resistance, high strength and modulus, and ease of melt processing (18) make this liquid crystal polymer an appropriate functional additive.

Other experiments were performed on various composites consisting of different particle configurations. Since the Nd-Fe-B particles given for the project have been analyzed to be between the sizes of 38 and 300 micron (with a few particles existing in the <38 and >300 micron regime as well), various combinations of monodispersed (particles of the same size) and polydispersed (particles of different sizes) were produced. Farris (19), Mangels and Williams (20), and Metzner (21) suggest that whether we have a system of particles that are all of the same average size (monodispersed) or one of varying sizes (polydispersed), one can observe a dramatic change in the viscosity at certain volume fractions between the two configurations. This change can be attributed to an enhancement of the maximum packing fraction. The general theory, researched by many authors, predicts that particles (specifically those which are spherical in nature) of various sizes (*i.e.* fine and coarse bimodal systems) allow better packing of the particles which leads to a more efficient arrangement allowing better flow of the melt. By systematically adjusting the size ratio of the Nd-Fe-B particles, it will also be shown that smaller particles can be accommodated in the spaces between the larger particles, resulting in a more efficient packing and low viscosities at high volume fraction of the particles as others (8, 22, 23) have reported for other bidispersed concentrated suspensions of spherical particles. Our future modeling efforts to be reported elsewhere will consider the important role of the shape factor (i.e. aspect ratio) of the anisotropic platelet Nd-Fe-B particles used as well as the geometry of the channel and type of flow (simple shear or elongational) involved. Although, most industrial materials such as the PBM of this study

contain non-spherical fillers and non-uniform size distributions, it is believed that the models based on filled polymer systems containing spherical fillers may be useful in interpreting the trends in viscosity-concentration behavior of melts of multimodal suspension systems.

Future and ongoing research on the subject of polymer bonded magnets involves investigating the effects of the presence of the filler on the physical properties of the polymer matrix. It has been discovered that PPS composites have quite a substantial strength (25) especially in polymer bonded magnet (PBM) systems such as ours. Due to the semi-crystallinity of PPS, it is believed that enhanced crystallization of the polymer at the binder-filler interfaces causes reinforcement sites to appear. The presence of filler in a semi-crystalline polymer can cause many changes to the mechanical properties of the polymer. Crystallinity studies through thermal analysis have yielded quantitative information, suggesting that the presence of inorganic fillers provides an adequate surface on which polymer chains can settle and crystallize. Some typical changes in the polymer are total degree of crystallinity, crystal phase and its orientation, number and size of crystalline particles, and the type of crystalline particle (24). Various particle sizes and distributions can offer different surface energies in which the crystallization can occur. Coupling agent promotes a change of interfacial properties of the filler particles, giving rise to better wetting between the filler and binder and ultimately increased physical strength of the composite (24-27). It is essential to understand the crystallization behavior of the system so that comprehension of the mechanical properties of these composites can be obtained.

For industrial applications our system needs to be capable of manufacture within commercial injection molding machines. Due to the processing windows open only within particular temperature and, ultimately, injection pressure ranges, the material may be

subjected to large or small shear rates during the process. Interest in information of the material over a broad range of shear is beneficial in order to ensure that one is operating the process under optimal conditions.

Much of the research on concentrated suspensions has included information regarding shear-thinning behavior at low shear rates of stabilized particulate suspensions due to shear induced ordering of the particles (28). Further research has shown that beyond a particular critical shear rate, shear-thickening behavior is observed for stabilized concentrated systems (29-30). Presumably, the hydrodynamic forces dominate over the particle-particle interactions that promote the ordered flow. In the regime where these interactions may predominate, microstructural formations can develop and lead to a yield stress that is necessary to break up these structures and induce flow of the melt composite. Low shear rate data was obtained in order to confirm and quantify this phenomenon. However, Husband et. al. (31) revealed that in studies of yield behavior of noncolloidal suspensions (particles greater than 10 microns) they do not cluster as much as the colloidal particles, suggesting that unlike colloidal particles interparticle effects are essentially dwarfed in comparison to the hydrodynamic forces applied. These authors discussed the typical pseudoplastic behavior of suspensions that exhibit no yield stress and a constant viscosity at low shear rates, depending upon the filler and the binder selected. The functionality of the yield stress to particle properties (size, distribution, shape, anisotropy, etc.) interests rheologists that are confined to working with concentrated systems where these yield effects tend to occur.

Purpose of the research problem

While significant research has been performed on the mechanical and thermal behavior of the PBM, insufficient attention has been paid to the flow properties of highly concentrated PBM systems. It is the goal of this research to properly obtain quantitative and qualitative information in regards to these filled systems. In particular viscosity measurements under a broad range of shear rates of these systems has yet to be professionally documented. Furthermore, it is important to optimize the composition of the PBMs as well in order to ensure minimal processing constraints. Information gleaned from these types of rheological measurements, which involves the use of various rheometric devices and techniques can elucidate and even alleviate current problems surrounding commonplace injection molding procedures. We will try to determine both theoretical and practical relationships between microstructure and performance properties of these novel, highly filled polymer composites. The objectives of this work are to:

1. Investigate the effect of a commercial liquid crystal polymer on the rheological properties (i.e. viscosity) of PPS at concentrations from 5 - 20 vol%.
2. Determine the viscosity effects on various PBM composites of different particle configurations.
3. Find a viscosity model based on the filler concentration that best describes the behavior of the PBM systems.
4. Investigate the effect on the crystallinity of the semi-crystalline PPS due to the presence of the Nd-Fe-B filler and a silane-coupling agent coated on the filler.

5. Develop quantitative viscosity curves over a broad shear rate ranging from 0.01 - 1000 rad s^{-1} at various filler concentrations (i.e. 5 vol%, 20%, 35% and 50%).
6. Determine existence of, and rough yield stress values, for various concentrated composites.

References

1. S. Bullen, Engineering Materials & Design, p.18 (1988).
2. J. Ormerod and S. Constantinides, J. Appl. Phys. **81**, 4816-4820 (1997).
3. J. Xiao, J. U. Otaigbe, and D.C. Jiles, J. Magn. Mag. Mater., **218**, 60-66 (2000a).
4. J. U. Otaigbe, H. S. Kim, and J. Xiao, Polym. Comp., **20**(5), 697-704, (1999a).
5. J. U. Otaigbe, J. Xiao, and S. Constantinides, J. Mat. Sci. Letters, **18**(4), 329-332 (1999b).
6. A. Einstein, Investigations on the Theory of the Brownian Movement, edited by R. Furth, Dover, New York, (1956).
7. G. K. Batchelor, J. Fluid Mech., **83**, 97-117 (1977).
8. D. C. H. Cheng, Powd. Tech., 37, 255-73 (1984).
9. J. C. van der Werff and C. G. De Kruif, J. Rheol., **33**(3), 421-454 (1989).
10. H. A. Barnes, J. Rheol., **33**, 329-366 (1989).
11. A. A. Zaman and B. M. Moudgil, J. Rheol., **42**(1), 21-39 (1998).
12. A. J. Polinski, M. E. Ryan, P. K. Gupta, S. G. Seshadri, and F. J. Frechette, J. Rheol., **32**, 751-771 (1988).
13. R. F. Probstein, M. Z. Sengun, and T. C. Tseng, J. Rheol., **38**, 811-829 (1994).
14. J. B. Jansma and S. Qutubuddin, J. Rheol., **39**(1), 161-178 (1995).
15. K. Sweeny and R. Geckler, J. Appl. Phys., **25**, 1135-1144 (1954).

16. J. Xiao and J. U. Otaigbe, J. Alloys & Compds, **309**, 100-106 (2000b)

17. A. Romo-Uribe, T. J. Lemmon, and A. H. Windle, J. Rheol., **41**(5), 1117-1145 (1997).

18. D. Dutta, R. A. Weiss, and K. W. Kristal, SPE ANTEC Tech Papers, **33**, 924-927 (1991).

19. R. J. Farris, J. Rheol., **12**(2), 281-301 (1968).

20. J. A. Mangels and R. M. Williams, Cer. Bulletin, **62**, No. 5, 601-606 (1983).

21. A. B. Metzner, J. Rheol., **29**(6), 739-775 (1985).

22. S. C. Goto and H. Kuno, J. Rheol., **28**, 197-205 (1984).

23. A. P. Shapiro and R. F. Probstein, Phys. Rev. Lett., **68**, 1422-1425 (1992).

24. Rothon, R. Particulate-Filled Polymer Composites; Longman Scientific & Technical: Essex, UK, 1995.

25. Han, C. D.; Snadford, C.; Yoo, H. J. Polym Eng Sci, 1978, 18(11), 849-854.

26. Boaira, M. S.; Chaffey, C. E. Polym Eng Sci, 1977, 17(10), 715-718.

27. J. M. Kenny and A. Maffezzoli, Polym. Eng. Sci., **31**, 607 (1991)

28. Jansma JB and Qutubuddin S (1995) Rheological behavior of concentrated calcium halophosphate suspensions. J. Rheol., 39(1): 161-178.

29. Boersma WH, Laven J, Stein HN (1991), Time-dependent behavior and wall slip in concentrated shear thickening dispersions. J. Rheol., 35(6): 1093-1120.

30. Fagan ME and Zukoski CF (1997) The rheology of charge stabilized silica suspensions. J. Rheol., 41(2): 373.

31. D. M. Husband, N. Asksel, and W. Gleissle, J. Rheol., **37**(2), 215 (1993).

CHAPTER 2. EFFECTS ON THE MELT RHEOLOGY OF SYSTEMS OF Nd-Fe-B PARTICLES SUSPENDED IN A POLY (PHENYLENE SULFIDE) AND LIQUID CRYSTALLINE POLYMER BLEND

A paper submitted to *Polymer Composites Journal*

Peter C. Guschl and Joshua U. Otaigbe

SYNOPSIS

The melt rheology of blends of a liquid crystalline polymer (LCP) and poly (phenylene sulfide) (PPS) and their composites with ferromagnetic Nd-Fe-B particles (MQP) was studied. We investigated the effects of LCP concentration, Nd-Fe-B particle volume fraction and size, distribution, and shear rate on the rheological properties of these composites. Enthalpy of fusion changes were observed due to the addition of the LCP and Nd-Fe-B particles to the polymer blends/composites. The shear rate and frequency dependencies of the materials revealed a viscosity reduction at low (1-3 wt. %) and moderate (10-15 wt. %) LCP concentrations, and strong effects on the shear-thinning characteristics of the melt. The suspensions of polydispersed Nd-Fe-B particle configurations in PPS that were of lower size ratios gave better processability, which is contradictory to previously reported behavior of suspensions containing spherical particles. Specifically, the compositions with unimodal and a bimodal distribution of Nd-Fe-B particles gave the lowest viscosities. The experimental data was correlated with semi-empirical viscosity model equations due to Maron-Pierce, Krieger-Dougherty, Eilers, and Thomas and were found to be consistent with the data. The maximum packing fraction, ϕ_m, of the MQP particles was estimated to be within the range of $0.78 \leq \phi_m \leq 1.0$ through graphical and parametric evaluation methods.

1. INTRODUCTION

The role of rheology of concentrated polymer systems is significant in today's industrial products, because it determines the processability of these materials under practical conditions. Polymer-bonded magnets (PBM) composed of polymer matrices and special rare earth transition metal magnetic alloys (e.g. Nd-Fe-B alloy) represent an important class of engineering materials used in electromechanical applications in automotive and non-automotive areas, where energy efficiency is a prime concern (1-5). The advantages of PBM over their metallic and ceramic counterparts include low weight, resistance to corrosion, ease of machining and forming, and capability for high production rates, but not high magnetic performance. The rheology of concentrated filler/polymer systems such as the PBMs of this study is important because it underscores the processability of these materials under practical conditions. Although, rheological studies of dilute and some concentrated suspensions have been previously reported for model monodisperse systems (6-15), it is widely recognized that rheological characterization and control of the viscosity of useful concentrated, non-spherical, polydisperse filler/polymer suspensions (e.g., PBM) is an inexact science due to the lack of theoretical models and experimental devices that can accurately define the complex flow behavior of such materials as a function of different physical and chemical parameters of the system. Further, systematic studies on rheological behavior of well-characterized, concentrated, polydisperse filler/polymer systems such as the PBMs of this study are very few (4).

Magnetic rare-earth alloy particles are badly corroded and oxidized under humid conditions and temperatures in excess of 100°C. To address this problem the magnetic industry is investigating the use of polymer binders as a potential solution. The flexible

nature, chemical resistance, and high thermal resilience of certain thermoplastic polymers, such as poly (phenylene sulfide) are of particular interest in the case of polymer-bonded magnets. These polymers (particularly thermoplastics) act as "shielding agents" for the rare-earth metal particles, reducing the degree of contact of the metal with oxygen, water vapor, and other potentially corrosive molecules present in the atmosphere. Furthermore, due to their flexibility and ease of molding, the polymer matrices allow magnetic materials to be molded and shaped into any desired part shape. However, many polymers have the disadvantage of degrading and crosslinking when exposed to elevated temperatures for long periods of time. In addition to the adverse temperature effect just mentioned, polymers are also well known to be very sensitive to elongational and shear deformation rates, especially at high rates that are likely to be encountered during processing.

Although the idea of polymer bonded magnets is a practical and very reasonable one, the presence of filler particles in a polymer matrix causes the viscosity of the material to increase rapidly as more and more fillers are added. This experimental fact explains why a limit of filler concentration (i.e. maximum packing fraction) exists beyond which the melt viscosity becomes intractable. It is desirable to obtain a composite of polymer and filler that is not too viscous to be molded at an optimal magnetic powder concentration. Ideally, the addition of magnetic fillers to a polymer matrix results in a material with optimal mechanical properties, magnetic properties (i.e. high coercivity, high remanence, and high energy product) and other beneficial properties such as stiffness and strength of the PBM composite.

The use of functional additives within a polyphenylene sulfide matrix has been previously reported to alleviate the aforementioned problems (4, 5, 16). The addition of a small amount of thermotropic liquid crystal polymer can lower the viscosity at low shear

rates as well as enhance the modulus and strength of the PBM. This observation can be attributed primarily to the orientation of the liquid crystal polymer chains in the direction of the shear, allowing fewer entanglements to form and a lower resistance to flow. It has been suggested that the liquid crystal polymer's unique rheological behavior is attributed to its flexible and rigid rod-like chains (17). However, it is important to note that certain liquid crystal polymers offer a better reduction of viscosity of particular polymer matrices than do others, due to increased phase separation between the polymer matrix and the LCP. Presumably, this higher degree of separation (*i.e.* immiscibility) allows numerous "slip boundaries" to be present within the matrix, providing regions in which viscosity reduction of the polymer blend can occur. Vectra A950 was the liquid crystal polymer of choice for the experiments described in this paper. Vectra A950 was chosen as a suitable additive because its melting temperature is comparable to that of the PPS used in the present study. Due to its random sequencing of the aromatic units, the Vectra A950 copolyester molecule is relatively linear and rigid. Additionally, its superior chemical and thermal resistance, high strength and modulus, and ease of melt processing (18) make this liquid crystal polymer an appropriate functional additive.

The presence of filler within a suspension is known to exhibit non-Newtonian pseudoplastic behavior such that the viscosity decreases with increasing shear rates (19). In other words, a Newtonian fluid can exhibit non-Newtonian behavior if sufficient amount of particles are suspended in it. This non-Newtonian behavior of filled polymer suspensions can be explained by considering certain mechanisms that cause the shear stress to orient or distort the particles against the effects of Brownian motion (20). In other words, the hydrodynamic forces predominate the thermal motion of the particles at high shear rates. It is this oriented

or distorted arrangement that offers a lower viscosity (lower resistance to flow) at increased shear rates than the melt viscosity of the matrix.

The particle configuration or distribution of the filler also strongly influences the processability of the polymer composite material. Farris (21), Mangels and Williams (22), and Metzner (23) suggest that whether one has a system of particles that are all of the same average size (monodispersed) or one of varying sizes (polydispersed), one can observe a dramatic change in the viscosity at certain volume fractions. The authors just mentioned used spherical particles in their studies. Although, most industrial materials such as the PBM of this study contain non-spherical fillers and non-uniform size distributions, it is believed that the models based on filled polymer systems containing spherical fillers may be useful in interpreting the trends in viscosity-concentration behavior of melts of multimodal suspension systems such as the PBM of this study.

Because of the complex heterogeneous nature of PBM, this paper does not attempt to describe quantitatively the viscosity-concentration behavior of the melts of the multimodal systems. Instead it discusses results of a systematic experimental approach aimed at accelerating the development of PBM with tailored properties for high temperatures and aggressive environments. It is felt that the work may be useful to scientists and engineers who must deal with inherent problems of PBM already mentioned. As will be shown later, our results appear to have some limited consistency with the trends predicted by a number of model equations derived for relatively simple filled systems of monodispersed or polydispersed, rigid spherical particles. By systematically adjusting the size ratio of the Nd-Fe-B particles, it will also be shown that smaller particles can be accommodated in the spaces between the larger particles, resulting in a more efficient packing and low viscosities at high

volume fraction of the particles like others (8, 24, 25) have reported for other bidispersed concentrated suspensions of spherical particles. Our future modeling efforts to be reported elsewhere will consider the important role of the shape factor (i.e. aspect ratio) of the platelet Nd-Fe-B particles used as well as the geometry of the channel and type of flow (simple shear or elongational) involved.

2. EXPERIMENTAL

2.1 Materials

A commercial thermotropic liquid crystalline copolyester (Vectra A950, Ticona Plastics), hereafter referred to as LCP, comprised of a 73 mol % hydroxybenzoic acid to 27 mol % hydroxynapthoic acid ratio, was used in this study. The melting temperature and density of the Vectra [Ticona Plastics (26)] are about 281±1°C and 1.400 g cm^{-3}, respectively. The melting temperature was determined from differential scanning calorimetry experiments discussed later.

Phillips Chemical Company provided the poly (phenylene sulfide) grade - Ryton Type PPS, which will hereafter be referred to as PPS. The PPS has been cured at a temperature below its melting point. The average molecular weight value of this grade is difficult to obtain and estimate due to its special synthesis conditions (27). The density, melting temperature, and glass transition temperature of the PPS grade is approximately 1.36 g cm^{-3}, 280°C, and 90°C, respectively.

The magnetic powder, manufactured by Magnequench, consists of varying particle sizes of a neodymium-iron-boron alloy ($Nd_2Fe_{14}B$) platelets (Figure 1). Specifically, the commercial powder used is MQP-B that has a density of 7.60 g cm^{-3} and a Curie temperature

of 360°C. The particle sizes used in these experiments ranged from 38-300 μm, separated into five particle size fractions corresponding to the sieve plates used: 38-75 μm, 75-106 μm, 106-150 μm, 150-212 μm, and 212-300 μm. The aspect ratio of the particles was experimentally determined to range from 0.2 to 10 (4). An image analysis of Figure 1 has showed that the aspect ratio of the MQP-B particles was within this aspect ratio range, with the majority of the particles having aspect ratios in the range of 1 to 5.

2.2 Differential Scanning Calorimetry

In order to investigate the effects of the additives on the enthalpy of fusion of the PPS matrices, DSC runs were performed on different blends and composites consisting of the LCP and/or MQP. The apparatus used was a Perkin Elmer Pyris 1 Differential Scanning Calorimeter. Scans performed on an indium metal standard at 10°C min^{-1} confirmed the accuracy of the experiments. Further, each run was performed in duplicate providing adequate reproducibility. Initially, baselines were determined for each run performed. The samples were each heated from ambient temperature to 400°C at a heating rate of 10°C min^{-1} under a nitrogen atmosphere. After each experiment the baseline curve was subtracted from the thermograms. Tables 1 and 2 show the DSC results obtained for PPS-LCP blends and PPS-MQP composites, respectively. The tables display peak temperature, peak area, and change in enthalpy of the system. A normalization value (discussed later) was calculated to allow valid comparisons in the change in enthalpy values of the materials tested.

2.3 Blend Preparation and Torque Rheometry

The polymer samples were dried in a vacuum oven (Model 5861) at 90°C for at least 24 hours prior to mixing in order to remove any moisture from the samples. Blends of PPS and LCP, with volume fractions of LCP ranging from 1% to 20%, were hand-mixed in the desired proportions prior to mixing (or melt blending) in the Haake Rheomix 600. Similarly, mixtures of 15% MQP-B + 12.5% LCP + 72.5% PPS were made. The following equation was used to determine the mass of material *j*, where *j* represents PPS, LCP, or MQP-B,

$$m_j = \phi_j \rho_j V \qquad (1)$$

ϕ_j is the volume fraction, ρ_j is the density, and V is the volume of the Haake Rheomix 600 mixing space. The volume fraction, ϕ_j, is the initial value desired for a particular blend. For example, if one desired to produce a 95/5 (v/v)% PPS-MQP composite, then one would measure m_{MQP} = (0.05)(7.60 g cm^{-3})(48.3 cm^3) = 18.354 g MQP. The actual volume of the Haake Rheomix (69 cm^3) is multiplied by 70% in order to allow for expansion of the blends during mixing. Similarly, the amount of PPS is determined, using the appropriate density and volume fraction values.

After hand mixing (i.e., measuring out desired amounts of the components into a plastic bag and shaking) the samples were poured into the Haake that was preheated to 320°C. The powders and polymer were allowed to equilibrate at the said temperature and at 5 RPM (~0.5 rad/s) for 3 minutes to allow particle agglomerates to break apart. Immediately following this equilibration, the rotor speed was increased by 5 RPM to 10RPM, and the torque data was recorded. Subsequently, torque measurements were taken after 2 minutes of mixing at shear rates that were increased by 5 RPM intervals. This process was continued

until the last set of data was obtained at 50 RPM. The overall mixing time was restricted to 21 minutes to avoid significant thermal degradation. The mixing volume was closed off on all sides (on both sides by two heating zones and on the top by a plunger) ensuring a constant volume and minimal sample contact with air and possible moisture. Values after the first minute during the two-minute intervals were used and averaged, because of the need for equilibration of the melt at different rotor speeds. Figure 2 shows two typical torque versus time plots obtained from the Haake measurements, displaying the initial increase in viscosity due to particle aggregates, the subsequent decrease, and the step increases resulting from the changes in rotor speed.

After the melt blending of the PBM was completed, the samples from the Haake were allowed to cool back to room temperature and then granulated into pellets/powders. The granulated samples were subsequently compression molded into disks (18.8mm diam. by 3.40mm thick) at 290°C and 24.1 - 27.6 MPa (3500 - 4000 psi) in order to reduce the amount of voids present. The resulting disks were used for the following shear rheometry experiments using the ARES rheometer as described in the next section. Scanning electron micrographs of typical PPS/LCP blends and PPS/MQP-B composites are shown in Figures 3 and 4.

2.4 Shear Rheometry

Dynamic experiments were performed on the Advanced Rheometric Expansion System (ARES, Rheometric Scientific) at 10% strain in a parallel plate configuration with 25-mm plates at a gap spacing of 2 mm, giving a flow space of at least 10 times the average particle size of 150 microns. The gap size used was assumed to be a reasonable size to

minimize particle migration effects such as reduced particle concentration near the walls of the parallel plates (28). In the sample composition range tested, it was found that the output signals were always sinusoidal, indicating an absence of nonlinear effects (29) caused by shear-induced structure in our filled polymer systems. Linearity (viscoelasticity) was maintained up to 30% strain. This information was determined by performing strain sweeps on the composites from 0.1% to 100% strain at a frequency of 10 rad s^{-1} and at 320°C. A linear strain of 10% was used for all materials studied. The dynamic frequency and steady rate sweeps were performed at either 280°C or 320°C and at frequencies and shear rates of 1-100 rad s^{-1} and 1-100 s^{-1}, respectively. Dynamic thermal stability tests were performed at 280°C or 320°C, 10 rad s^{-1}, and 10% strain. All tests were performed in triplicate. For example, the standard deviation was calculated for three complex viscosity experiments at three frequencies of a blend of 85% PPS and 15% LCP. The standard deviations at 1, 10, and 100 rad s^{-1} were 42.47, 12.06, and 2.84 Pa-s, respectively. The data shown in the results section (4.) are averages of these measurements. Test times were at least 4 minutes (run time from 1-100 rad s^{-1}) for the dynamic and steady shear sweeps and 30 minutes (selected in order to observe long-term effects above the melt temperature) for the thermal stability tests.

2.5 Variable Pressure Scanning Electron Microscopy (VP-SEM)

Figures 3 and 4 were obtained using a Hitachi S-2460N VP-SEM. These micrographs were created under a beam current of 0.5 nA, a 25 mm working distance, a 40 Pa (0.3 torr) Helium atmosphere, an accelerated voltage of 20kV and a magnification of 300x. Figure 3a was scanned under a pressure of 80 Pa (0.6 torr), because 40 Pa was insufficient to prevent

charging. The samples under examination were compression molded, as discussed previously, and fractured with a razor blade, exposing the surface to be viewed.

3. VISCOSITY MODEL EQUATIONS

Farris (21), Metzner (23), Lee (30), Brodnyan (31), and others have reported a number of different mathematical models that describe the viscosity of suspensions as a function of the volume fraction of the suspended particles. Some of these models generally refer to basic suspensions consisting of spherical particles dispersed in a Newtonian or a non-Newtonian matrix, which represent simpler systems than the present PBM. We found the insightful review by Metzner (23) and earlier theoretical studies of the rheology of suspensions of solids in polymeric (10) and other liquids (8) to be of especial interest in this study by alerting us to behavioral possibilities that might be exhibited by our PBM. We now show in this section the extent of agreement or otherwise of our experimental results with those calculated from some of the available model equations for understanding the role of different variables such as particle size and shape, particle size distribution, and volume fraction of the particles on flow properties of our suspensions. Apparent viscosity data extracted from the Haake mixer was used to test the applicability of most of these models to our PBM. In order to get a more accurate value of the viscosity, we calculated it from the following equation (32):

$$\eta = \frac{2\Gamma}{\pi L (R_e + R_i)^2 (1 + g^{n+1})\dot{\gamma}} \tag{2}$$

In this equation, Γ is the torque on the rotors, L is the length of the rotor, R_e is the effective radius (i.e. distance from the center of the rotor to the wall of the mixer), R_i is the radius of the rotor, and g is the rotor ratio. Since the rotors have the same rate, g=1 and the $(1+g^{n+1})$ term in Equation (2) equals two and cancels the two in the numerator, leaving an expression based only on the geometry and physical parameters of the mixer.

We selected three rotor speeds from the Haake Rheomix data: 1.05, 3.14, and 5.24 rad s^{-1} (equivalently, 10, 30 and 50 RPM) to analyze a range of the viscosities at different volume fractions of MQP. Figure 5 represents a graph of relative viscosity (ratio of suspension viscosity to polymer matrix viscosity) versus volume fraction of the MQP, from 0%-75% by volume, present in the PPS matrix at the three rotor speeds, using Equation (2). Most equations that relate viscosity to volume fraction of the suspended particle use a relative viscosity, $\dot{\eta}_r$ (i.e. the viscosity ratio of the viscosity of the filled system to that of the unfilled system). One can observe the general increase in viscosity as more MQP is added to the blend (see Figure 5). The lines that are drawn in this figure represent guides for the reader to observe this increase in viscosity with addition of MQP.

The first model applied to our PBM was developed by Maron and Pierce (22-23), and described by Equation (3). This empirical equation is typically given with an A parameter value equal to unity and shows an inverse relationship to the volume change of the spacing between particles. Equation (4) is a modified form of Equation (3) developed by Krieger and Dougherty (20), where the maximum packing fraction and the volume fraction of the particles, are denoted by ϕ_m and ϕ, respectively.

$$\eta_r = A\left[1-\left(\phi/\phi_m\right)\right]^{-2} \tag{3}$$

$$\eta_r = \left[1-\left(\phi/\phi_m\right)\right]^{-[\eta]\phi_m} \tag{4}$$

Because the parameter A (which depends upon the shape of the particles) and the maximum packing density (dependent upon particle configuration) are unknown for the geometry of the particle of this study, the viscosity values are compared to the monodispersed spherical particle case (i.e. $A = 1.3$, $\phi_m = 0.68$), where the ϕ_m parameter is an average maximum packing fraction for monodispersed spheres in low and high shear limit cases. The following statement has been made by Rothon (33) that "when comparing spherical data to non-spherical data: if the values are close, then a low aspect ratio is assumed; if greater than the spherical case, then the filler is either porous or has some degree of anisotropy." Since the MQP-B particles have been found to be within the aspect ratio range of 0.2 to 10 (4), the closeness of our experimental results to the calculated values from spherical particle models can be rationalized. The $[\eta]$ parameter in Equation (4) is the intrinsic viscosity of the suspension. Through a method of nonlinear least squares regression, the intrinsic viscosities were obtained. The following numbers 2.7958, 2.9042, and 2.5230, shown in Table 3, are the intrinsic viscosity values at the three shear rates mentioned earlier and are relatively close to the dilute, monodispersed value of 2.5. ϕ_m values close to or equal to unity were fitted to Equations (3) and (4) and the values obtained are given in Table III.

The Thomas expansion of Einstein's equation for dilute monodispersed spherical suspensions, Equation (5) (23), shows good agreement with the experimental data in Figure

6, and it reveals more reasonable values of relative viscosity at higher volume fractions (> 50%).

$$\eta_r = 1 + 2.5\phi + 10.05\phi^2 + A\exp(B\phi) \qquad (5)$$

The coefficients in Equation (5) are physical constants dependent upon the particles of the system (i.e. 2.5 is the shape factor for a monodispersed spherical system). A and B are given as 0.00273 and 16.6, respectively, in Metzner's review paper (23). The value of 2.5 was used here in order to adjust the equation for only a two-parameter fitting. The two parameters seemed to vary irregularly with shear rate, but we can see that the B constant remains relatively close to the monodisperse sphere case (see Table III).

Eilers's equation (6) (34) is also in good agreement with our experimental data (see Figure 6). In fact, this equation seems to have a better fit to our data compared to the other equations already discussed. In order to have the values fit the experimental points, we used nonlinear regression to find ϕ_m. The values were found to increase with shear rate (see Table 3).

$$\eta_r = \left\{1 + \frac{1.25\phi}{\left[1 - \left(\phi/\phi_m\right)\right]}\right\}^2 \qquad (6)$$

The fitted ϕ_m values are in good agreement with experimentally determined parameter values as shown in Figure 7, which is a graphical evaluation of the maximum packing fraction (35). In this figure ϕ_m corresponds to the point where the vertical and horizontal axes meet. Since volume fractions as high as only 0.75 were investigated, it is not possible to precisely evaluate the maximum packing fraction experimentally. However, Figure 7 shows that the value of this parameter is roughly 0.78 or higher.

The deviation from the simple, monodispersed, spherical case is shown in Table 3 for Equations (3), (4), (5), and (6). The fitted parameters were found for nine composites of PPS (PPS)-LCP-MQP at the following volume fractions of MQP: 0%, 5%, 20%, 35%, 50%, 60%, 65%, 70% and 75%. Typically, these equations fit experimental data reasonably well for most of the volume fractions until the system becomes more concentrated (~50% loading of MQP) (see Figure 6). The parameters A and ϕ_m from Equation (3) and most of the other parameter values for the other three equations appear to increase with shear rate. van der Werff and de Kruif (9) observed that the value of the maximum packing fraction is a function of shear rate, due to an ordering phenomenon of the particles under shear flow. The information revealed from this regression method suggests that the geometry of the MQP particles within the composite exhibits higher packing densities than that of a spherical system. According to Rothon (36) many non-spherical particles (i.e. cubes, rectangles, and plates) can have ordered packing fractions of unity but most have less dense random packing than spheres, due to the difficulty of particle movement with respect to one another. As the maximum packing density is approached, the relative volume fraction reaches the value of 1. When this occurs, the viscosity approaches infinity, exhibiting solid-like behavior. The equations of Mooney, Frankel and Acrivos (23), Chong (34), and the modified infinite power

series equation (37) were also fitted, but they yielded poorer comparisons to our system, therefore these equations and their predictions are not given in this paper.

4. RESULTS

4.1 Dynamic Thermal Stability

In an effort to determine the maximum melt processing temperature, we measured the time dependencies of the complex viscosity of the PPS polymer at 280°C and 320°C in air and nitrogen. Figure 8 shows the time dependencies of complex viscosity of the PPS grade of PPS at 280°C and 320°C, fixed shear rate (10 rad s^{-1}), and in air and nitrogen atmospheres. Figure 8 shows that the polymer is strongly thermally unstable under oscillatory shear flow at both 280°C and 320°C after roughly 500 and 100 seconds, respectively. This observed thermal instability was significantly reduced, as well as the complex viscosity, when the tests were performed in a nitrogen atmosphere. The PPS polymer appeared to be relatively thermally stable in the nitrogen atmosphere over the entire experimental time window (1800 seconds). The poor thermal stability of the polymer in air is ascribed to crosslinking or polymer oxidation to an extent that depends on the polymerization reactions used to produce the polymers (17, 19, 27, 38). As expected the poor thermal stability of the polymer was observed to be exacerbated at 320°C in an air atmosphere (Figure 8). The results indicate that the polymer is relatively thermally stable in the temperature range of 280°- 320°C and nitrogen atmosphere over the experimental time window covered in this study.

To determine the effect of the presence of the LCP (Vectra A950) on the thermal stability of the PPS polymer, we performed similar dynamic thermal stability tests at 280°C

to those just described using the PPS polymer blended with 1-4% LCP. The results obtained are compared with those acquired for the pure PPS and pure LCP in Figure 9. The pure LCP showed poor thermal stability under the test conditions. Blending the PPS with small amounts of the LCP (1-4%) increased the viscosity of the PPS while the 1-2% PPS/LCP blends showed a small improvement in the thermal stability over the experimental time window. The poor thermal stability of the pure LCP may be ascribed to the reported strong dependence of LCP rheology on previous thermal or preshear treatment due to the relatively long relaxation times of the LCP and the reported concept of percent of "melted" resin (i.e. amount of resin in the solid-nematic phase) (39). The observed complex viscosity rise with time of the LCP is consistent with formation of high-melting crystals at elevated temperatures, as others have found for another thermotropic LCP (40, 41). The viscosity growth was attributed to factors such as recrystallization of the LCP phase (40, 41), chemical interaction between the LCP (a copolyester) and the PPS, or to the potential transesterification reactions of the LCP (17). Similar trends in the time dependencies of complex viscosity at 320°C (not shown) of the PPS, LCP and their blends were observed.

Similar thermal stability analysis was performed on PPS-MQP-B composites in order to investigate the effect of oxidation of the metallic powders on the complex viscosity of the polymer. Figure 10 shows complex viscosity versus time curves for PPS and two composites of 5 % and 10 % MQP in either an air or nitrogen atmosphere at 280°C. As expected, a significant improvement in thermal stability of the composites was observed in nitrogen atmosphere. Approximately a 26 % increase in the complex viscosity of the 5 % filled sample and a 15% increase for the 10 % filled composite was found. The percent increase in complex viscosity of these composites is roughly tripled in air. Although no oxidation was

expected on the surface of the filler particles in the nitrogen atmosphere, increases in viscosity were apparent to a greater extent than observed for the pure polymer and PPS-LCP blends. Therefore, we can surmise that the MQP particles initiate faster cross-linking at the polymer-filler interface.

Thermal stability tests at 320°C reveal, as expected, a shorter stability window at a higher temperature. A test run of a 15 % filled PPS-MQP sample was heated under the same test conditions as the earlier experiments at both 280°C and 320°C in nitrogen (graph not shown). A more substantial increase in complex viscosity was indeed observed for the latter case. However, in perspective of the experiments following this analysis, only a time window of 250 seconds (~4 minutes) is needed in order to run a frequency sweep for a sample from 1 rad s^{-1} to 100 rad s^{-1}. In this timeframe, only a 6.35% increase and a 11.95 % increase in complex viscosity was observed for the tests performed at 280°C and 320°C, respectively. The presence of the nitrogen during the experiment appeared to suppress the complex viscosity increase in the tests performed in air by a factor of 10, giving more reliable data from the experiments performed at 320°C.

4.2 Torque Rheometry (Haake Rheomix)

The Haake mixer allowed us to measure the effects of shear and deformation on the mixing/blending of a sample of pure powders at low shear rates, resulting in a homogeneous blend. The data recorded during the mixing process consisted of torque measurements experienced by the rotors as they sheared the molten material. Average values of torque and rotor speed were used to determine the apparent viscosity at a given shear rate. Equation (7) represents this relationship:

$$\eta_a = \frac{\Gamma}{RPM} = \frac{\tau}{\dot{\gamma}} \tag{7}$$

where η_a is the apparent viscosity, Γ is the torque, RPM is the rotor speed, τ is the shear stress, and $\dot{\gamma}$ is the shear rate. Figures 11 and 12 represent apparent viscosity versus shear rate data.

The concept of adding a liquid crystalline polymer (LCP) to other polymers to enhance processability is widely known (17, 18, 41, 42, 43, 44). However, the amount of LCP needed to provide optimal viscosity reduction in a particular polymer matrix is unknown. The first set of data corresponding to the apparent viscosities of five compositions of LCP and PPS versus the shear rate (rotor speed) is shown in Figure 11a. The five curves show shear-thinning behavior as expected. One can see from this figure that initially an increase in apparent viscosity occurs as LCP is added. However, it is obvious that the apparent viscosity does drop close to, but not lower than, the value of the pure PPS curve in the 15/85 LCP/PPS blend at the various shear rates. Generally, it appears that a moderate concentration of LCP (~10-20% by volume) in the PPS-LCP blend yields a composite with a reduced viscosity. However, Whitehouse *et. al.* (44) suggested that a small percentage of LCP (0.2, 0.5, and 2 % by weight) might exhibit a lower viscosity profile. Their experiments involved a thermotropic LCP consisting of hydroxybenzoic acid, hydroxyquinone and sebacic acid blended with high-density polyethylene. Blends of LCP/PPS mixtures containing lower LCP concentrations than before were prepared and tested to investigate this concept. Figure 11b shows the apparent viscosity versus shear rate curves for five composites at low concentrations of LCP. The figure shows that the LCP increases the PPS matrix

viscosity but only until a 2 % concentration is reached. The 3 % curve drops down closer to that of the neat PPS curve. In contrast with the results shown in Figure 11a, the 15 % LCP/PPS blend is actually of lower viscosity than the 3 % blend. This fact supports our expectation that a moderate concentration is more beneficial in our PPS-LCP blend. It is important to note that the preceding results were merely intended to show the unique rheological behavior of these blends as they are sheared and heated for the first time.

Samples were mixed in the Haake before the experiments just described by loading different MQP particle sizes and distributions into the LCP/PPS matrix. A constant ratio of LCP: PPS concentration (ϕ_{LCP}: ϕ_{PPS} = 0.176), corresponding to a 15 % volume fraction of LCP within the PPS matrix, was maintained as the different particle configurations were added at a 15 % volume fraction (i.e., 72.5 % PPS, 12.5 % LCP, 15 % MQP). This moderate volume fraction allowed us to investigate particle polydispersity effects at a more reliable volume fraction range in which more reproducible data could be obtained. It is understood that higher particle loadings might show more significant modality effects, but the reproducibility of data obtained from such systems is strongly compromised (8). Eight samples were prepared, consisting of various combinations of the particle sizes, as already described in the Experimental section. Table 4 shows these different combinations and their respective ranges of particle sizes. The concept for these experiments arose primarily from the earlier works of Farris (21), Mangels and Williams (22), and Metzner (23). Their research suggests that the viscosity of a suspension depends upon the configuration or modality of the particles within a suspension. Although their research was based upon systems containing spheres of various sizes, it is believed that the platelets of the MQP may behave similarly as discussed in Section 3 of this paper. The system, 1mod150 in Table 4, was selected based on

our previous work (3,4) under the assumption that MQP-B would yield similar results as MQP-O. In that work the authors showed that in a unimodal system, the 106-150 micron range had the lowest complex viscosity in the frequency range of 1 - 100 rad s^{-1}.

For the bimodal systems the correct ratio of fines to coarse particles that would yield the lowest viscosity is unknown. Following the work of van der Werff and de Kruif (9), we constructed Figure 13 that reveals our reasoning for using a 50-50 mixture of fines (38-75 microns) to coarse (212-300 microns) ratio. A minimum in the apparent viscosity of these curves appears at the 50% fines point in this figure. Figure 12 shows the apparent viscosity versus shear rate curves for the different configurations (sizes and modality) of the MQP powder in the PPS/LCP blend matrix. This graph shows that a slight change in the distribution of the particles can affect the apparent viscosity of the suspension in a significant way. One can see that the bimodal system consisting of particles with average sizes of 90.5 and 128 microns (2mod150) yields the lowest viscosity at each shear rate beyond ~2 rad s^{-1}. Higher viscosities are observed for the other bimodal systems. Furthermore, for these bimodal systems, a more pronounced shear thinning behavior seems to have occurred, whereas less shear thinning is apparent for the lower viscosity systems. Interestingly, the trimodal configurations appear to exhibit a lower viscosity at low shear rates than that of some of the bimodal ones. Further discussion on this observation will be given in the next section.

4.3 Shear Rheology (ARES)

The ARES rheometer was used in order to perform various rheological tests under two different deformations: steady and oscillatory shear amongst other possible deformation

histories. Unlike the Haake Rheomix, the ARES is capable of operating at shear rates and frequencies in the range of 0.00625 - 625 s^{-1} and 0.001 - 100 rad s^{-1}, respectively. The samples mixed via the Haake runs were utilized again in the ARES experiments. Performing rheological experiments under the two deformation modes allowed measurements to be obtained under small strains within a linear viscoelastic regime (dynamic) and under continuous deformation (steady shear) over a range of frequencies and shear rates.

The initial five concentrations of LCP in PPS (0%-20% by volume) were studied with oscillatory shear flow experiments in the ARES from 1 - 100 rad s^{-1} at 320°C. The results obtained are shown in Figure 14. Figure 14a shows that an increase in LCP concentration results in a rise in the complex viscosity. However, the presence of 10% LCP appears to yield a viscosity drop at 1 rad s^{-1}. In Figure 14b one can see an initial drop in viscosity at small concentrations, a rise at slightly higher concentrations, and finally another drop at 5% LCP. It is believed that since the ARES can operate under a larger range of frequencies, more information on the flow behavior of the composites can be obtained. However, because the material used in the ARES had previously been heated and sheared many times (heated, mixed, heated, and compression-molded) before the experimental runs, it is believed that cross-linking and chain entanglement may have occurred within the polymer matrix and LCP phases (38). These effects are investigated to some extent in this paper; however, further research focusing on the chemical responses to shear and extended heating on the materials is needed. The results of this further research will be published elsewhere. For comparison to the dynamic shear mode of deformation, the steady shear viscosities of these composites were plotted versus LCP concentration in a similar way in Figure 15. It is evident from Figs 14 & 15 that the mode of deformation has a strong affect on the flow properties of the

systems. Figure 14 shows that minima in these curves appear at low and moderate concentrations (1, 2, 3 and 10%).

The curves shown earlier in Figure 11 and 12 exhibit excellent agreement with the power law model, when graphed as log viscosity versus log shear rate. The power law equation obeys the following expression:

$$\eta = m\dot{\gamma}^{n-1} \tag{8}$$

where m and n are the consistency factor and the power law index, respectively.

The steady shear viscosity versus shear rate plots (not shown) were not quite as uniformly linear with a well-defined slope as the complex viscosity curves, showing a possible Newtonian region at shear rates less than or around 1 s^{-1}. One could observe this by plotting steady shear viscosity versus shear rate from Fig 15. Exact agreement (i.e. similar rheologies) between the two deformation modes was not expected and was not observed in comparison between these two deformation experiments (not shown). The Cox-Merz rule was reasonably valid for the pure polymer case. However, the presence of LCP and MQP in PPS created large deviations between the dynamic and steady shear curves, due to the heterogeneous nature of the blends/composites.

Adverse effects on measurements such as edge fracture, end effects and possible wall slip for concentrated dispersions may lead to unreliable data under steady shear testing. However, considerations were made, such as use of a large enough gap height during parallel plate rheometry measurements, to minimize these effects. Further inconsistencies may arise with the parallel plate geometry, because the shear rate is a function of the radial position of

the plates (due to an inhomogeneous strain) (19). Corrections can be made to account for an "apparent" shear rate. Edge fracture, for instance, was not noticed below our maximum shear rate of 100 s^{-1} for the blends. Emphasis was placed upon the dynamic (oscillatory) measurements for reasons of reducing effects of any such instabilities. Oscillatory measurements were obtained under small strain testing in order to ensure linear viscoelastic responses to the deformation.

By calculating the power law index, *n*, and consistency factor, *m*, for the samples of PPS/LCP blends, an interesting characteristic of the LCP becomes apparent. Figure 16a and 16b show how the index and consistency are affected by different amounts of LCP, respectively. For guidance each curve has a regressed polynomial plotted through the data points. The power law index and consistency factor curves follow a quadratic expression of the following form $Y = 0.6917 - 0.01935X + (5.914E\text{-}4)\ X^2$ and a cubic equation of this form $Y = 166 + 11.8X + 2.772X^2 - 0.1106X^3$, respectively. A maximum index is reached in this plot around the 1% LCP concentration mark, and then it decreases as more LCP is added to the PPS matrix. It seems that the viscosity is lower at smaller concentrations of LCP, but the shear thinning behavior appears to be at a minimum as a consequence. A minimum consistency factor is observed around 1%, and it increases almost linearly after 5% LCP.

The effect on the relative viscosity of the presence of MQP in the PPS-LCP blend is shown in Figure 17. This figure shows a relative viscosity versus shear rate plot for eight loadings of MQP ranging from 5% to 75% in the PPS-LCP blend. Clearly this figure shows that the viscosity increases profoundly with higher loadings of MQP. One can also observe from this figure the significant shear-thinning effect the MQP particles have on the flow behavior of the polymer matrix at high loadings (>65%).

Modality effects were again analyzed but by way of the ARES rheometer. As mentioned earlier, the tests were performed at 320°C and 10% strain. Complex viscosity versus frequency curves were plotted in order to determine a minimal viscosity particle size dispersity at this particular loading of 15%. Figure 18 shows the results obtained. The curves are labeled in terms of their particle modality as before. It appears that the unimodal and a few bimodal systems possess the lowest curves. Reasons for this observation are not clear at this time. Systems of polydisperse spheres are reported to yield better processability because of the enhanced packing that occurs between the particles of varying size in broader distributions (21, 22, 23). This was not observed for our system of polydisperse platelets, making our results inconsistent with earlier reports on the rheological behavior of polydispersed spherical systems. Varying the MQP particle size distribution among different combinations of the (38-75), (75-106), (106-150) and (38-75), (106-150), (212-300) size distributions seemed to effect the complex viscosity as well.

5. DISCUSSION

DSC analysis of the materials show that the addition of LCP to the system appears to affect the PPS matrix by reducing the area of the melting temperature peak and the associated change in enthalpy (ΔH). It can be seen in Table 1 that the presence of LCP does not significantly affect the melting temperature. This is reasonable due to the fact that LCP (Vectra A950) melts at about the same temperature as the PPS (see Table 1). We can also see that the peak area and ΔH of pure LCP are very small compared to that of pure PPS and the PPS-LCP blends. Further, Table 1 shows that adding LCP to the PPS matrix decreases the peak area and ΔH of the latter. In order to investigate whether or not this result is due to the

fact that less PPS is present in the system at high concentrations of LCP, a normalization value of the change in enthalpy [ΔH (norm)] was calculated. Basically, ΔH (norm) is the ΔH value of pure PPS multiplied by the respective LCP volume fraction in the system (e.g. with a 95/5 blend of PPS/LCP, ΔH (norm) = 0.95*26.5 = 25.2). We can see that the ΔH values are close to the normalization values, but not quite equal. This suggests that the presence of LCP in the system is causing the heat capacity of the composite to be lower than that of the pure PPS, since

$$\Delta H = \int C_p dT \tag{9}$$

where C_p is the heat capacity of the material.

An unusual observation is noticed when 20% of the LCP is added to the PPS. The peak area and ΔH increased slightly (see Table 1). This observation has been confirmed in replicated tests. The reason for this observation is not well understood at this time, but may be due to a phase inversion process at this volume fraction of LCP in the PPS (4).

The introduction of MQP into the polymer matrix yields expected trends on the DSC curves. Table 2 shows the effects of MQP addition to the PPS. Melt temperatures are not changed considerably, albeit slightly reduced. However, peak area and changes in enthalpy are reduced significantly, beyond the normalization values. Again, heat capacity changes due to the presence of the filler confirmed the trends in the ΔH changes observed for the unfilled PPS-LCP blends. Rothon (36) explains that the presence of inorganic particles can modify the cure processes of cured polymers by lowering the overall exotherm. This in turn reduces the cure temperature and kinetics of the polymer. Further thermal analysis (i.e. filler effects on crystallinity) on these composites will be published later (50).

Subjecting the polymer blends and composites to temperatures at and above their melting point for an hour and a half under air or nitrogen atmosphere caused an abrupt rise in complex viscosity after certain exposure times (Figures 8, 9, & 10). It is difficult to completely explain the reasons for this phenomenon without performing structural analyses on the specimens. However, it is believed that cross-linking and branching between the polymer chains and/or filler particles allow domains of entanglements to form, ultimately impeding the flow of the melt and, thus, increasing the viscosity (17). Furthermore, because of this cross-linking, entanglements are more likely to appear, further increasing the viscosity. Another important aspect is the concept of transesterification of the liquid crystals. At higher temperatures longer copolyester chains are likely to form linear and possibly longer chains, as more LCP is present in the matrix (see Figure 9). The combination of the PPS and LCP together seemed to produce a higher-viscosity material than either of the material alone at certain LCP concentrations. Figure 10 shows that the presence of the filler affects the complex viscosity of the matrix by increasing it initially and with time, due to an increased cross-linking between the polymer and filler. Possibly, an oxide layer on the surface of the filler may promote faster crosslinking. It is obvious that the elimination of oxygen in the environment during the experiments drastically reduced the occurrence of this apparent viscosity increase.

From the viscosity versus shear rate graphs of the various LCP-PPS blends (Figures 11, 14, 15, & 16), it is apparent that the presence of Vectra A950 liquid crystal polymer affects the PPS in a number of ways. Of critical importance is the fact that the viscosity is strongly affected. The viscosity decrease observed can be attributed to the formation of an oriented LCP phase (43). This allows less resistance to flow in a certain flow direction.

However, it seems that the viscosity increases are observed after a certain concentration of LCP is reached. An explanation of this phenomenon may be ascribed to mutual solubility between the LCP and PPS and phase-boundary transesterification (43). The latter effect in addition to a possible recrystallization of the LCP phase could be also responsible for rises in viscosity as well as viscosity reductions to an extent that depends on the type of LCP, the LCP volume fraction, temperature, shear rate and aging time. The longer the ester chains of the LCP within the polymer matrix, then the more likely entanglements may arise, leading to a larger resistance to flow or higher viscosity. This explanation is supported by the fact that a lower molecular weight polymer has a lower viscosity than the same polymer at a higher molecular weight ($\eta = KM^{3.4}$) (46). Furthermore, higher concentrations of LCP imply a higher potential for longer ester chains to form. As mentioned earlier, viscosity increases may also be attributed to polymer-polymer interactions present at higher LCP volume fractions, which can cause a higher degree of entanglement. Ibar (38) suggests that the polymer chains may be entangling with themselves (PPS-PPS or LCP-LCP) or other polymers (PPS-LCP), causing obstacles that restrict flow at higher molecular weights. Reducing the effect of entanglement through disentanglement would alleviate this problem.

The liquid crystal polymer acts as a shear-thinning agent when blended with the polymer matrix (see Figures 11, 14, 15 & 16). At certain concentrations the blend exhibits more non-Newtonian behavior. Due to curiosity, we investigated the effect of adding even more LCP (e.g. 50%) and noticed that the viscosity continued to increase rapidly and gave rise to a lower power law index. It is reasonable to expect that this viscosity increase will continue and the index will remain constant, suggesting a shear-thinning limiting behavior. Scanning electron micrographs, Figure 3, show three blends of 3%, 10%, and 50% LCP in

PPS. A uniform matrix is observed for the first picture, suggesting a single-phase dispersion of the polymers. The other micrographs show two distinct phases in which the dark-colored spots, representing the LCP phase, appear. The 10% LCP blend appears to have a uniform dispersion of the two phases where the majority of the LCP spots are of the 10-micron size. The 50% blend of LCP in PPS, displayed for the intent of viewing a sample of high LCP loading, shows aggregation of the LCP spots, which seem to be of the order of 15- to 20-microns. This aggregation causes a reinforcement of the PPS matrix, allowing the viscosity and the strength of the material to increase.

Differences between the Haake Rheomix and ARES data were observed when comparing viscosity versus shear rate curves. Because polymers behave differently under certain conditions due to the shear and thermal histories of the LCP and the PPS as well as the geometry of the apparatus in which measurements are produced, this discrepancy between the data from the two rheometers can be rationalized. The initial Haake mixing runs could have deformed the initial shape of the LCP from ellipsoidal to fibril within the existing matrix (44). Once in a fibril shape the LCP copolyester chain is less susceptible to entanglements with the matrix chains and itself becoming more orientable (44). Furthermore, the fibrils can act as lubrication agents present between the PPS chains, allowing "slip surfaces" to exist. Similarly for the PPS-MQP composites, the flow of MQP-B powder particles in the continuous polymer phase could be shear-dependent as well, due to the sliding of the platelet-shaped particles that is exacerbated at high shear rates. The initial Haake mixing process broke up any agglomerations between the particles, allowing formation of homogeneous dispersions consisting of oriented particles distributed within the matrix.

Further explanation of the discrepancies between the results of the two rheometric data can be discussed in terms of the preparation of the blends. Geiger (45) found that the viscosity of a thermotropic liquid crystal polymer was lower if the melt was pre-sheared by feeding the viscometer from an extruder (melt-fed) as compared to measurements made by filling the rheometer reservoir with solid pellets (pellet fed) (46). Basically, the Haake runs were pellet-fed and the ARES runs were "melt-fed." In this study, the samples for the ARES runs, as described before, were blended first in the Haake mixer, allowed to cool, granulated and then molded into disks.

Difficulty arises in comparing apparent viscosity (from Haake data) and complex or steady shear viscosity values especially when the shear rate/frequency ranges are different. The Haake data represents information of the blends and composites that are initially subjected to heat and shear within a shear rate range of 1 - 5 rad s^{-1}. In contrast, the ARES experiments allowed tests on the presheared/preheated samples under a broader range of shear rates/frequencies (i.e. 1 -100 rad s^{-1} and 1 - 100 s^{-1}). It is important to note that two rheometers were needed to reliably characterize the melt rheology of the complex heterogeneous materials of this study.

Investigation of the applicability of the Cox-Merz rule to our systems was performed. As expected, the addition of an immiscible material (Vectra A950) to the PPS matrix caused the two curves of complex viscosity versus frequency and steady shear viscosity versus shear rate to diverge away from each other, making the complex viscosity larger than the steady shear viscosity (data not shown). Al-Hadithi, *et al.* (47) noted a similar phenomenon in their paper describing the flow properties of a series of polymers, colloidal systems, and other

structured fluids. These discrepancies just mentioned arise due to the heterogeneous nature of our polymer blends (48).

Figures 5, 10, 12, 13, 17 & 18 show that the presence of the ferromagnetic MQP particles within the PPS matrix has a significant effect on the processing properties of the polymer. Furthermore, one can see that different arrangements of these particles can also induce various physical effects on the system. Firstly, Figure 13 shows the effect on apparent viscosity of particle size ratio. As expected, we can see that the unimodal system representing 0% fines exhibits a lower apparent viscosity than the 100% fines configuration. Because of the higher surface area of the smaller particles, the smaller particles in the 100% fines interact with each other more than the larger particles in the 0% fines case. Systems with smaller particles are not to be added to the PPS matrix due to the increased aggregation effect because of the particles' larger surface areas (49). Aggregation takes place below a certain particle size in which adhesion dominates over shear forces. This aggregation is easily reduced with larger particles and larger shear rates in order to exceed the adhesive forces (50). In a previous paper (4), we observed that the complex viscosity increased as the particles exceeded the range of 106-150 microns. It is hypothesized that beyond a certain particle size, the particles may begin to impede the flow of the melt by behaving like an aggregation of smaller particles.

As discussed earlier, the configuration of the embedded particles determines how easily the suspension flows. Figures 12 & 18 show a number of particle modalities of the MQP powder in a PPS-LCP blend. It is surmised that certain configurations exhibit better packing due to a broader particle size distribution. This hypothesis is supported by Rothon (36), "when different sizes of similar shapes are mixed, then improvements in packing

similar to those observed with spheres are usually obtained." This enhanced packing allows a highly concentrated composite to exhibit a low viscosity when compared to a suspension with unimodal particles at the same concentration (23). One can see from Figures 12 & 18 that although the configuration 1mod150 is unimodal, it still exhibits a relatively lower viscosity curve than those of higher modal systems. This observation contradicts Rothon's statement. It is believed that the viscosity would be larger if a smaller particle size were chosen (4). We see in this case that the samples containing particles with more narrow size configurations yield better processing results. The multimodal systems, such as 2mod300A and 3mod150, display high viscosities possibly due to the presence of particles that are possibly too small in combination with other smaller particles, leading to agglomerations that are difficult to disperse uniformly (52). The rationale for these observations is not completely understood at this time. However, we believe that the main reason lies in the fact that we are dealing with non-spherical, anisotropic particles, which may exhibit better packing at lower configurations of particles size, i.e. when the particles are of roughly the same size. Reported claims that a larger packing fraction may be obtained with a wide distribution of sizes and a larger proportion of bigger particles can be found in the literature (36). It is, however, important to realize that fillers with the same average particle size can have largely differing distributions, and it is the distribution that is generally more important in determining the particle effects on the properties of polymer composites (33). Although the concept just mentioned has been employed by a number of industries to achieve lower viscosities at a very high volume fraction of the particles (24, 25), systematic studies such as the present one on rheological behavior of well characterized polydisperse filled polymer suspensions are

scanty in the open literature. It is hoped that the present study will provide useful guidelines to future experimental studies and theory development for the little-studied PBMs.

Figure 4 shows micrographs of two composites loaded with 20% and 50% MQP, respectively. These micrographs show that at 20% loading, particle-particle interactions begin to appear whereas at 50% loading excessive clustering is observed. There is no preferential orientation of particles observed in Figure 4. But, after the suspension has been sheared, alignment along the shear direction is expected. Figures 17 & 18 show that the presence of the MQP particles increases the viscosity quite considerably. The shear-thinning behavior of the PPS does not appear to be affected very much by the MQP particles at low loading fractions (Figure 17). A similar observation was also observed by Nicodemo *et al.* (51). One can see that at the dilute (5%) and semi-dilute concentrations (35%) a lesser degree of shear thinning is observed. It can be seen from Figure 17 that after 50% MQP is added to the system, a significant thinning of the viscosity occurs. This observation can be ascribed to an increase in local shear rates in the fluid around the particles than average shear rates (19). The high concentrations of particles present in the system cause a larger increase in local rates. Similar results were reported by van der Werff and de Kruif (9) who found that shear-thinning effects within anisotropic dispersions originate in the particles' orientations and in the non-Newtonian flow properties of the entangled polymer matrix. It is understood that concentrated systems (greater than 35%) do tend to exhibit complex rheological properties with poor reproducibility (8). However, these properties obtained through use of a torque rheometer were found to be useful in providing a qualitative assessment of the shear-thinning behavior of the systems with higher volume fractions (>35%). It is noteworthy that such

highly concentrated systems cannot be reliably tested using conventional rotational rheometers such as the ARES.

6. CONCLUSIONS

The results of this study show that the addition of Vectra A950 liquid crystal polymer and the Nd-Fe-B particles to the PPS polymer grossly affects the PPS matrix viscosity via internal structural changes and phase separations. A viscosity reduction is apparent at small and moderate concentrations (1%-3%) and (10%-15%) of LCP in the PPS. Higher LCP concentrations gave an unexpected increase in viscosity of the blends possibly due to agglomerations of the LCP phase within the matrix. The degree of interaction between the two polymer components is difficult to quantify, but the results obtained suggest that they are partially miscible. As expected, under long exposure to high temperatures and shear deformation and flow conditions, the polymer blend components were found to exhibit changes in structure and properties (i.e., viscosity). A reduction of these changes was observed by performing experiments within a nitrogen atmosphere.

Addition of the platelet-shaped Nd-Fe-B particles strongly affected the rheological properties of the system. The distribution of these particles was found to be the critical factor that needs to be controlled to obtain high maximum packing densities at minimal viscosities for the composites. Specifically, the unimodal and bimodal system (1mod150 and 2mod150) gave rise to the system with the lowest viscosity at a volume fraction of 15% Nd-Fe-B. Higher Nd-Fe-B volume fractions (up to 75 vol. %) in the composites showed high viscosities that are melt-processible in conventional plastics processing equipment. However, it is believed that such high Nd-Fe-B volume fractions may compromise other properties such as the tensile

strength and toughness of the materials for the targeted applications. These properties are being investigated.

Comparisons between measured viscosity data for bimodal suspensions of the Nd-Fe-B particles at various volume fractions and fixed particle sizes (75-106 microns and 106-150 microns) in a PPS-LCP blend and calculated viscosity values at these corresponding volume fractions showed that certain equations may be beneficially used to some degree to describe the viscosity of the materials studied. The Maron-Pierce, Krieger-Dougherty, Thomas, and Eilers equations show excellent agreement at each of the Nd-Fe-B concentrations with slight deviation within the range of 35%-70% Nd-Fe-B concentrations. Maximum packing fractions were estimated graphically and parametrically from these models to be in the range of 0.78 to 1.00.

Finally, this study shows that, whereas much theoretical work has been published on relatively simple suspensions of spherical particles in polymeric liquids, very little information on concentrated, suspensions of non-spherical, polydisperse particles in polymeric liquids such as the present PBMs is available in the open literature. This was a surprise considering their relative technological importance. Much work on PBMs or similar polymeric materials may be available in undisclosed files within the industry. Despite the relative complex nature of the PBMs, it is very interesting to note that their viscosity is consistent with some of the semi-empirical viscosity models reported for relatively simple suspensions containing spherical particles. With the advent of advanced analytical tools and increasing interest in interdisciplinary research, it is likely that the present study will provide a useful basis and motivation for future experiments and theory development for the little-studied but intriguing and commercially important PBMs. The experiments point to the need

for a theory that explicitly takes the shape factor (i.e., aspect ratio), particle-particle interactions, and particle distribution of the of the Nd-Fe-B platelet particles in the composites into account.

ACKNOWLEDGEMENTS

The financial support of the U. S. National Science Foundation through Grant No. DMR-9712688 is gratefully acknowledged. We are particularly grateful to Arnold Engineering Company, Phillips Petroleum Company, and Ames Laboratory without whose collaboration and support this work would have been impossible.

REFERENCES

1. S. Bullen, Engineering Materials & Design, p.18 (1988).

2. J. Ormerod and S. Constantinides, J. Appl. Phys. **81**, 4816 (1997).

3. J. Xiao, J. U. Otaigbe, and D.C. Jiles, J. Magn. Mag. Mater., **218**, 60 (2000).

4. J. U. Otaigbe, H. S. Kim, and J. Xiao, Polym. Comp., **20**(5), 697, (1999).

5. J. U. Otaigbe, J. Xiao, and S. Constantinides, J. Mat. Sci. Letters, **18**(4), 329 (1999).

6. A. Einstein, Investigations on the Theory of the Brownian Movement, edited by R. Furth, Dover, New York, (1956).

7. G. K. Batchelor, J. Fluid Mech., **83**, 97 (1977).

8. D. C. H. Cheng, Powd. Tech., 37, 255 (1984).

9. J. C. van der Werff and C. G. De Kruif, J. Rheol., **33**(3), 421 (1989).

10. H. A. Barnes, J. Rheol., **33**, 329 (1989).

11. A. A. Zaman and B. M. Moudgil, J. Rheol., **42**(1), 21 (1998).

12. A. J. Polinski, M. E. Ryan, P. K. Gupta, S. G. Seshadri, and F. J. Frechette, J. Rheol., **32**, 751 (1988).

13. R. F. Probstein, M. Z. Sengun, and T. C. Tseng, J. Rheol., **38**, 811 (1994).

14. J. B. Jansma and S. Qutubuddin, J. Rheol., **39**(1), 161 (1995).

15. K. Sweeny and R. Geckler, J. Appl. Phys., **25**, 1135 (1954).

16. J. Xiao and J. U. Otaigbe, J. Alloys & Compds, **309**, 100 (2000)

17. A. Romo-Uribe, T. J. Lemmon, and A. H. Windle, J. Rheol., **41**(5), 1117 (1997).

18. D. Dutta, R. A. Weiss, and K. W. Kristal, SPE ANTEC Tech Papers, **33**, 924 (1991).

19. C. W. Macosko, Rheology Principles, Measurements, and Applications, Wiley-VCH New York (1994).

20. I. M. Krieger and T. J. Dougherty, J. Rheol., **3**, 137 (1959).

21. R. J. Farris, J. Rheol., **12**(2), 281 (1968).

22. J. A. Mangels and R. M. Williams, Cer. Bulletin, **62**, No. 5, 601 (1983).

23. A. B. Metzner, J. Rheol., **29**(6), 739 (1985).

24. S. C. Goto and H. Kuno, J. Rheol., **28**, 197 (1984).

25. A. P. Shapiro and R. F. Probstein, Phys. Rev. Lett., **68**, 1422 (1992).

26. Ticona Plastics Product Information Sheet of Vectra A950, Stock Number VB0067.

27. J. Geibel, private communication, Philips Petroleum Company, Bartlesville, OK (2000).

28. Y. Cohen and A. B. Metzner, AICHE Journal, **27**, 705 (1981).

29. F. Gadala-Maria and A. Acrivos, J. Rheol., **24**, 799 (1980).

30. D. I. Lee, J. Rheol., **13**(2), 273 (1969).

31. J. G. Brodnyan, J. Rheol., **3**, 61 (1959).

32. M. Bousmina, A. Ait-Kadi, and J. B. Faisant, J. Rheol., **43**(2), 415 (1999).

33. R. Rothon, Adv. Polym. Sci., **139**, 67 (1999).

34. S. J. Stedman, J. R. G. Evans, and J. Woodthorpe, J. Mater. Sci., **25**, 1833 (1990).

35. J. S. Chong, E. B. Christiansen, and A. D. Baer, J. Appl. Polym. Sci., **15**, 2007 (1971).

36. R. Rothon, Particulate-Filled Polymer Composites, Longman Scientific & Technical, Essex, UK (1995).

37. M. J. Edirisinghe. and J. R. G. Evans, Int. J. High Technology Ceramics, **2**, 1 (1986).

38. J. P. Ibar, SPE ANTEC Tech. Papers, **45**, 1900 (1999).

39. P. D. Frayer and P. J. Huspeni, J. Rheol., **34**, 1199 (1999).

40. Y. G. Lin and H. H. Winter, Macromolecules, **21**(8), 2439 (1988).

41. Y. G. Lin and H. H. Winter, Macromolecules, **24**, 2877 (1991).

42. F. N. Cogswell, U.S. Patent No. 4386174 (1983).

43. W. N. Kim and Denn, M. M., J. Rheol., **36**(8), 1477 (1992).

44. C. Whitehouse, H. Lu, and P. Gao, Polym. Eng. and Sci., **37**, 1944 (1997).

45. K. Geiger, Abstracts of the 6th Annual Meeting, The Polymer Processing Society, Paper 10-09, (1990)

46. K. F. Wissbrun, J. Rheol., **37**(5), 777 (1993).

47. T. S. R. Al-Hadithi, H. A. Barnes, and K. Walters, Coll. Polym Sci., **270**(1), 40 (1992).

48. D. Doraiswamy, A. N. Mujumdar, I. Tsao, A. N. Beris, S. C. Danforth, and A. B. Metzner, J. Rheol., **35**(4), 647 (1991).

49. J. Jancar, Adv. Polym. Sci., **139**, 1 (1999).

50. P. C. Guschl, *M.S. Thesis*, Iowa State University (2000).

51. L. Nicodemo, L. Nicolais, and R. F. Landel, Chem. Eng. Sci., **29** (3), 729 (1974).

52. D. M. Bigg and R. G. Barry, SPE ANTEC Tech. Papers., **44**, 997 (1998).

LIST OF FIGURES

Figure 7. Graphical evaluation of maximum solids packing fraction at 320°C

Figure 8. Dynamic thermal stability analysis of PPS (PPS) in an air or nitrogen atmosphere at 280°C and 320°C

Figure 9. Dynamic thermal stability analysis of PPS (PPS) / LCP blends (1% - 10%) in a nitrogen atmosphere at 280°C

Figure 10. Dynamic thermal stability analysis of PPS (PPS) / MQP-B composites (5% and 10%) in an air or nitrogen atmosphere at 280°C

Figure 11. Effect on apparent viscosity of PPS (PPS) of the presence of LCP at the following concentrations: a) 0%, 5%, 10%, 15%, and 20% and b) 0%, 1%, 2%, 3%, 4%, and 5% LCP at 320°C (lines drawn through data points as guides for the reader)

Figure 12. Effects of particle dispersity and shear rates on apparent viscosity of the PPS (PPS) / MQP-B PBMs at 15% loading at 320°C

Figure 13. Calculated apparent viscosities showing dependence on particle size ratio for 50% loaded bimodal suspensions of MQP-B powder at 320°C in Haake Rheomix

Figure 14. Effect of LCP concentration in PPS (PPS) from ranges a) 0%-20% and b) 0%-5% on complex viscosity at three frequencies: 1, 10, 100 rad s^{-1} at 320°C and 10% strain in a nitrogen atmosphere

Figure 15. Effect of LCP concentration in PPS (PPS) from ranges a) 0%-20% and b) 0%-5% on steady shear viscosity at three shear rates: 1, 10, 100 s^{-1} at 320°C in a nitrogen atmosphere

Figure 16. Effect of LCP concentrations in PPS (PPS) on a) power law index and b) consistency factor at 320°C

Figure 17. The effect of MQP on the shear-thinning behavior of PPS (PPS) - LCP blend (85%-15%) at concentrations of 5%, 20%, 35%, 50%, 60%, 65%, 70% and 75% at 320°C. The MQP particles are unsieved in these cases

Figure 18. Particle size and dispersity effects on complex viscosity (320°C, 10% strain) (see Table 4 for guidance of the materials discussed in the text)

Table I. DSC runs performed on various PPS - LCP blends (100/0, 95/5, 90/10, 85/15 and 0/100) from 50°C to 400°C at 10°C min^{-1}

LCP Concentration (%)	Melt Temperature (C)	Area (mJ)	ΔH (J/g)	ΔH(norm) (J/g)
0	279.7	77.0	26.5	26.5
5	279.8	76.0	26.3	25.2
10	280.7	69.2	22.8	23.9
15	280.3	67.4	22.0	22.6
20	277.6	73.3	24.8	20.2
100	281.1	0.47	0.16	0.00

Table II. DSC runs performed on various PPS - MQP blends (100/0, 95/5, 90/10, and 85/15) from 50°C to 400°C at 10°C min^{-1}

MQP Concentration (%)	Melt Temperature (C)	Area (mJ)	ΔH (J/g)	ΔH(norm) (J/g)
0	279.7	77.0	26.5	26.5
5	279.2	77.7	25.3	25.2
10	280.7	50.7	17.3	23.9
15	278.1	44.8	14.6	22.6

Table III. Experimental viscosities using Equation (3) and calculated viscosities of the following equations with regressed parameter values

	$\dot{\gamma}$ = 1.05 rad s^{-1}	$\dot{\gamma}$ = 3.14 rad s^{-1}	$\dot{\gamma}$ = 5.24 rad s^{-1}	Monodispersed Spheres
Maron & Pierce [Eq. 3] $\eta_r = A\left[1-\left(\frac{\phi}{\phi_m}\right)\right]^{-2}$	A	A	A	A
	1.506	3.284	2.090	1.300
	ϕ_m	ϕ_m	ϕ_m	ϕ_m
	0.864	1.000	1.000	0.680
Krieger & Dougherty [Eq. 4] $\eta_r = \left[1-\left(\frac{\phi}{\phi_m}\right)\right]^{-[\eta]\phi_m}$	[η]	[η]	[η]	[η]
	2.796	2.904	2.523	2.500
	ϕ_m	ϕ_m	ϕ_m	ϕ_m
	0.905	1.000	1.000	0.680
Thomas [Eq. 5] $\eta_r = 1+2.5\phi+10.05\phi^2+A\exp(B\phi)$	A(10^{-4})	A(10^{-4})	A(10^{-4})	A(10^{-4})
	3.6	2950	1.3	27.3
	B	B	B	B
	16.37	6.63	16.06	16.60
Eilers [Eq. 6] $\eta_r = \left\langle 1+\frac{1.25\phi}{\left[1-\left(\frac{\phi}{\phi_m}\right)\right]}\right\rangle^2$	ϕ_m	ϕ_m	ϕ_m	ϕ_m
	0.844	0.879	0.942	0.680

Table IV. Particle configurations and average particle sizes of Nd-Fe-B powder in PPS-LCP matrix

Name	Modality	Particle Size Range (μm)	Average Particle Size (μm)
1mod150	1	106-150	128
2mod150A	2	38-75, 106-150	109.25
2mod150	2	75-106, 106-150	92.25
2mod212	2	106-150, 150-212	154.5
2mod300A	2	38-75, 212-300	192
2mod300	2	106-150, 212-300	156.25
3mod150	3	38-75, 75-106, 106-150	91.67
3mod300	3	38-75, 106-150, 212-300	121.83

Guschl and Otaigbe, Figure 1

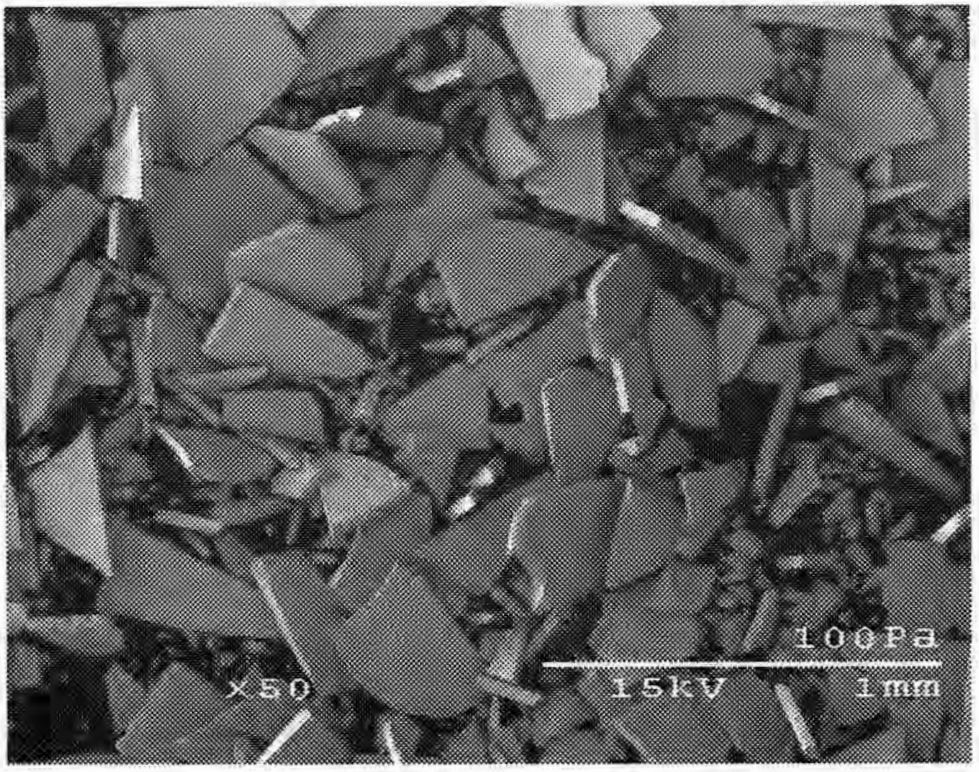

Guschl and Otaigbe, Figure 2

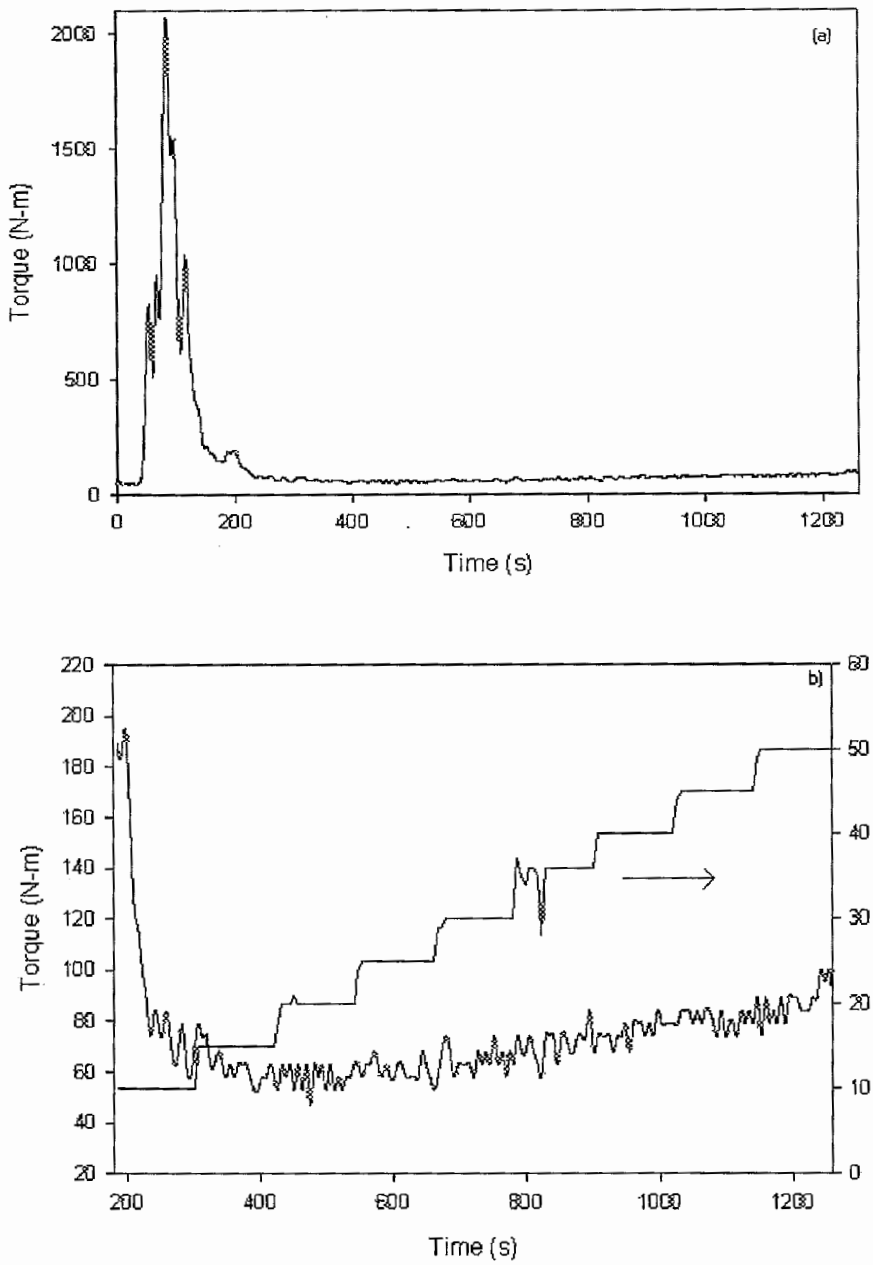

Guschl and Otaigbe, Figure 3

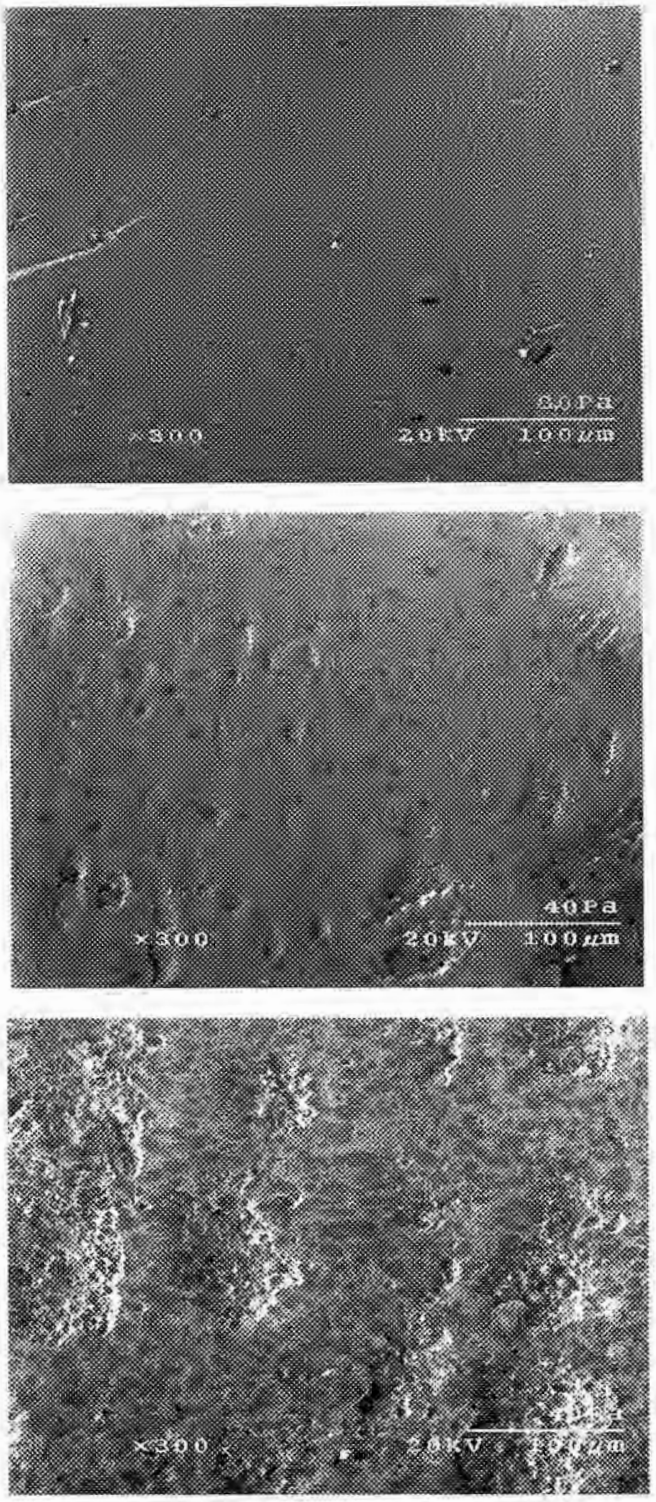

Guschl and Otaigbe, Figure 4

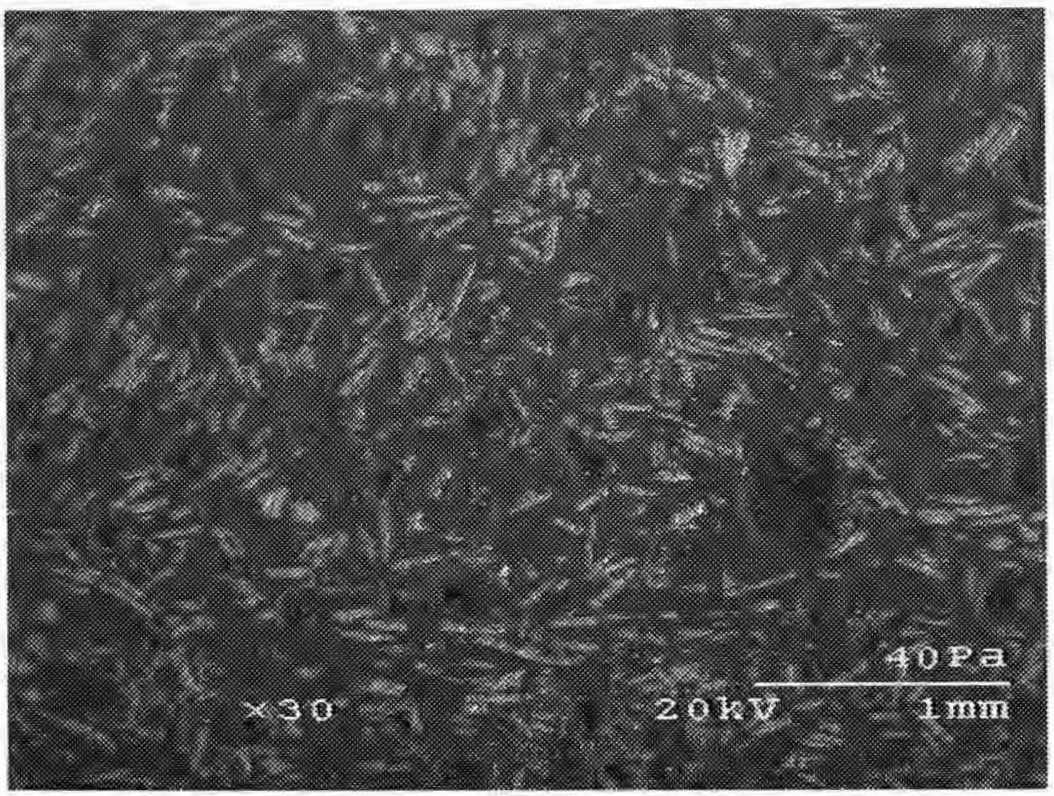

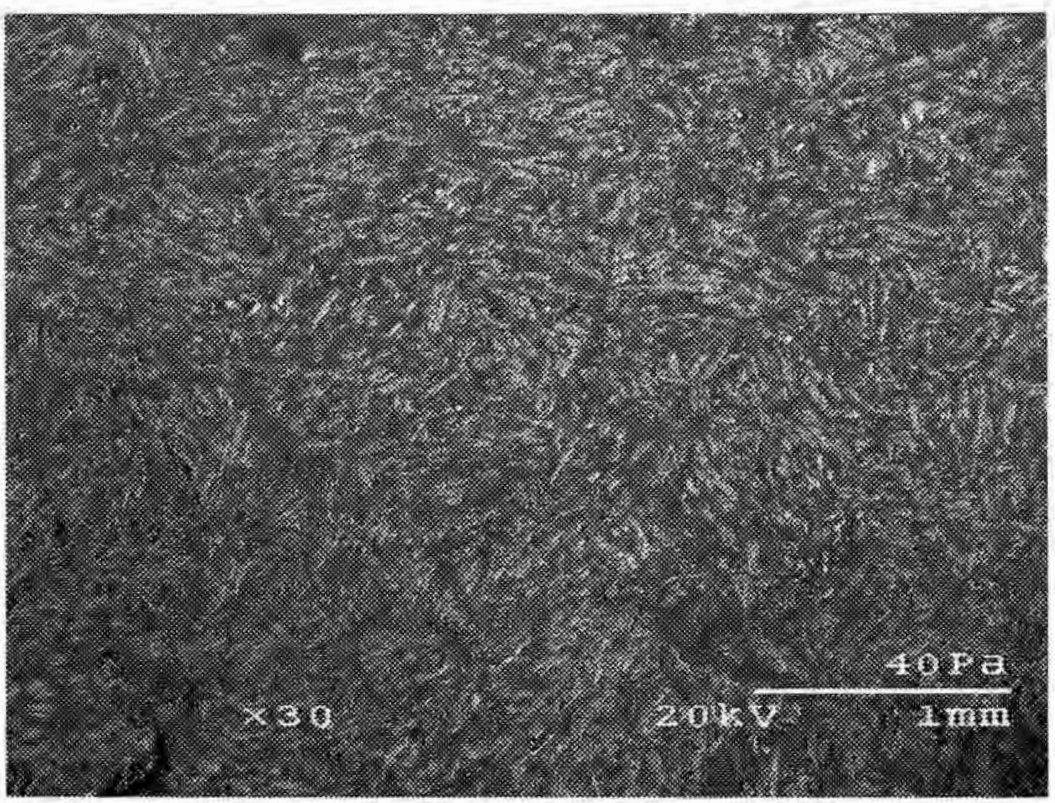

Guschl and Otaigbe, Figure 5

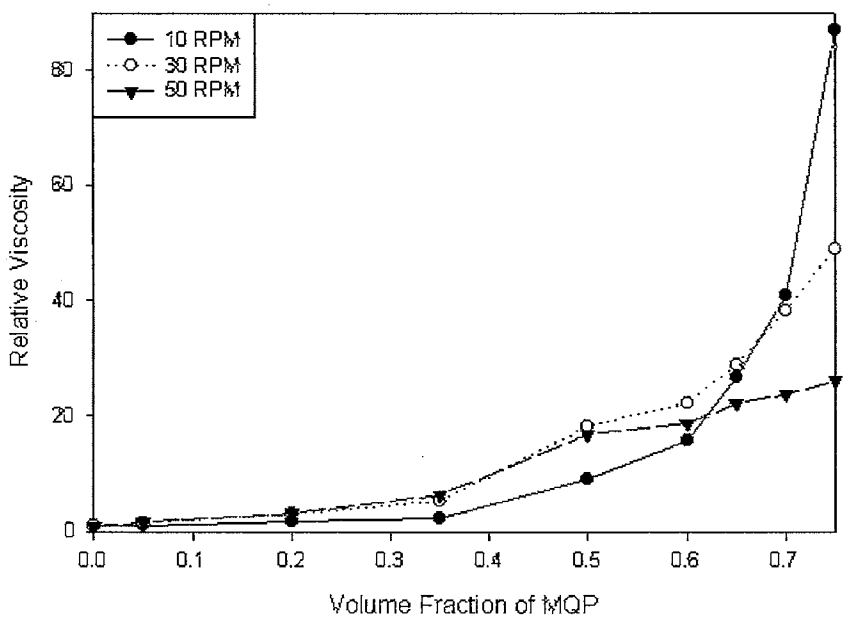

Guschl and Otaigbe, Figure 6

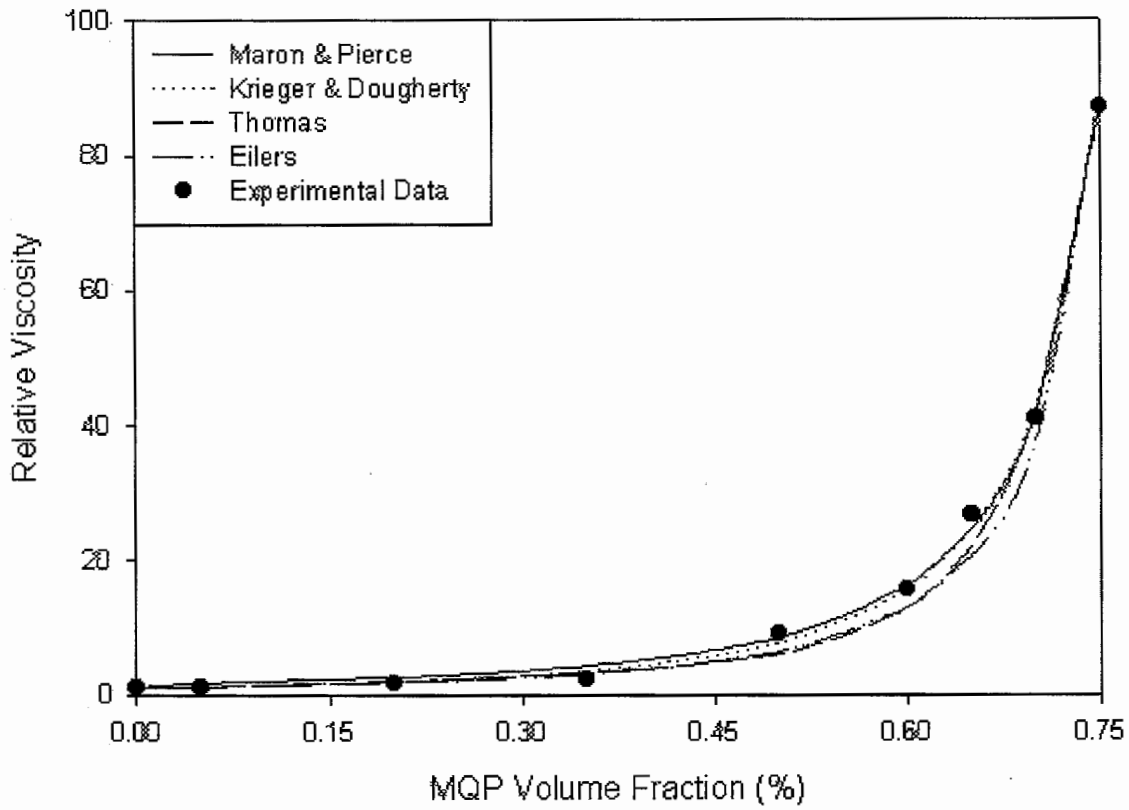

Guschl and Otaigbe, Figure 7

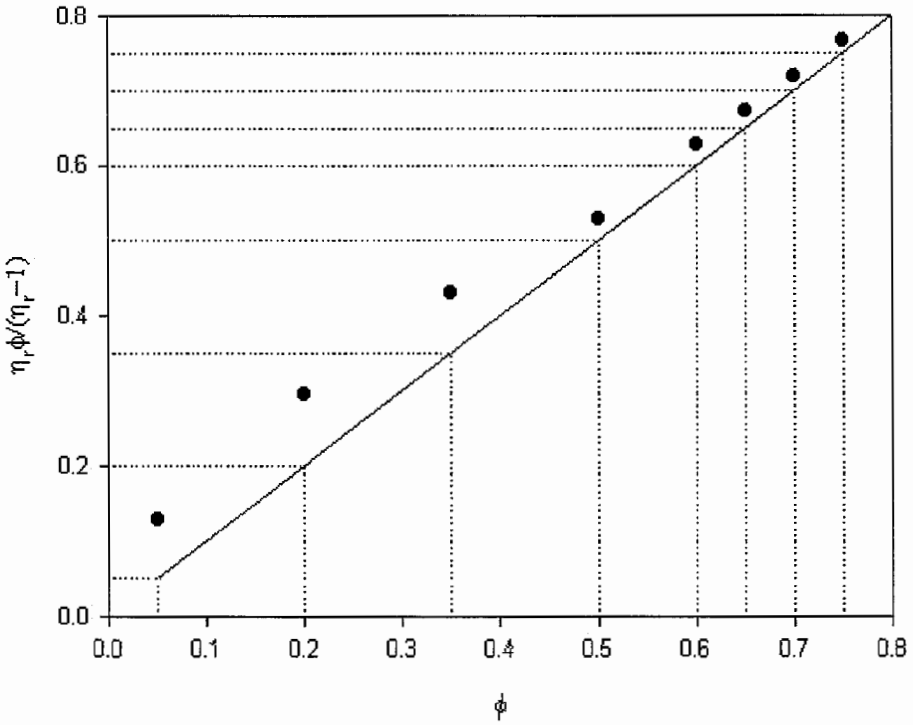

Guschl and Otaigbe, Figure 8

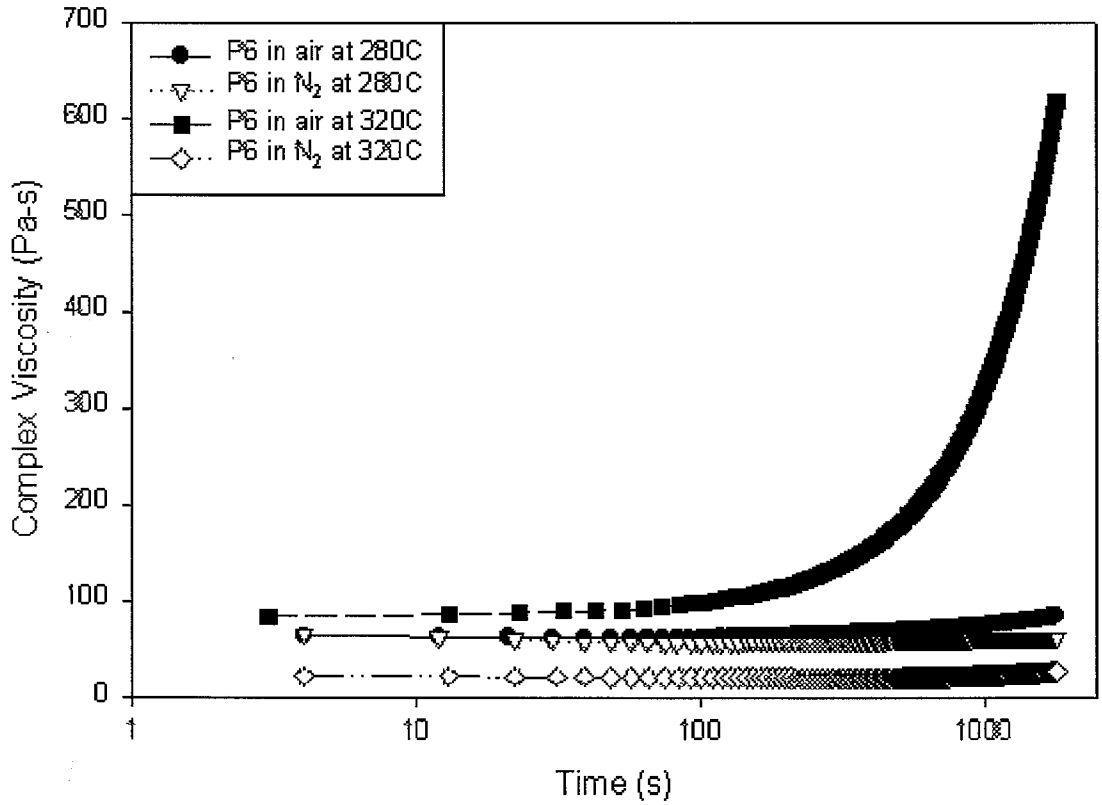

Guschl and Otaigbe, Figure 9

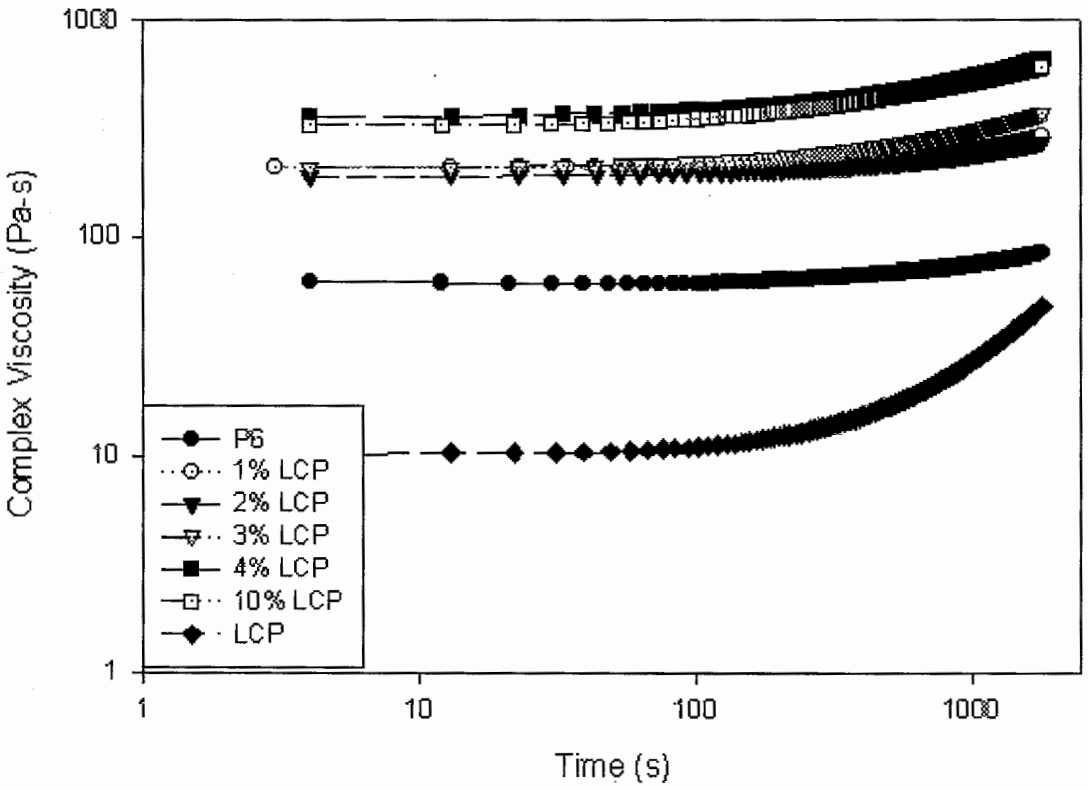

Guschl and Otaigbe, Figure 10

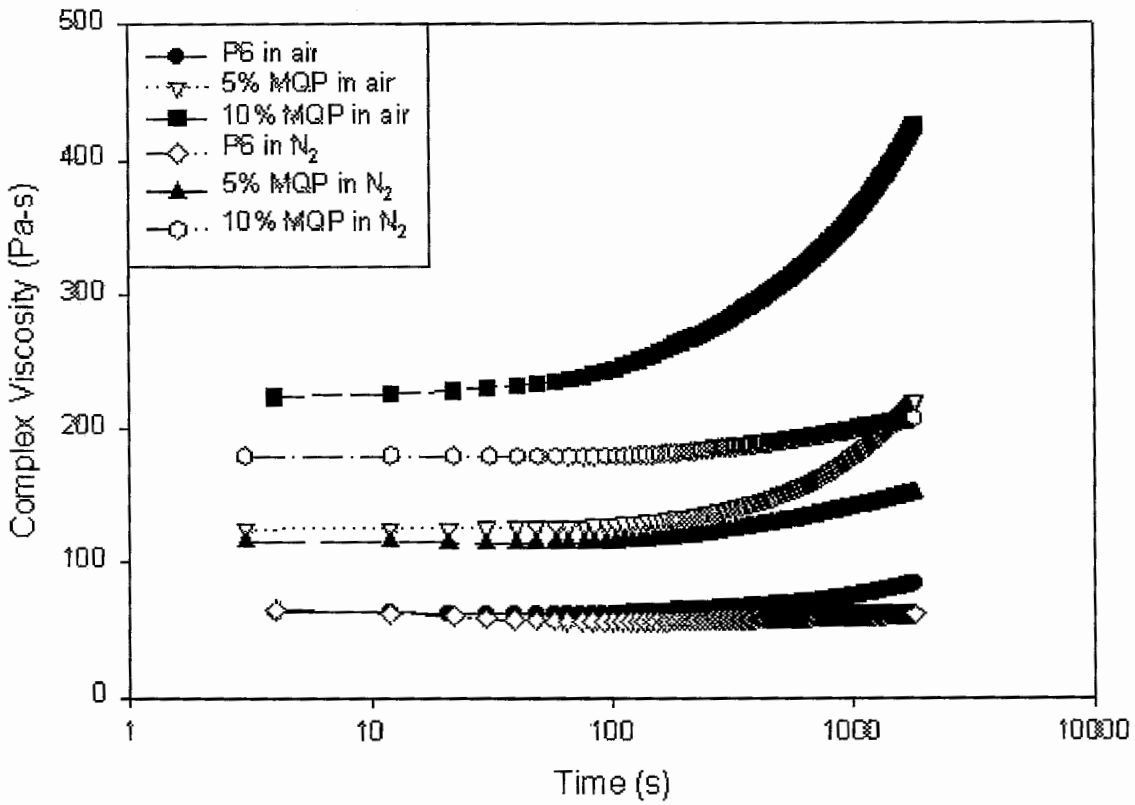

Guschl and Otaigbe, Figure 11

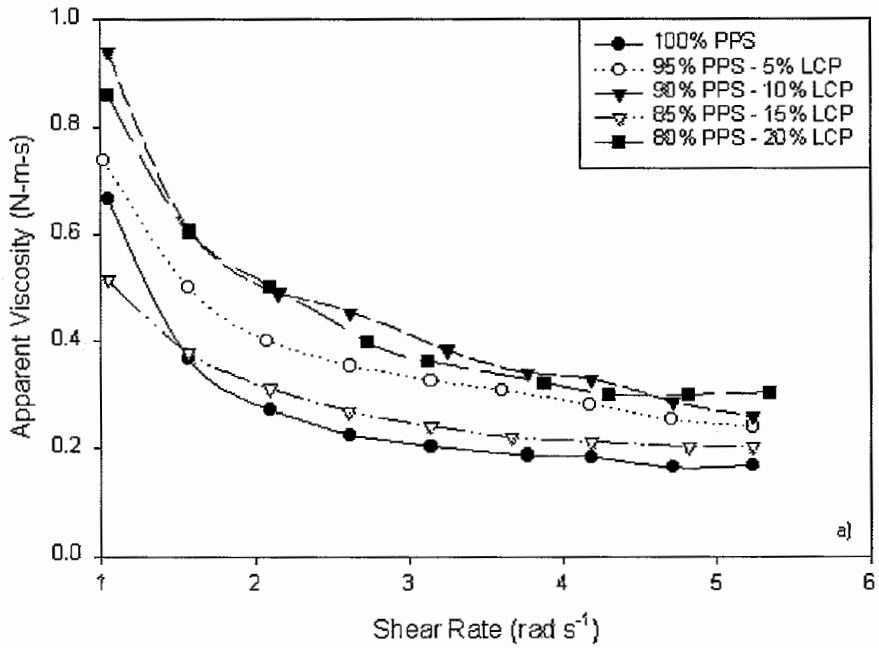

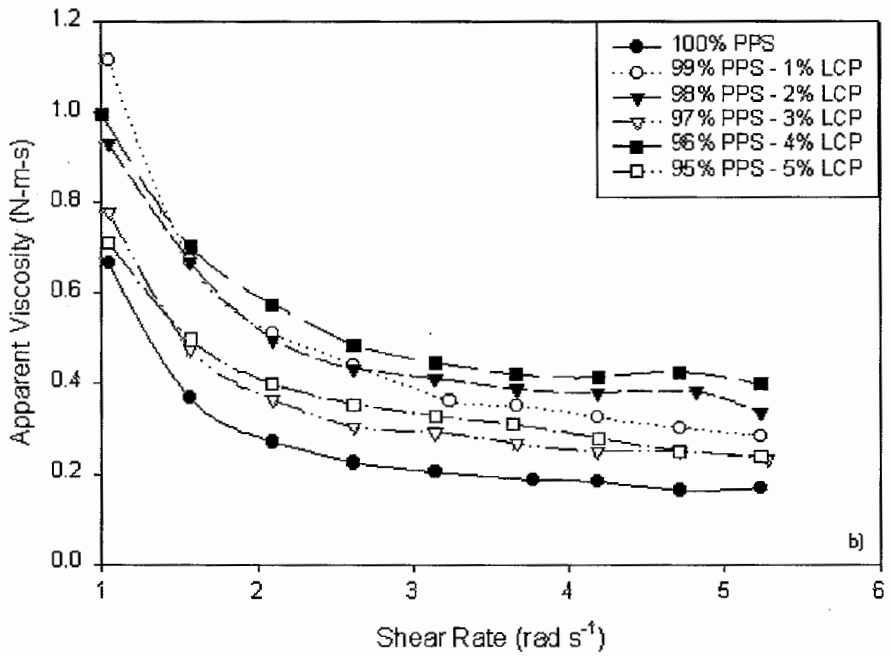

Guschl and Otaigbe, Figure 12

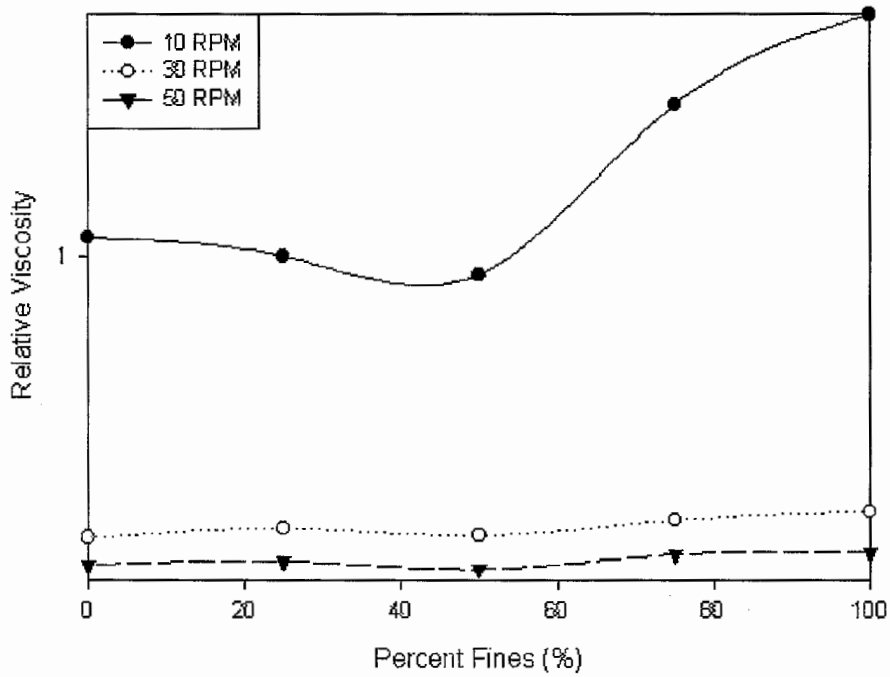

Guschl and Otaigbe, Figure 13

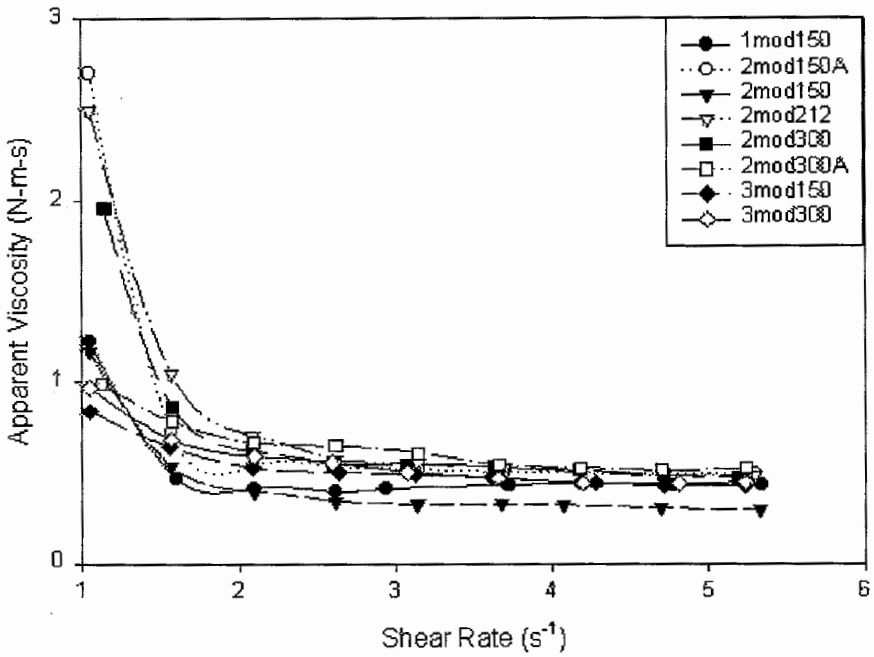

Guschl and Otaigbe, Figure 14

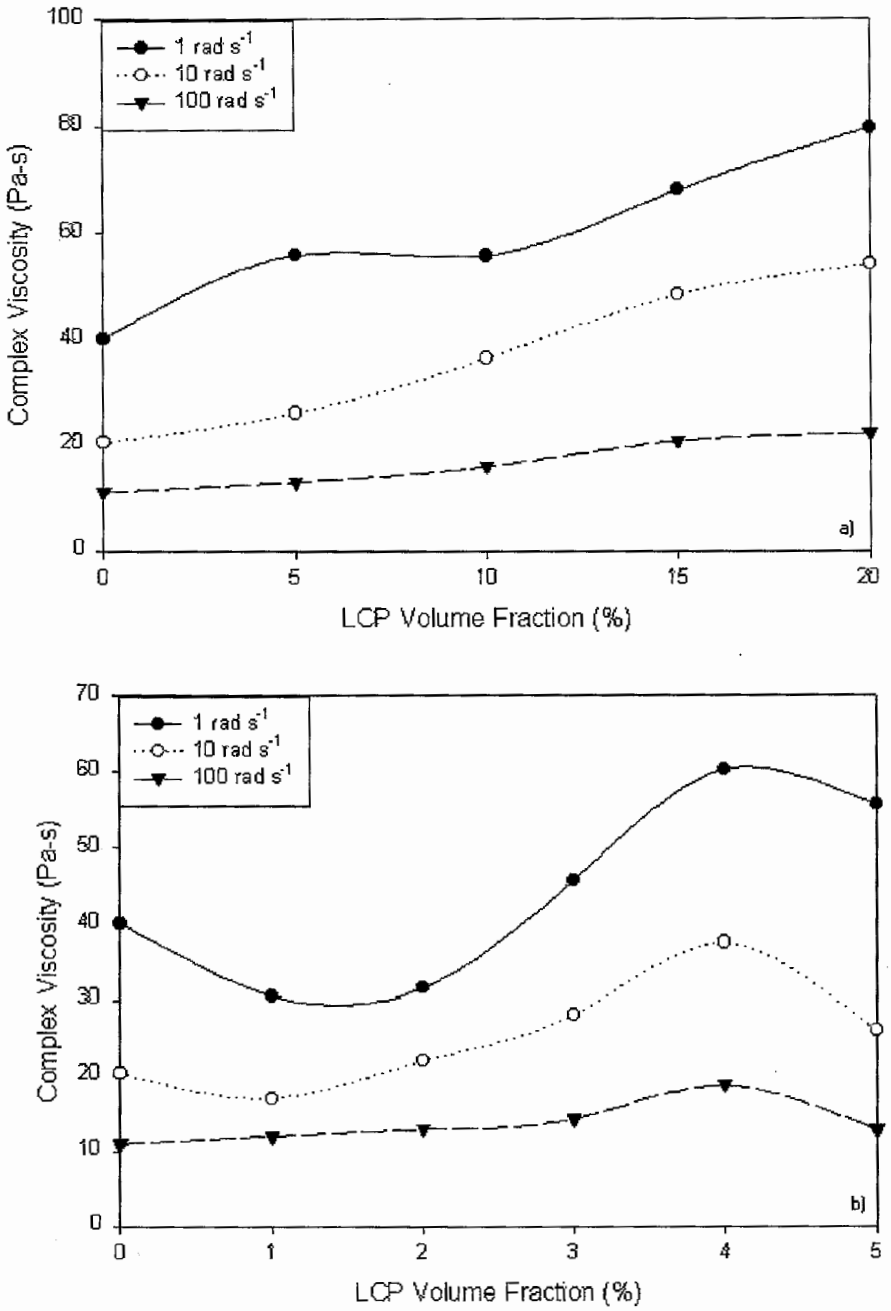

Guschl and Otaigbe, Figure 15

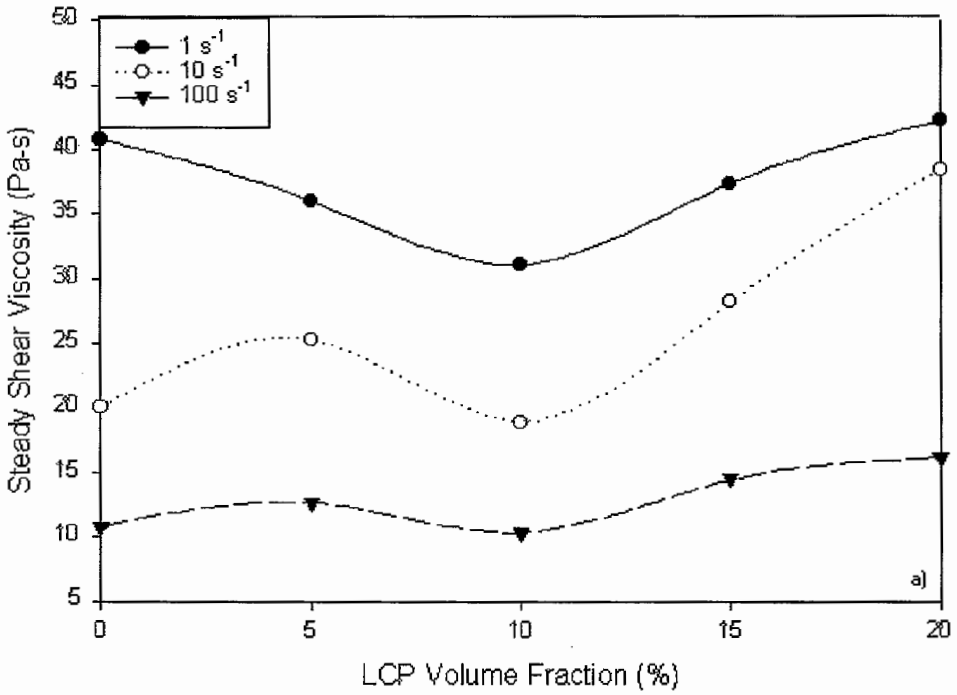

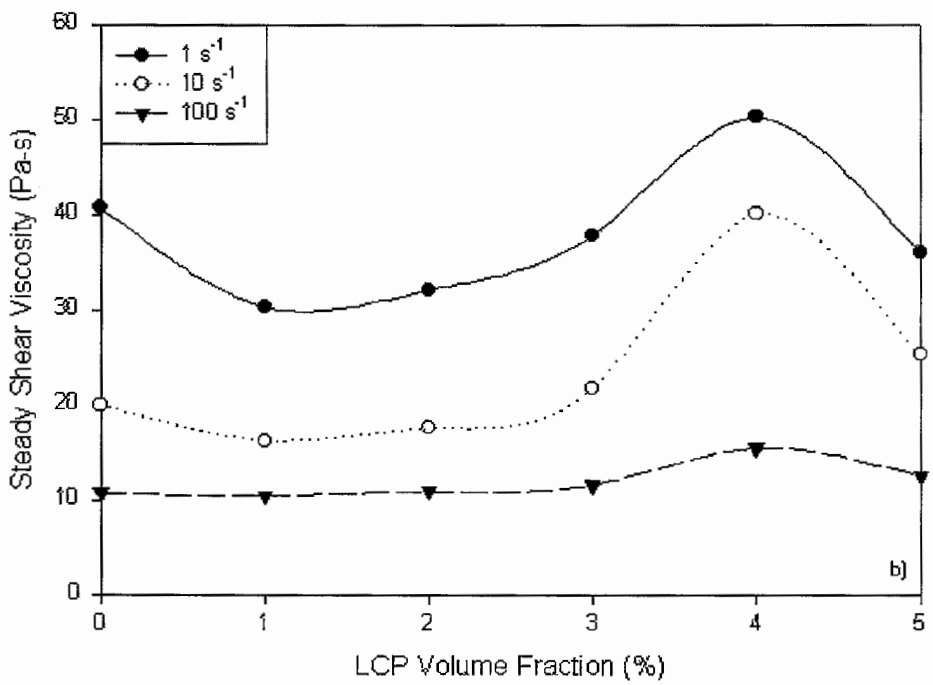

Guschl and Otaigbe, Figure 16

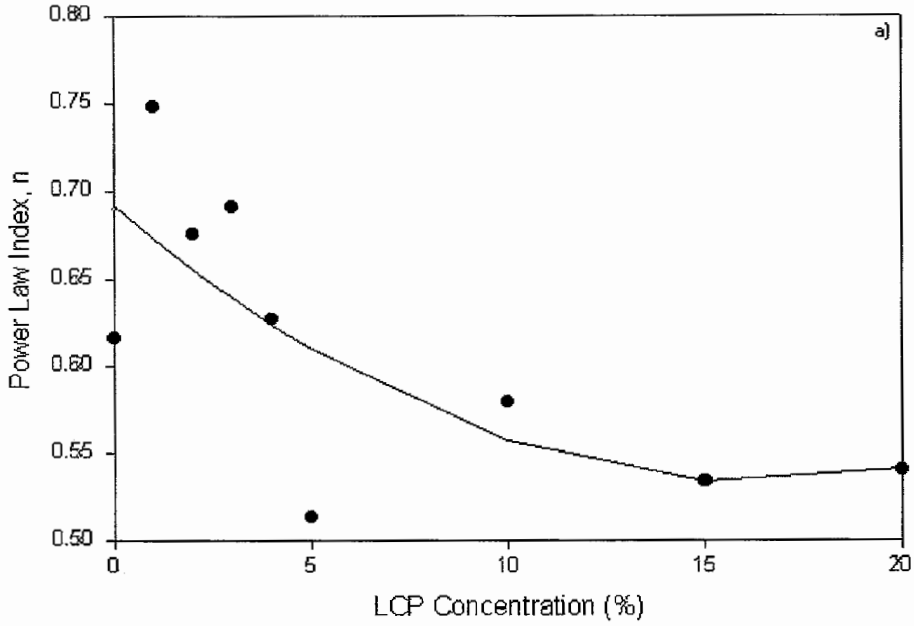

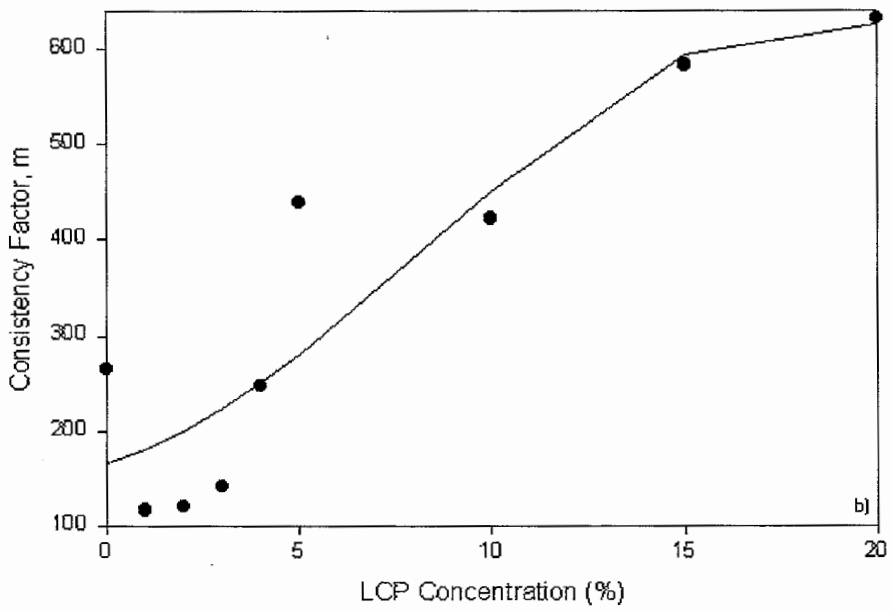

Guschl and Otaigbe, Figure 17

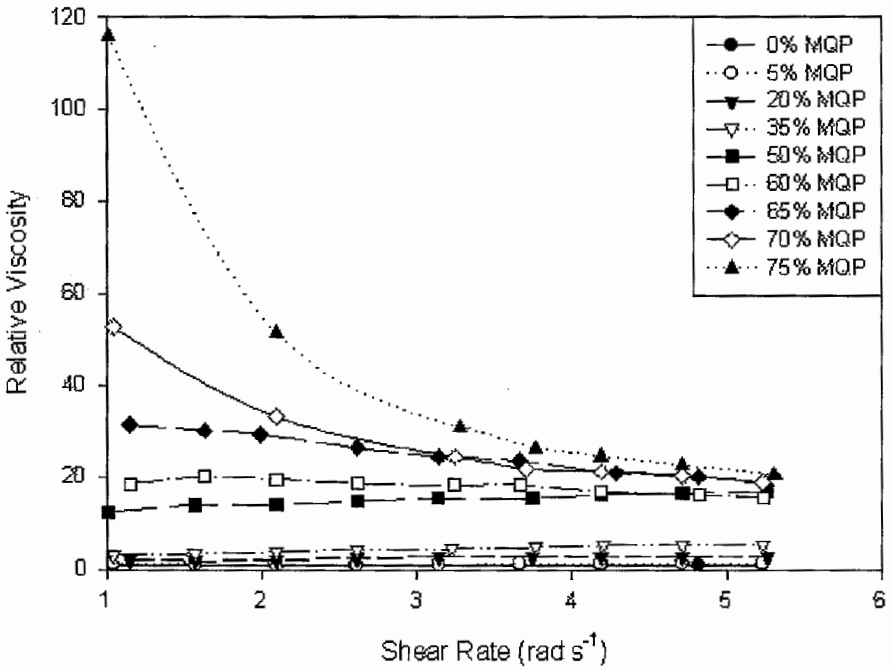

Guschl and Otaigbe, Figure 18

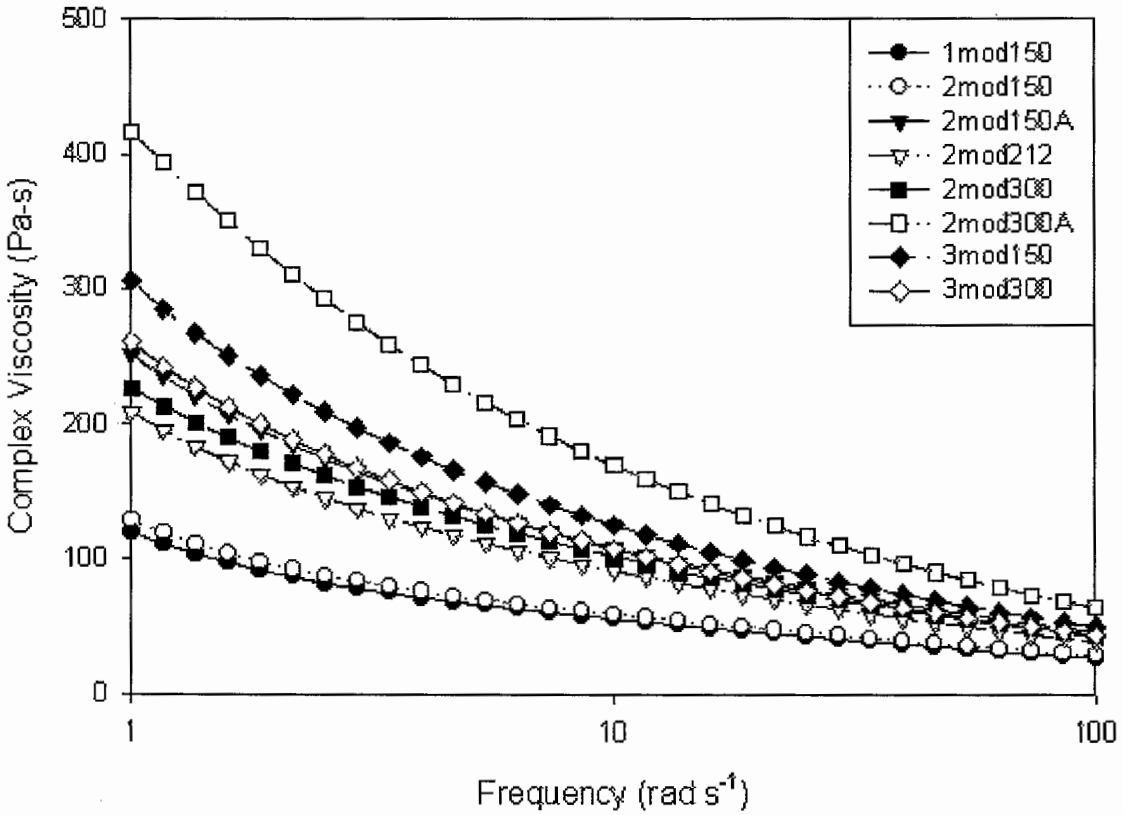

CHAPTER 3. EFFECTS OF A Nd-Fe-B MAGNETIC FILLER ON THE CRYSTALLIZATION OF POLY (PHENYLENE SULFIDE)

A paper submitted to the *Journal of Applied Polymer Science*

Peter C. Guschl, Hyun Seog Kim, and Joshua Otaigbe

SYNOPSIS

The crystallization of poly (phenylene sulfide) (PPS) in a polymer-magnetic powder suspension was studied. Isothermal crystallization behavior was analyzed by way of differential scanning calorimetry (DSC), and the kinetics were described via the Johnson-Mehl-Avrami (JMA) equation. The major effects of particle size and the presence of a coupling agent coated on the filler particles on the crystallization kinetics was the variability upon the JMA parameters and the crystallization times. Smaller particles exhibited longer induction and half times, whereas the larger particles tended to have shorter crystallization times. Particles ranging fro 38 to 150 appeared to have similar crystallization times and no significant change in value of JMA index with melt crystallization temperature. As a result of the analyses, the dynamic mechanical properties were determined, linking together the fundamental polymer characteristics of crystallinity and the physical properties of the PPS binder. The enhancement of the wetting of the filler to the binder was promoted through the coupling agent. The storage modulus was generally decreased due to the smaller particles and the lack of coupling agent. Conversely, the loss modulus was enhanced due to the smaller particles and presence of coupling agent.

KEYWORDS: polymer crystallinity, magnetic filler, dynamic mechanical property, silane coupling agent, polymer bonded magnets

1. INTRODUCTION

Poly (phenylene sulfide) (PPS) has been known as a high performance, engineering thermoplastic that can operate at high temperatures (1,2). However, due to its low impact strength PPS has been considered inappropriate for such applications requiring high strength materials. It has been discovered that PPS composites have quite a substantial strength, though, (3) especially in polymer bonded magnet (PBM) systems such as ours. Due to the semi-crystallinity of PPS, it is believed that enhanced crystallization of the polymer at the binder-filler interfaces creates reinforcement sites. Thus, it is essential to understand the crystallization behavior of the system so that comprehension of the mechanical properties of these composites can be attained.

Because of their advantages such as low weight, resistance to corrosion and ease of machining, PBMs have been recognized as a practical material for many electromechanical capabilities. For better thermal stability and enhanced performance of the PBMs, a high temperature coating, silane-coupling agent is employed, allowing better wetting between the binder and filler as well as proper oxidative shielding (4,5). Previous studies have investigated the rheological consequences due to the variation of the particle sizes and the presence of this coupling agent (6), as well as other additives, such as liquid crystalline polymers, introduced into the composite system (7).

The presence of filler in a semi-crystalline polymer can cause many changes to the physical properties of the polymer. Some of these typical changes are total degree of

crystallinity, crystal phase and its orientation, number and size of crystalline particles, and the type of crystalline particle (8). The surface of the filler particles acts as an active site on which the polymer chains can easily adhere, allowing other chains to initiate an ordered crystalline structure around the particle. Various particle sizes and distributions can offer different surface energies in which the crystallization can occur. Coupling agent promotes a change of interfacial properties of the filler particles, giving rise to better wetting between the filler and binder and ultimately increased physical strength of the composite (8-10). This study offers an investigation of these particle sizes and a coupling agent and how they affect the characteristics of crystallinity of PPS. The crystallinity of a polymer composite/blend is an important property in terms of the physical strength and morphology of the material. Enhanced crystallinity underscores the consistency and ultimately the flow properties of the composite under high loadings of filler.

2. EXPERIMENTAL

2.1 Materials

Phillips Chemical Company provided the poly (phenylene sulfide) grade - Ryton Type P6. The P6 has been cured at a temperature below its melting point. The average molecular weight value of the P6 is difficult to obtain and estimate due to its synthesis conditions. The density, melting point, and glass transition temperature of the PPS grade is approximately 1.36 g cm^{-3}, 285°C, and 90°C, respectively.

The magnetic powder, manufactured by Magnequench, consists of varying particle sizes of a neodymium-iron-boron alloy ($Nd_2Fe_{14}B$) that are produced in platelet form. Specifically, the commercial powder used is MQP-O and has a density of 7.61 g cm^{-3} and

Curie temperature of 299°C, respectively. The particle sizes utilized in these experiments ranged from 38-300 μm, separated into five particle size fractions corresponding to the sieve plates used: 38-75 μm, 75-106 μm, 106-150 μm, 150-212 μm, and 212-300 μm. The aspect ratio of the MQP powder was determined to be within the range of 0.2 to 10 (6).

In order to prevent oxidation and to sustain the coupling effect between the polymer binder and magnetic powder, 3-aminopropyltriethoxy silane (A1100, Huls) was used. The MQP-O powders were treated with this coupling agent through simple immersion in an aqueous solution (1 wt.% silane). To enhance the wetting of the coupling agent to the powders, we utilized an ultrasonic homogenizer to the powder/silane mixture for a period of five minutes. After the silane treatment, the excess solution was decanted and the powder was dried at 80°C in a vacuum oven (Model 5861). This method was found to produce the coupled MQP-O powders with reproducible results.

The desired amounts of the coupled powder were hand-mixed with the PPS in a plastic bag prior to compression molding and Haake Rheomix 600 mixing. Rectangular plates (60 mm x 60 mm x 1.2 mm) were compression-molded under a pressure of 7 MPa at 290°C, held for 10 minutes, and allowed to cool in air to ambient temperature under the same pressure. Thin rectangular bars (18 mm x 1.5 mm x 1 mm) were produced in order to perform dynamical mechanical measurements, whereas small pieces were taken for the crystallization kinetic study.

2.2 Differential Scanning Calorimetry

A differential scanning calorimeter (DSC Pyris 1, Perkin-Elmer thermal analysis system) was used to determine the crystallization behavior of our samples. The sample was

cooled rapidly from above its melting point to a particular melt crystallization temperature, and then the crystallization was measured under isothermal conditions. Scanning an indium metal standard at 10°C min^{-1} checks the accuracy of the experiments. For the isothermal kinetics study, 10.0 ± 1.0 mg samples were crimped in an aluminum pan and heated from ambient temperature to 320°C at a rate of 10°C min^{-1} in a nitrogen atmosphere. The samples were held at this temperature for 10 minutes in order to ensure a total melting of the crystals within the polymer. Four crystallization temperatures, 245, 250, 255, and 260°C, were selected for the isothermal kinetic runs, and the samples were quenched to each isothermal temperature from the holding temperature.

2.3 Dynamic Mechanical Analysis (DMA)

Rectangular DMA test specimens [dimensions stated in Materials section (2.1)] were cut from the compression molded samples using a slow-speed cutter. A dynamic mechanical analyzer (Perkin-Elmer DMA 7) was used to perform the testing through a three-point bend configuration; using a specimen span length of 15 mm. Storage (E') and loss (E'') moduli were measured at a frequency of 1 Hz. Temperatures were scanned for each sample at a rate of 2°C min^{-1} from 50°C to 220°C. E' linearity was maintained at stress levels producing a displacement amplitude of 30 microns. Confirmation of this linearity was performed through stress scan experiments run at a constant rate of 2 mN min^{-1}, a frequency of 1 Hz, and a temperature of 25°C. Linearity was assumed to hold for different values determined at the higher temperatures tested.

3. RESULTS AND DISCUSSION

3.1 Isothermal Crystallization Behavior

In order to describe the kinetics of the crystallization behavior, the Johnson-Mehl-Avrami (JMA) equation, also known as the "stretched exponential" equation, was employed, revealing the relationship between the degree of crystallization, X, and time, t.

$$X(t,T) = 1 - \exp(-kt^n) \quad (1)$$

The k and n parameters are constants, where k contains several material constants and is defined as the propagation rate constant of the crystal, and n is a number that depends upon the geometry of the growth process. X is defined as the time- and temperature-dependent ratio of the crystallized mass to the original amorphous polymer mass. Avrami has treated intermediate heterogeneous nucleation cases in which the rate of nucleation decreases exponentially with time (3). The results show that the JMA index represented a greater dimensionality in the growth process (see Table 1) (11).

For the isothermal kinetics studies, pure PPS was observed on the temperature range of 230 to 265°C. It was noticed that in experiments below 240°C, crystallization was too fast to measure accurately, and above 265°C, the crystallization was too slow. However, stable thermograms were observed for the following temperatures: 245, 250, 255, and 260°C. The results of the thermogram data (see Figure 1) reveal that the time needed for the crystallization peak to develop is a strong function of temperature such that at higher temperatures more crystallization time is required. The higher degree of thermal energy that the material possesses at the larger melt crystallization temperatures inhibits the growth of structured formations of crystals. Once enough energy has dissipated after the quenching and

subsequent cooling, crystal growth increases. Analysis of the relative crystallinity at each temperature was performed through the division of the area of the crystallization peak at various times by the value of theoretical heat of melting over the entire thermogram area, represented by the following equation (12).

$$X_c = \frac{\int_0^t (dH/dT)dT}{\int_0^\infty (dH/dT)dT} \tag{2}$$

The JMA analysis of this data for relative crystallinity is represented in Figure 2. Through application of the JMA equation on the partially integrated heat flow changes during isothermal crystallization, the JMA parameters could be determined. Rearrangement of Equation (1) by applying a double logarithm to both sides of the equation yields a linear form with variables $\ln[-\ln(1-X)]$ and $\ln t$ and slope n and intercept $\ln k$. With these results the JMA parameters appear to be either strong or weak functions of temperature. The JMA index n increases for the neat PPS samples and decreases weakly with temperature, but it appears to lessen as the coupling agent is employed (see Figure 3). The rate constant k decreases significantly as the temperature increases (not shown). Minkova *et. al.* (13) confirm these observations of the JMA parameters with crystallization temperature as they performed their melt crystallization procedure on PPS from 200 – 240°C. The neat PPS and uncoated composite of MQP-O/PPS showed indices in between 4.0 and 2.5 as the temperature was increased. The coated composite, however, exhibited a smaller range of 2.5 to 2.0. With these results the crystal growth mechanism and nucleation type were changed due to the addition of the coupling agent [see Table 1 (11)].

Once information regarding the *k* and *n* parameters was known, then the half time of the crystal growth was determined. This is the time required to obtain a relative crystallinity of 50% (X = 0.5). Applying this value to Equation (1) gives the following equation:

$$t_{1/2} = \left(\frac{\ln 2}{k}\right)^{1/n} \qquad (2)$$

Figure 4 represents how fast the crystallization of the neat PPS, uncoated and coated MQP-O/PPS suspension systems grow with temperature. Strong polymer-filler attractive forces can explain the general rise in half time with crystallization temperature. Kowalewski and Galeski (4) claim that these interactions would slow down the growth rate of crystallization by acting as hindrances for the transport of polymer molecules to the active crystallization sites. The presence of the powder and coupling agent seems to accelerate the crystallization of the suspension, especially when present at lower melt crystallization temperatures. This observation can be explained as an adhesion effect of the coupling agent to the filler particles that provides nucleation enhancements of the semi-crystalline binder (14). The enhancement of nucleation can be attributed to an increase in the number of active nucleation sites on the surface of the filler particles. Such results suggest that there are no strong interactions between the PPS and MQP filler.

The effect of particle size on the crystallization behavior was also investigated. Figures 5 and 6 show the relationships of the JMA index and half time on crystallization temperature for the different particle sizes, respectively. It appears that the monodispersed composite of average particle size 128 microns (106 – 150 micron range) yielded the lowest index range that did not change much with temperature. The mixture of particles of each size (polydispersed) showed the largest drop in index value from about 3.3 to 2.4. The size is an

important factor regarding the surface energy of the particles. As this changes the interaction behavior of the components of the suspension, the filler and polymer, is be altered (14).

Calculation of the crystallization induction time was graphically determined through a linear extrapolation method, since direct calculation was not possible through use of the JMA equation. Figure 7 represents a graph of relative crystallinity versus the crystallization time. The induction of crystallization can be found by determining the line tangent to the curve during the rise in relative crystallinity. Extrapolating back to the initial relative crystallinity value allows one to evaluate the induction time. Figure 8 reveals the trend of induction time with crystallization temperature and how it is affected by the presence of the filler particles and coupling agent. Apparently, the MQP powder instigates a shorter induction period for the polymer crystals to grow. The coupling agent contracts this induction time further. Similar trends were observed regarding the half time versus temperature data in Figure 4; however, the induction times appeared to be more sensitive to the presence of filler and coupling agent. Also, the rise in induction time with temperature was not as drastic as the samples containing filler and coupling agent. In regards to particle size, the induction time (shown in Figure 9) behaved similarly to that of the half time. Larger particles induce a quicker crystallization, specifically those in the 106-150 micron range, in terms of both half and induction time. Furthermore, the unimodal systems of finer particles (i.e. less than 38 microns) tended to have slower induction times.

3.2 Dynamic Mechanical Analysis

The mechanical properties of the filled polymeric composite were investigated, showing a significant improvement in the storage (elastic component) and loss (viscous component) moduli due to the presence of the coupling agent (Figure 10 & 11). The filler induced roughly a 33% increase in storage modulus of the neat PPS, initially at 40°C, whereas the coupling agent initiated an increase of about 56%. The reasons for these observations can be attributed to the effects of adhesion and nucleation enhancement between the filler and binder previously mentioned (14). Figure 12 represents the effect of three different particle sizes on the storage modulus and tan delta (ratio of loss to storage modulus). Essentially, the larger particles (> 150 microns) show at temperatures above the glass transition the highest storage modulus and lowest phase angle values. Because the presence of the filler and coupling agent strengthens the polymer (increasing storage modulus) and creates a more viscous material (increasing loss modulus) a change in phase angle was observed. The improved strength effect is larger than the increased viscosity effect for larger particles.

4. CONCLUSIONS

This paper has shown that the crystallization behavior of a semi-crystalline binder, PPS, was significantly changed due to the presence of an inorganic filler and a silane-coupling agent. It was observed that the MQP-O powder acted as a nucleation agent, initiating faster crystallization by reducing the half time and induction time of crystallization. Particle size did not appear to affect the crystallinity of the composite significantly, but small particles did exhibit the longest crystallization times. The JMA index, n, seemed to be at a

minimum for the 106-150 micron particle range and did not vary severely with crystallization temperature, much like the coated MQP particles. Large particles and coated particles, greater than 150 microns, seemed to have the highest storage modulus and the lowest loss angle, tan δ, for temperatures above the glass transition temperature. The presence of the particles in a mixture of different sizes did not appear to affect the crystallization behavior significantly; however, the largest change in the JMA index *n* was observed for this particle configuration. The coupling agent further enhances this crystallization via improved wetting between the particle and polymer chains. The net effect of this faster growth causes an internal strengthening to occur within the composite, giving rise to an increased storage modulus and improvement in mechanical properties.

ACKNOWLEDGEMENTS

The financial support from the U. S. National Science Foundation through Grant No. DMR-9712688 is highly appreciated. We are particularly grateful to Group Arnold and Mr. Steve Constantinides, without whose collaboration this work would have been impossible.

REFERENCES

1. Wayne, H.; Brady, D. J. Polym Eng Sci, 1976, 16, 831-835.

2. Brady, D. J. J Appl Polym Sci, 1976, 20, 2541-2551.

3. Kenny, J. M.; Maffezzoli A. Polym Eng Sci, 1991, 31(8), 607-614.

4. Kowalewski, T.; Galeski, A. J Appl Polym Sci, 1986, 32, 2919-2934.

5. Long, Y.; Shanks, R. A.; Stachurski, Z. H. Prog Polym Sci, 1995, 20, 651-701.

6. Otaigbe, J. U.; Kim, H. S.; Xiao, J. Polym Comp, 1999, 20(5), 697-704.

7. Guschl, P. C.; Otaigbe J. U., Properties of blends of a thermotropic liquid crystalline polymer and poly (phenylene sulfide) filled with ferromagnetic powder of Nd-Fe-B alloys, submitted to Polym Comp (2000).

8. Rothon, R. Particulate-Filled Polymer Composites; Longman Scientific & Technical: Essex, UK, 1995.

9. Han, C. D.; Snadford, C.; Yoo, H. J. Polym Eng Sci, 1978, 18(11), 849-854.

10. Boaira, M. S.; Chaffey, C. E. Polym Eng Sci, 1977, 17(10), 715-718.

11. Schultz, J. Polymer Material Science; Prentice-Hall, Inc.: Englewood Cliffs, New Jersey, 1974.

12. Brostow, W.; Seo, K.;. Baek, J. B. Polym Eng Sci, 1995, 35(12), 1016-1021.

13. Minkova, L.; Paci, M.; Pracella, M.; Magagnini, P. Polym Eng Sci, 1992, 32(1), 57-64.

14. Denault, J.; Vu-khanh, T. Polym Comp, 1992, 13(5), 372-379.

15. Mitusuishi, K.; Uneo, S.; Kodama, S.; Kawasaki, H. J Appl Polym Sci, 1991, 43, 2043-2049.

LIST OF FIGURES

Figure 8. Effect of filler and coupling agent on the estimated induction time of crystallization for a 15 vol% MQP suspension at the four isothermal crystallization temperatures

Figure 9. Effect of particle size (for uncoated MQP) on the estimated induction time of crystallization for a 15 vol% MQP suspension at the four isothermal crystallization temperatures

Figure 10. Effect of the presence of filler and coupling agent on the storage modulus of the suspension between the temperature range of 40 - 220°C

Figure 11. Effect of the presence of filler and coupling agent on the loss modulus of the suspensions of 15 vol% MQP between the temperature range of 50 - 150°C

Figure 12. Effects of particle size on the storage modulus and phase angle shift of the suspensions of 15 vol% MQP (uncoated) between the temperature range of 60 - 220°C

Table 1. Johnson-Mehl-Avrami index for Isothermal Polymer Crystallization and Interpretation (6)

JMA Index,n	Nucleation	Growth Geometry	Growth Control
2	Instantaneous	Disc	Interface
2	Homogeneous	Disc	Diffusion
2	Homogeneous	Rod	Interface
2.5	Homogeneous	Sphere	Diffusion
3	Instantaneous	Sphere	Interface
3	Homogeneous	Disc	Interface
4	Homogeneous	Sphere	Interface

Guschl, *et. al.*, Figure 1

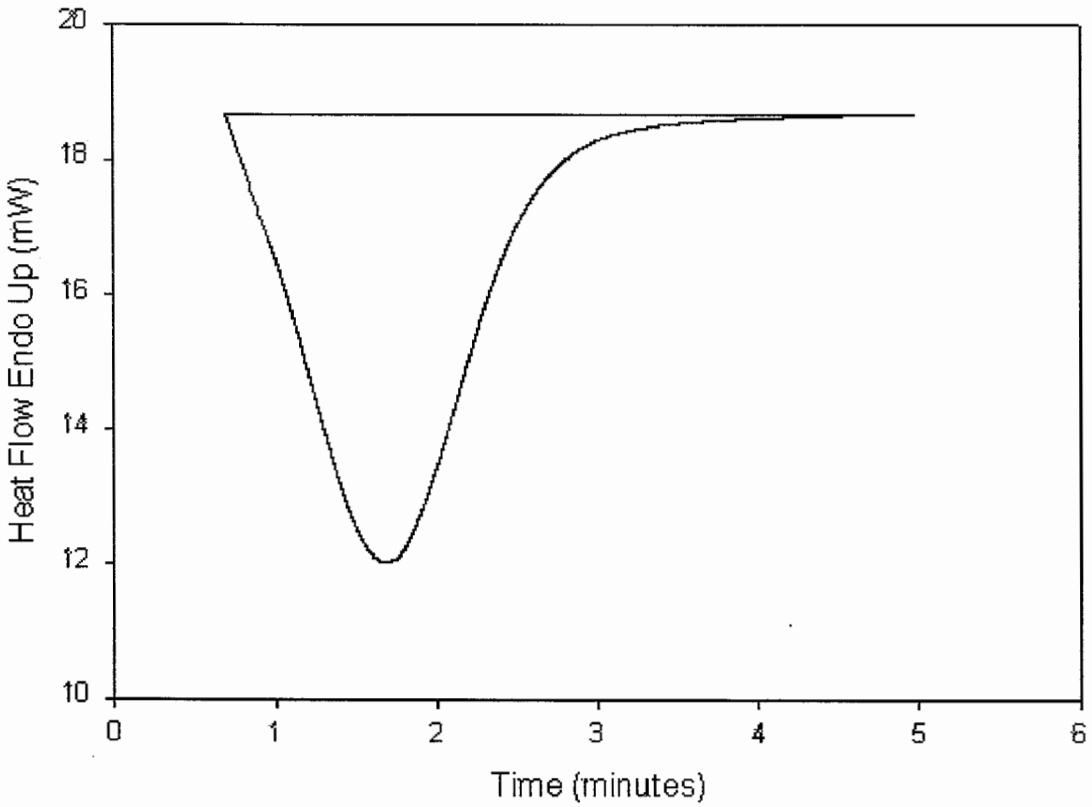

Guschl, *et. al.*, Figure 2

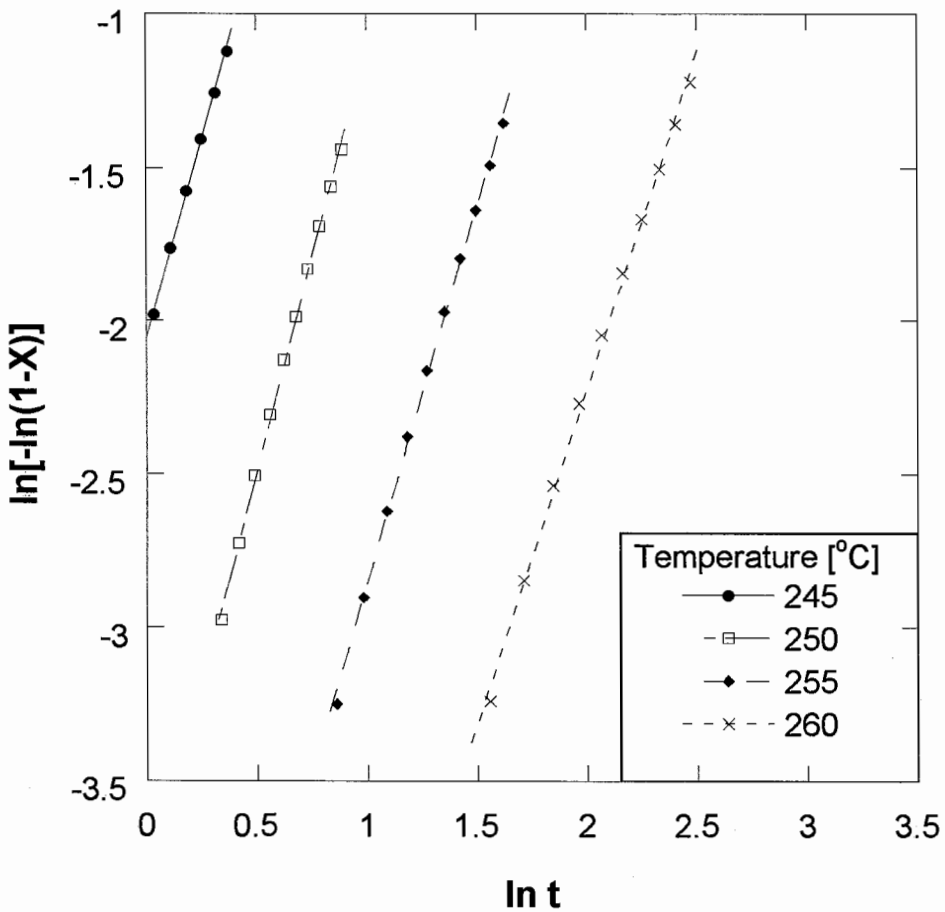

Guschl, *et. al.*, Figure 3

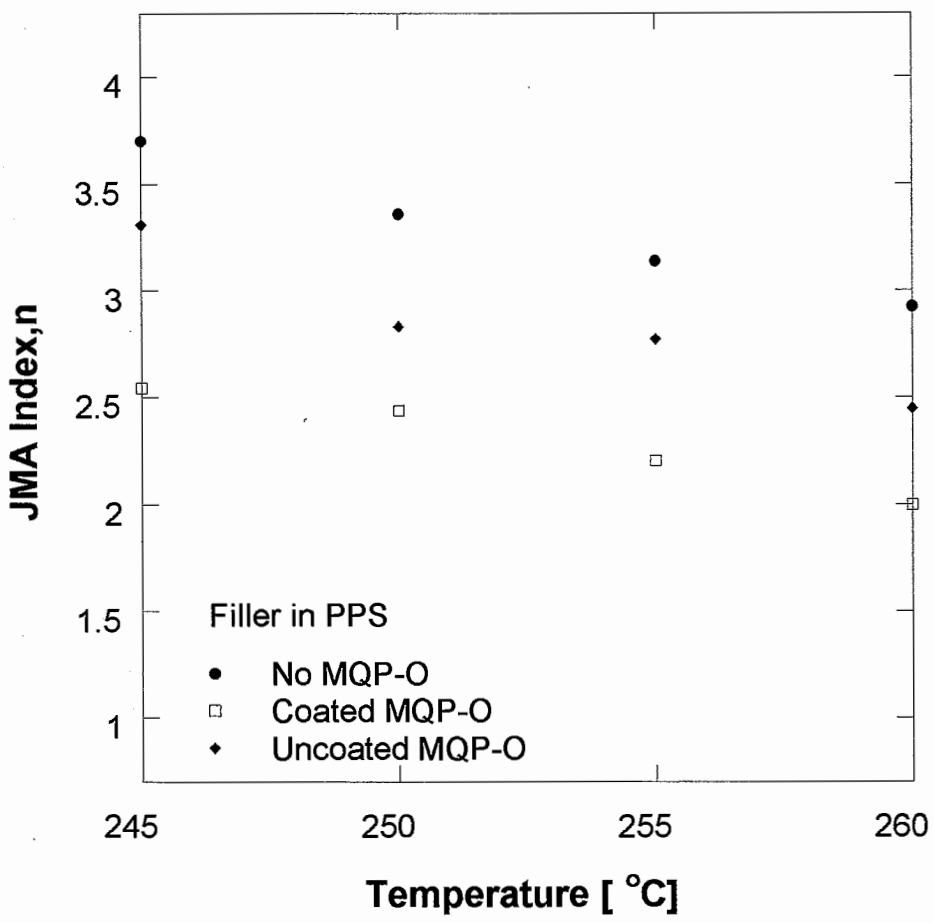

Guschl, *et. al.*, Figure 4

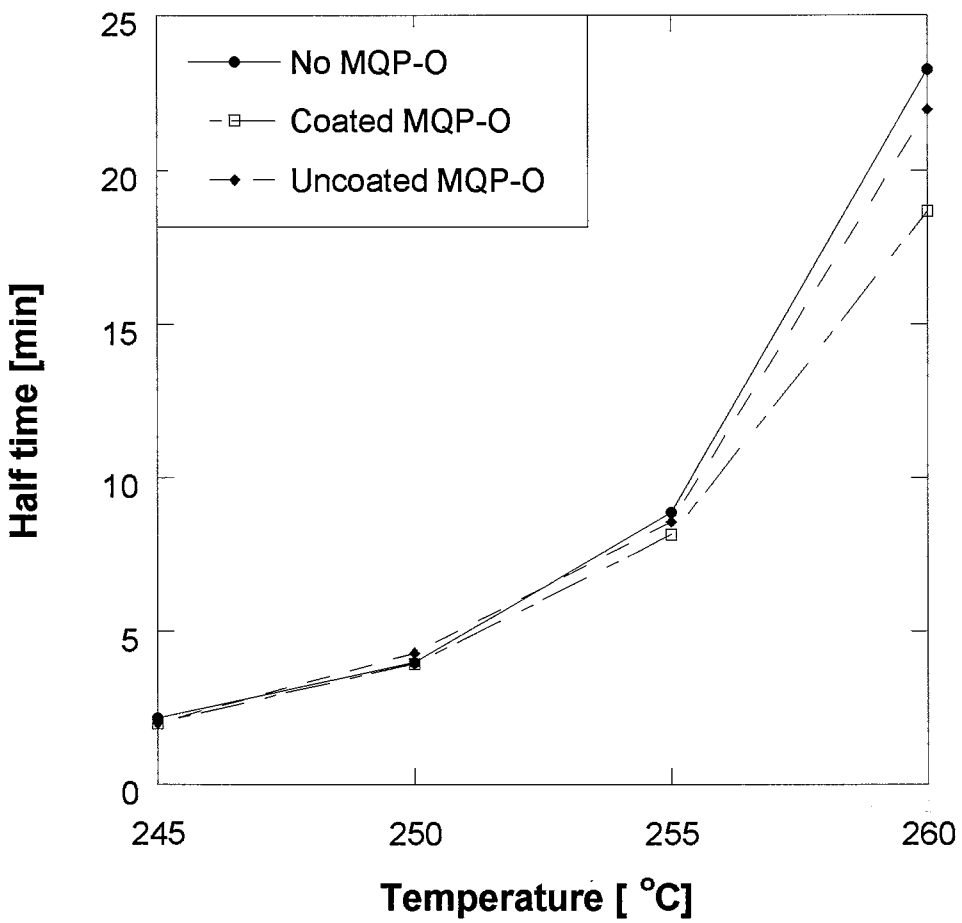

Guschl, *et. al.*, Figure 5

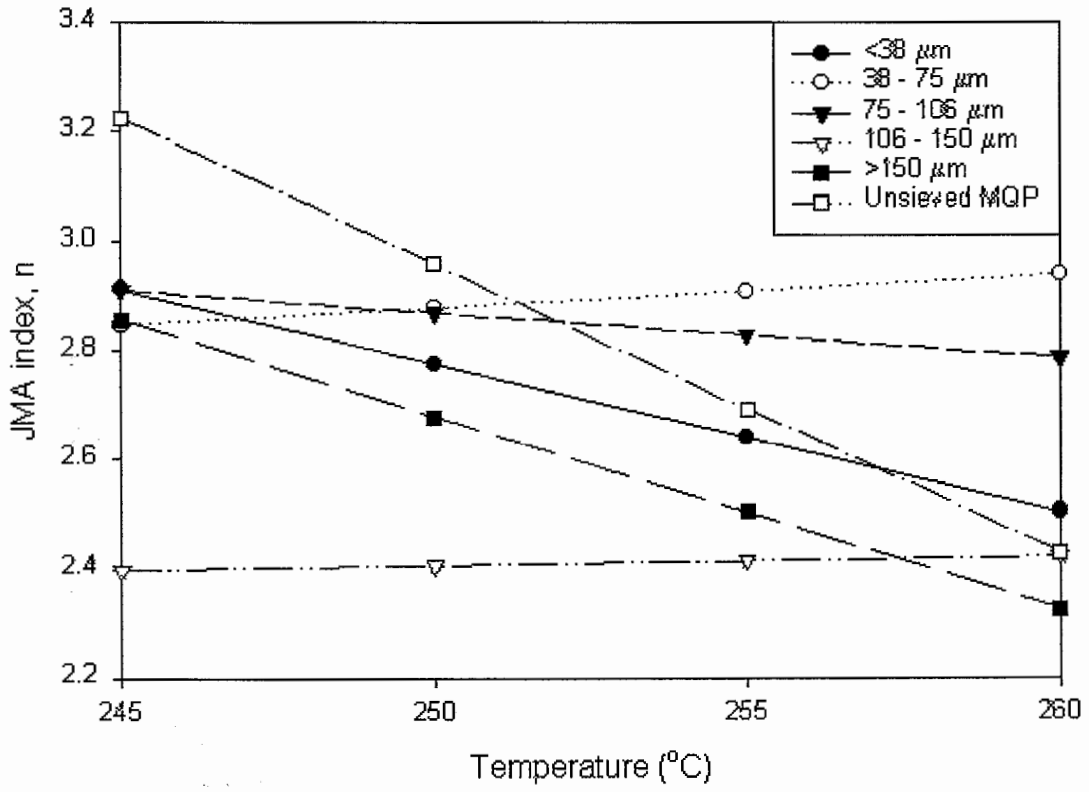

Guschl, *et. al.*, Figure 6

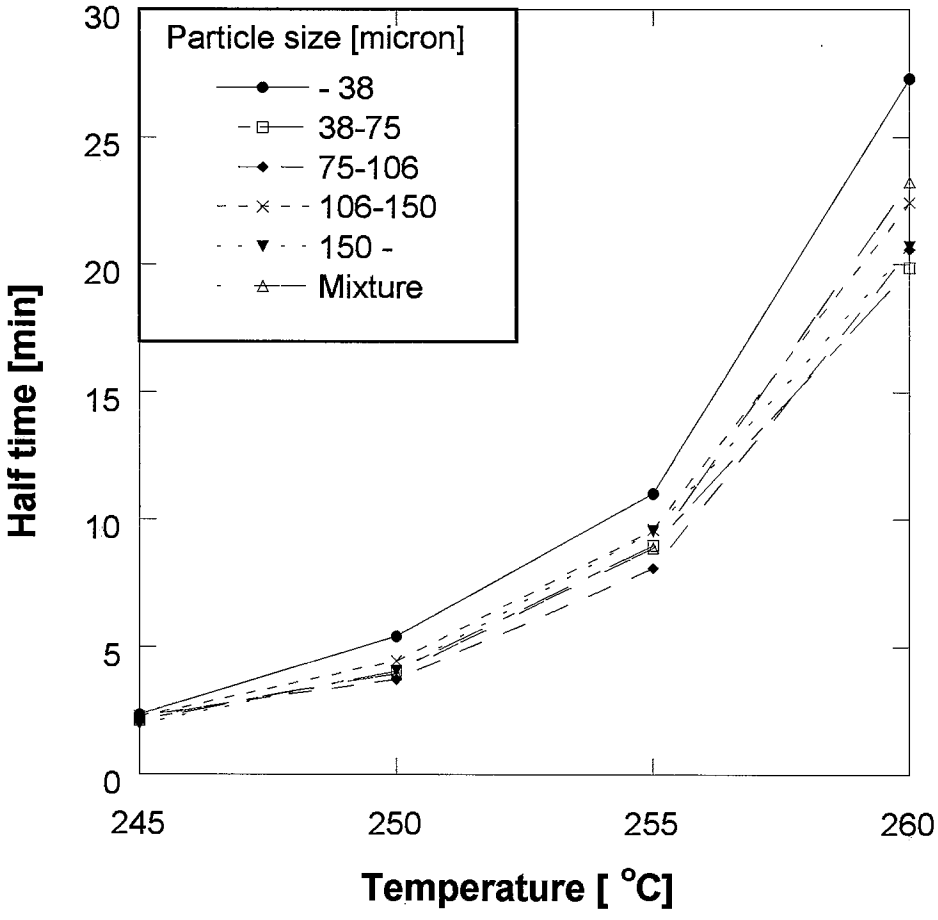

Guschl, *et. al.*, Figure 7

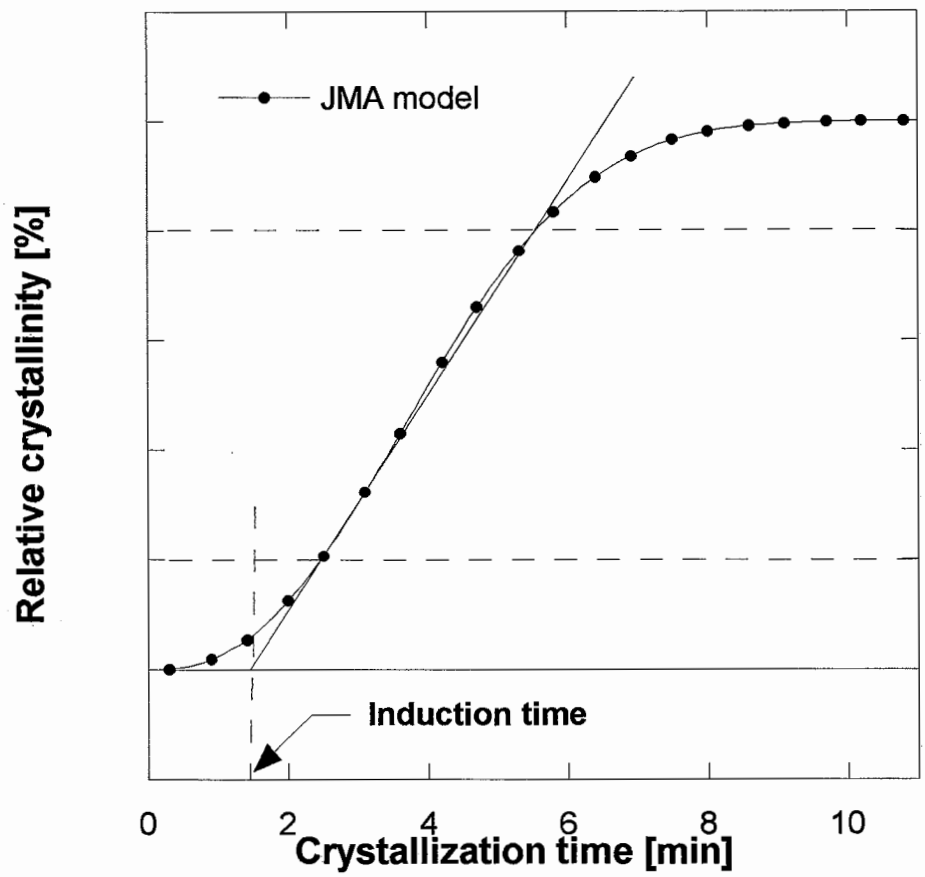

Guschl, *et. al.*, Figure 8

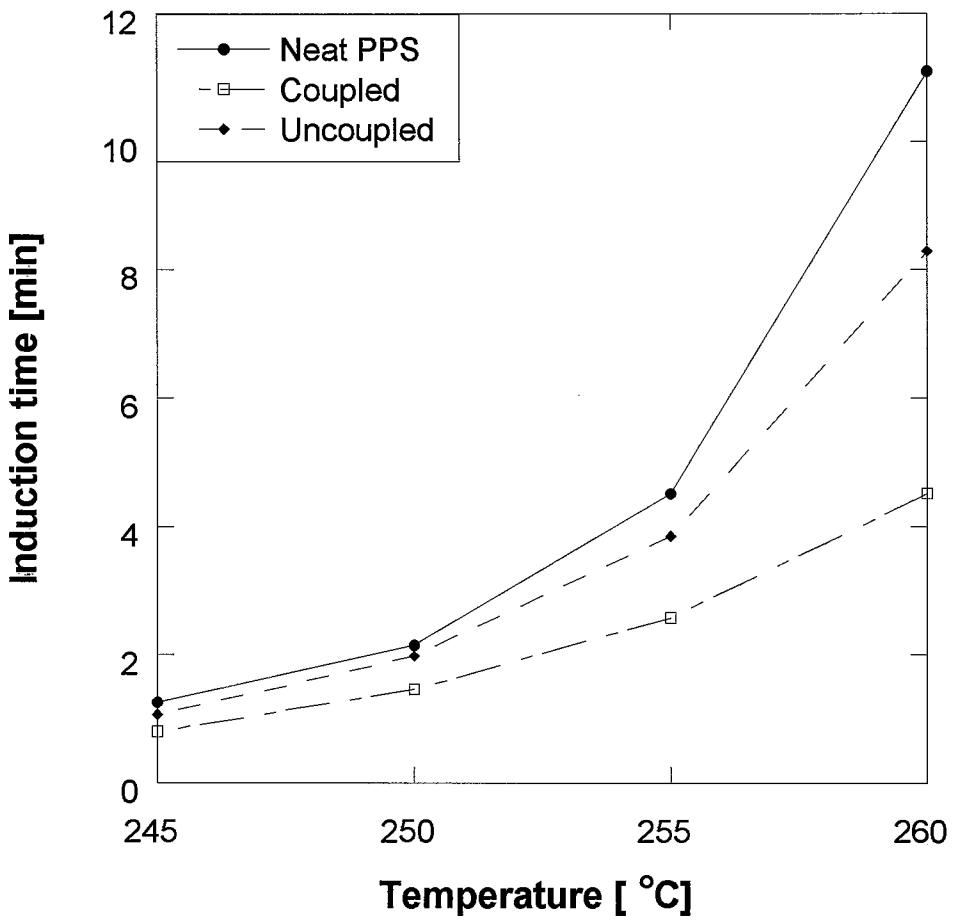

Guschl, *et. al.*, Figure 9

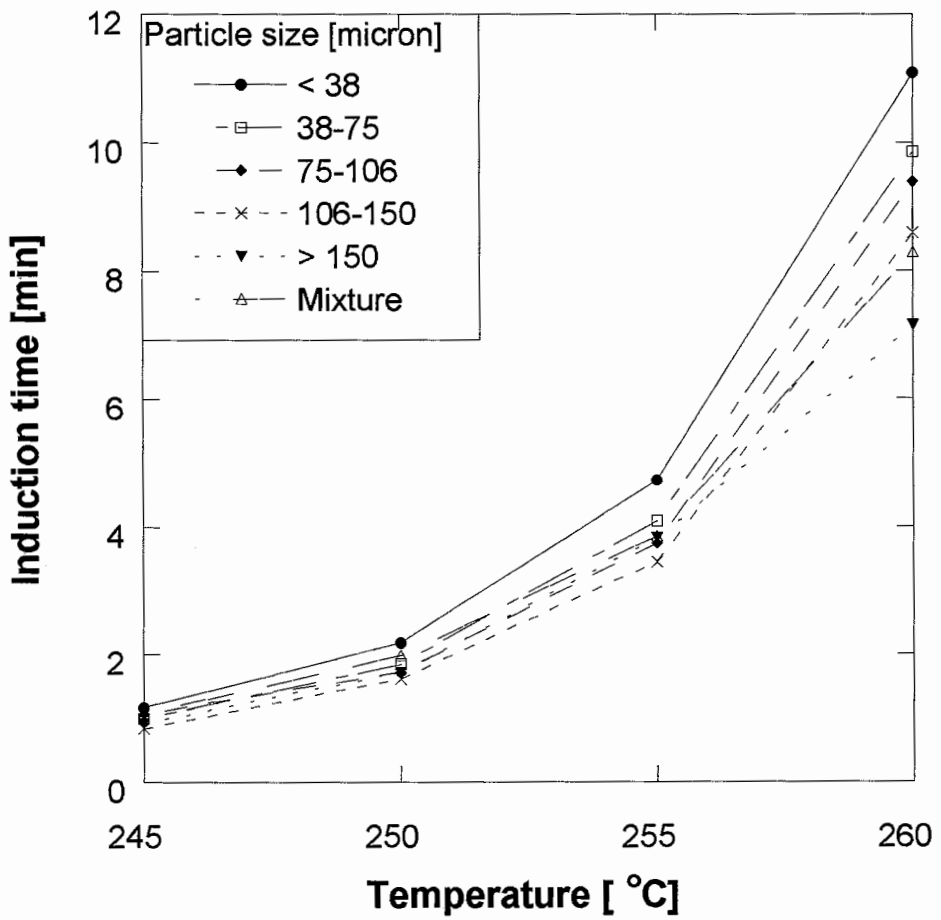

Guschl, *et. al.*, Figure 10

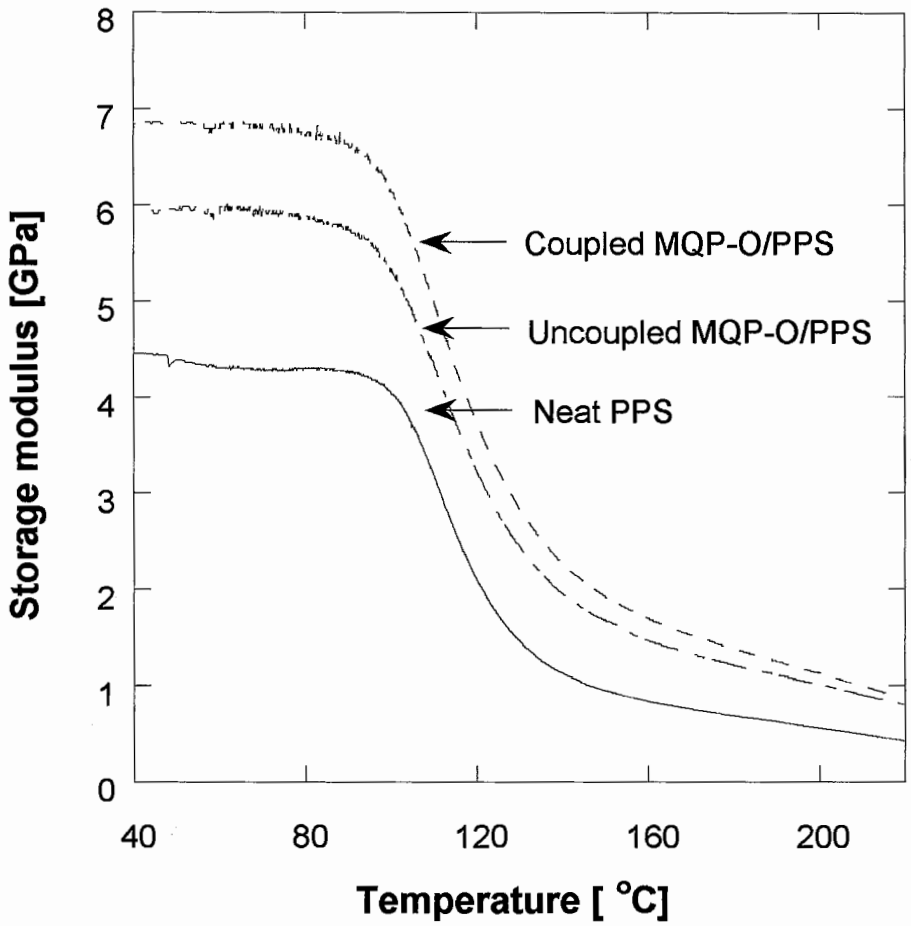

Guschl, *et. al.*, Figure 11

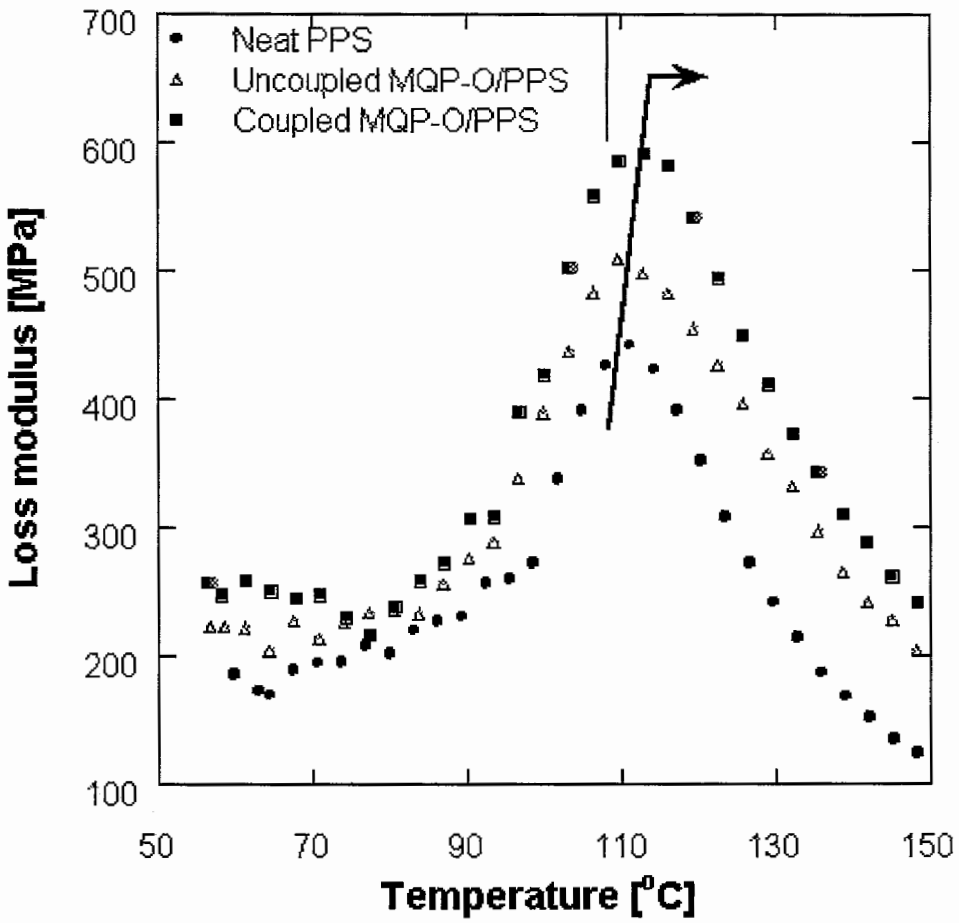

Guschl, *et. al.*, Figure 12

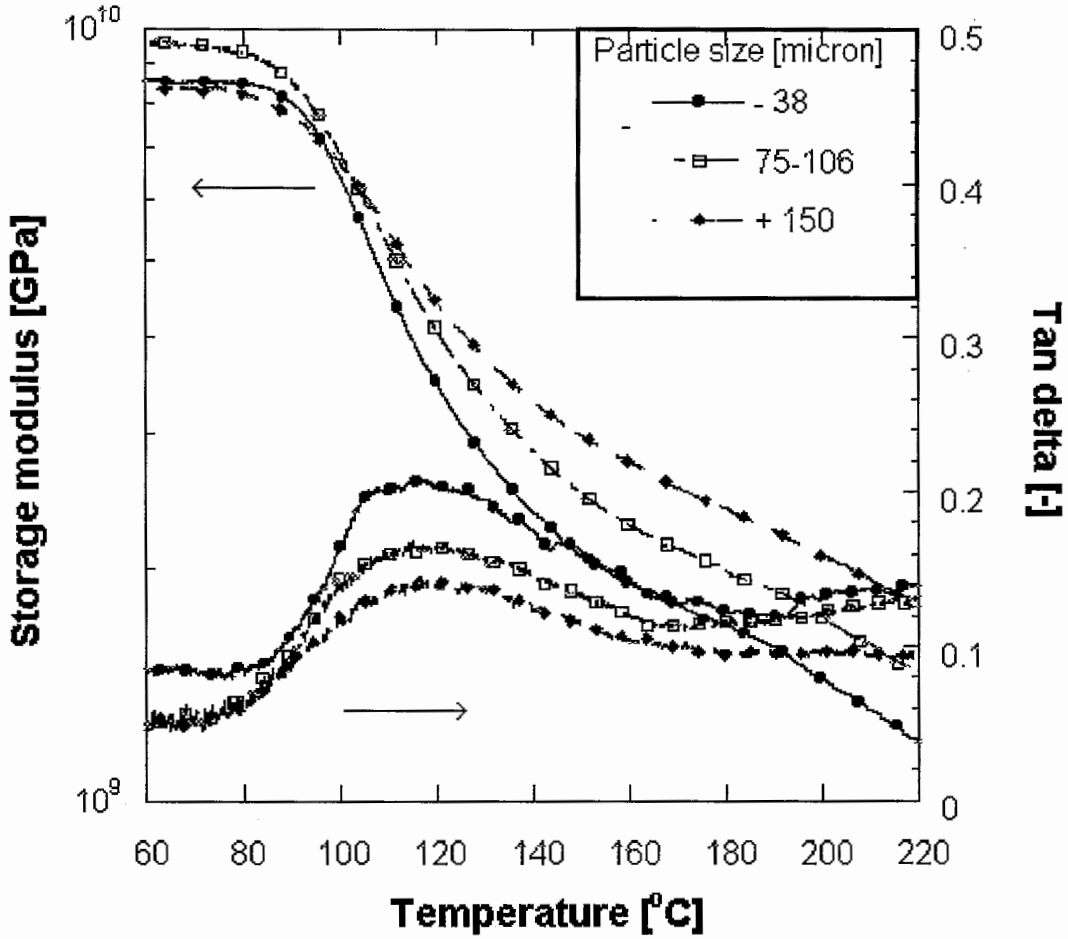

CHAPTER 4. LONG RANGE RHEOLOGICAL AND YIELD BEHAVIOR OF A Nd-Fe-B MAGNETIC FILLER SUSPENDED IN POLY (PHENYLENE SULFIDE)

A paper submitted to *Rheological Acta*

Peter C. Guschl and Joshua Otaigbe

SYNOPSIS

The rheological properties of the composite material of a poly (phenylene sulfide) (PPS)/magnetic powder suspension were studied. Both complex and steady shear viscosity data were obtained at 320°C for various concentrations of a Nd-Fe-B magnetic filler within the polymer matrix, ranging from 0 - 50 vol %, from very low to moderate frequencies and shear rates (ω □ 0.1 to 100 rad s^{-1} and $\dot{\gamma}$ □ 0.01 to 5 s^{-1}) (parallel plate rheometry) and up to high shear rates (100 s^{-1} □ $\dot{\gamma}$ < 1200 s^{-1}) (capillary rheometry). The results show that a Newtonian plateau exists at shear rates less than 1 rad s^{-1} whereas distinct shear-thinning (power law) behavior is apparent at larger shear rates. For the 35% and 50% MQP suspensions, deviations between the steady shear and complex viscosities were observed at higher shear rates/frequencies. Yield behavior was subsequently analyzed for the samples ϕ □ 35 vol% in the low shear regime. The estimated yield stress grows exponentially with volume fraction of filler as discovered through linear extrapolation and nonlinear least squares regression to the Bingham model. The values of the yield stress through these methods are respectively 0.027 to 26.1 Pa and 0.024 to 71.5 Pa for the suspensions ranging from 0 to 35% MQP in PPS.

KEYWORDS: suspension rheology, yield stress, polymer rheology, capillary rheometry

1. INTRODUCTION

The role of rheology of concentrated polymer systems is quite significant in industry today, because it helps to determine the processability of complex materials under practical conditions. Polymer-bonded magnets (PBM) comprised of polymer matrices and special rare earth magnetic alloys (e.g. Nd-Fe-B alloy) represent an important class of engineering materials used in electromechanical applications in automotive and non-automotive areas, where energy efficiency is a prime concern [Bullen (1988), Ormerod and Constantinides (1997), Otaigbe et. al (1999a), Otaigbe et. al. (1999b), Xiao et. al. (2000)]. Higher magnetic capabilities are possible when more magnetic filler is available in the system. Unfortunately, the composite's processability is strongly compromised at higher concentrations. For industrial applications our system is to be capable of manufacture within commercial injection molding machines. Due to the processing windows open only within particular temperature and, ultimately, injection pressure ranges, the material may be subjected to large or small shear rates during the process. Interest in information over a broad range of shear is beneficial for reassurance that one is operating the process under optimal conditions.

Earlier studies have investigated the introduction of certain additives into these composites, such as liquid crystal polymers and coupling agents, as well as particular particle configurations, in the search for the optimal conditions in the reduction of the material's viscosity [Otaigbe et.al. (1999b), Guschl and Otaigbe (2000)]. Results have shown that the presence of such additives does indeed reduce the resistance to flow at certain concentrations of a particular liquid crystal polymer and silane-coupling agent. The mechanisms involved in

this viscosity reduction entail provision of immiscible slip layers and improved wetting between the filler and binder, respectively. Furthermore, narrow particle dispersity configurations (one or two different sizes) were found to yield the lowest processability, due to the unique anisotropic, non-spherical nature of the filler particles.

Although extensive research has been conducted on the rheology of various suspensions [Einstein (1956), Krieger and Dougherty (1959), Farris (1968), Chong (1971), Cheng (1984), Metzner (1985), Barnes (1989)], less rheometric work has been contributed to that of non-colloidal, non-spherical suspensions, such as our system. Much of this research has included information regarding shear-thinning behavior at low shear rates of stabilized particulate suspensions due to shear induced ordering of the particles [Jansma and Qutubuddin (1995)]. Further research has shown that beyond a particular critical shear rate shear-thickening behavior is observed for stabilized concentrated systems [Boersma et. al. (1990), Fagan and Zukoski (1997)]. Presumably, the hydrodynamic forces dominate over the particle-particle interactions that promote the ordered flow. These forces, however, play an important role regarding noncolloidal particles where particle-particle interactions may be neglected. Barnes (1989) implied that under the appropriate circumstances, all suspensions of colloidal or noncolloidal solid particles would exhibit this thickening behavior. He states that the critical shear rate is basically reduced for larger particles as opposed to smaller colloidal ones. Furthermore, Beazley (1980) claims that more anisotropic particles will more readily produce this effect, specifically at lower solids concentrations. This work investigates the possibility of shear thickening of PBM composites through the long range rheological testing.

In conjunction with the long-range rheological behavior, the yield behavior, although controversial, of these composites is important in which to be aware for processing purposes. Fagan and Zukoski (1997) described the presence of a suspension yield stress, τ_y, as "based on a microscopic deformation mechanism where, under shear, arrays of particles deform slowly up to a critical strain at which point they rapidly move to new semi-stationary positions." The author continues to suggest that this apparent yield stress would be a weak function of particle volume fraction, particle diameter and strength of interparticle repulsions. Husband et. al. (1993) studied yield behavior of noncolloidal suspensions, suggesting that unlike colloidal particles interparticle effects are essentially dwarfed in comparison to the hydrodynamic forces applied. These authors discuss the typical pseudoplastic behavior of suspensions that exhibit no yield stress and a constant viscosity at low shear rates, depending upon the filler and the binder selected. Similar models, such as the Bingham model, signify materials whose shear stresses behave linearly with shear rate. The Bingham model was selected for analysis due to this simple, linear relationship viewed experimentally at low shear rates. The functionality of the yield stress to particle properties (size, distribution, shape, anisotropy, etc.) interests rheologists that are confined to working with concentrated systems where these yield effects tend to occur. The secondary purpose of this study was to observe and possibly quantify any detectable yield behavior for the PBM composites.

2. EXPERIMENTAL

2.1 Materials

Phillips Chemical Company provided the poly (phenylene sulfide) grade - Ryton Type P6. The P6 has been cured at a temperature below its melting point. The average

molecular weight value of the P6 is difficult to obtain and estimate due to its synthesis conditions. The density, melting point, and glass transition temperature of the PPS grade is approximately 1.36 g cm^{-3}, 285°C, and 90°C, respectively.

The magnetic powder, manufactured by Magnequench, consists of varying particle sizes of a neodymium-iron-boron alloy ($Nd_2Fe_{14}B$) that exist in platelet form. Specifically, the commercial powder used is MQP-O and has a density of 7.61 g cm^{-3} and Curie temperature of 299°C, respectively. The particle sizes utilized in these experiments, for both powders, ranged from 38-300 μm, separated into five particle size fractions corresponding to the sieve plates used: 38-75 μm, 75-106 μm, 106-150 μm, 150-212 μm, and 212-300 μm. The aspect ratio of the particles was experimentally determined to range from 0.2 to 10 [Otaigbe et. al. (1999a)].

2.2 Variable Pressure Scanning Electron Microscopy (VP-SEM)

Figures 2a and 2b were obtained using a Hitachi S-2460N VP-SEM. These micrographs were created under a beam current of 0.5 nA, a 25 mm working distance, a 40 Pa (0.3 torr) Helium atmosphere, an accelerated voltage of 20kV and a magnification of 300x. The samples under examination were extruded through a 1-mm die during the capillary rheometry experiments in Section 2.4. The extrudate from the die was cut into small cylindrical pieces that were embedded in an epoxy and polished in order to scan a flat surface of the samples.

2.3 Shear Rheology

Dynamic and steady shear experiments were performed on the Advanced Rheometric Expansion System (ARES, Rheometric Scientific) in a parallel-plate configuration with 25-mm plates and a gap height of 2.0 mm, giving a flow space of at least 10 times the average particle size of 150 microns. The gap size used was assumed to be a reasonable size to minimize the effects of the reduced particle concentration near the walls of the parallel plates [Cohen and Metzner (1981)]. In the sample composition range tested, it was found that the output signals were always sinusoidal, indicating an absence of nonlinear effects [Gadal-Maria and Acrivos (1980)] caused by shear-induced structure in our filled polymer systems. Strain sweep tests were performed on each of the different compositions from 0.1% to 100% strain at a frequency of 10 rad s^{-1} and at 320°C. Linearity (viscoelasticity) was maintained up to 30% strain for the composites with a volume fraction less than or equal to 5%. The 20% and 35% composites showed critical strains of about 10% and 0.5%, respectively. Due to its high viscosity and large stresses on the torque transducers, the 50 vol% MQP suspension was not analyzed by way of the ARES rheometer. Two torque transducers that operate under the torque ranges of 0 - 200 ft-lb (278 N-m) and 0 - 2000 ft-lb (2780 N-m) were available. The dynamic frequency and steady rate sweeps were performed at 320°C at frequencies and shear rates of 0.1 - 100 rad s^{-1} and 0.00625 - 5 s^{-1}, respectively. Edge fracture difficulties arose when shear rates greater than 5 s^{-1} were exceeded during steady shear testing. Due to the thermal stability window, measurements could only be made between particular frequencies and shear rates at a given time. Dynamic measurements were made from the three following frequency ranges: 0.1 - 0.2 rad s^{-1}, 0.2 - 0.5 rad s^{-1}, and 0.5 - 100 rad s^{-1}. Steady shear measurements were taken at the three following shear rate ranges: 0.00625 - 0.05 s^{-1}, 0.01 -

0.3 s^{-1}, and 0.05 - 5 s^{-1}. Dynamic thermal stability tests performed at 320°C, 10 rad s^{-1}, and the appropriate strain for the material analyzed, show a processing window of only 4 minutes (240 seconds). Testing after 4 minutes may yield inexact data due to the crosslinkability and ultimately the increase in viscosity of the polymer matrix used in this study. All tests were performed in triplicate. The data shown in the results section are averages of these measurements.

The yield stress was determined as the lowest stress that created a steady deformation and was found by increasing the shear rate in a stepwise manner. A controlled shear rate test was performed through extrapolation of shear stress to very low shear rates. Yield stresses were also calculated from nonlinear least squares regression to fitted parameters from the Bingham model.

2.4 Capillary Rheometry

A Göttfert Rheo-Tester 1500 was used for the high shear capillary rheometry. Experiments performed on the samples were run at 320°C between shear rates of 5.76 - 1152 s^{-1} with two dies with different length/diameter ratios (20mm/1mm and 30mm/1mm). Results from each die were obtained and compared, showing excellent agreement between the two sets of data. Due to the availability of only these two dies, a proper Bagley correction analysis could not be effectively performed. Two pressure transducers were utilized in order to effectively receive data under high filler loading. The first transducer was a mid-range transducer [0 - 5000 psi (34,960 kPa)], and the second was a high-range transducer [0 - 20,000 psi (139,840 kPa)]. The dry samples in powder form were added to the barrel of the rheometer and subsequently tamped during loading for tight packing in order to reduce the

amount of air pockets present in the extrudate. Apparent shear stress, viscosity and shear rate data were obtained from this procedure. True shear rate was then calculated by the following equations [Crawford (19980]:

$$\dot{\gamma} = \left(\frac{3n+1}{4n}\right)\frac{4Q}{\pi R^3} \tag{1}$$

$$\dot{\gamma}_{app} = \frac{4Q}{\pi R^3} \tag{2}$$

where n is the power law index, Q is the volumetric flow rate, R is the radius of the die, $\dot{\gamma}$ is the true shear rate, and $\dot{\gamma}_{app}$ is the apparent shear rate.

3. RESULTS AND DISCUSSION

The shear rheology of this research revealed that the suspensions studied exhibit unique flow properties under two deformation modes over a broad range of shear rates. Figure 1 shows the complex viscosity and how it is affected by increasing frequency for the suspensions containing 0%, 5%, 20% and 35% volume fractions of the MQP filler in PPS at 320°C. A shear-thinning relationship between the complex viscosity and the frequency is noticed. Power law indices for each curve were determined to be 0.726, 0.675, 0.603, and 0.577 in order of increasing filler volume fraction. The increased shear-thinning characteristic with filler concentration was expected due to this observation in an earlier study of similar composites [Guschl and Otaigbe (2000)]. It is apparent that the anisotropic nature of the filler particles aided in this rheological behavior. Further inspection of Figure 1 shows that as the frequency of shear decreases a slight Newtonian region of the curve begins to appear as others have noted for many polymer suspensions [Husband et. al. (1993)]. This

region is considered to be under conditions of competitive low hydrodynamic forces and high thermal and attractive forces between the particles where little to no uniform alignment of the particles takes place. We see that once sufficient shear is applied to the material, then the particles' anisotropy is utilized through orientation along the direction of shear. Figure 2a illustrates this observation for the 35% and 50% MQP suspensions. Both samples show particle orientation around the edges of the picture. These edges represent the walls of the die of the capillary from which the suspensions were extruded. The particles appear to possess a random alignment towards the centerline of the die, exhibiting a layer of particles oriented in the direction of highest shear at the edges. These observations are in agreement with previously published works [Rothon (1995)].

In addition to the shear rheology data, capillary rheometry information was obtained for the more concentrated suspensions studied (ϕ = 0.35 and 0.50) in order to obtain quantitative information. Figure 1 shows the results of the experiments with a particular die (L/D = 20/1). Under the shear rates applied, due to the speed of the piston, the high shear-thinning behavior of the composite was continued and exists beyond the already analyzed frequency of 100 rad s^{-1}. The curves of the 35% and 50% MQP suspensions have power law indices of 0.406 and 0.364, respectively. The 50% suspension curve shows a greater degree of non-Newtonian shear-thinning behavior, supporting the conclusion that as the filler concentration increases the psuedoplasticity rises as well. These two curves show no apparent signs of shear-thickening behavior at a particular critical shear rate, as predicted by others [Beazley (1980)] due to the anisotropy of the particles in the suspension. Further investigation of lower shear rates of the 50% and more highly concentrated suspensions are needed in order to absolutely confirm the existence of this claim.

Figure 3 represents the steady shear behavior of the same suspensions discussed previously. The data presented shows steady shear viscosity of these composites at low shear rates ($\dot{\gamma} < 0.1$ s^{-1}) whereas the dynamic measurements were tested at $\omega \geq 0.1$ rad s^{-1}. One can observe a more defined Newtonian plateau region for these curves. The pure PPS curve shows the longest plateau region the ends around a shear rate of roughly 0.5 s^{-1}. The 5% composite also exhibits this region up to a shear rate of 0.25 s^{-1}. The plateau regions vanish as higher filler concentrations are reached. This observation can be explained due to the anisotropy and increased presence of the particles. When more anisotropic particles are present in the system, then a higher degree of orientation occurs under shear.

Analysis of the information retrieved from the two deformation modes was performed and graphed in Figure 4. The pure PPS and 5% MQP suspension exhibit excellent agreement between the complex and dynamic viscosities. Discrepancies appear at the higher filler volume fractions (not shown). This observation was expected due to the highly filled systems. Al-Hadithi, *et al.* (1992) noted a similar phenomenon in their paper describing the flow properties of a series of polymers, colloidal systems, and other structured fluids. These deviations just mentioned arise due to the heterogeneous nature of our polymer blends [Doraiswamy et. al. (1991)]. Agreement does, however, begin to appear at the lower shear rate/frequency regime of the figure. This phenomenon can be attributed to the Cox-Merz rule:

$$\lim_{\omega \to 0} \eta^* = \lim_{\dot{\gamma} \to 0} \eta \qquad (1)$$

where ω is the frequency, η^* is the complex viscosity, and η is the steady shear viscosity.

The investigation of the existence of yield behavior in these complex systems was explored. Figure 5 shows the four composites in the low shear rate region. Due to limitations with our controlled shear rate rheometer accurate stress values could not be determined below a certain shear rate. Because of the existence of the Newtonian region at low shear rates, linear extrapolation can be utilized in order to estimate the yield stress. Since the experimental shear stress data in this low shear rate range is linear with $\dot{\gamma}$, an assumption of Bingham behavior was made. This figure gives the yield stress values for the pure PPS, 5% MQP, 20% MQP, and 35% suspensions as 0.027, 0.084, 1.27, and 26.1 Pa, respectively. This increase in yield stress was expected due to the reduction in spacing between particles at higher loadings of filler. Because of this lack of separation between the particles, microstructural formation is more likely to occur. An exponential rise in yield stress with filler fraction was predicted [Rothon (1995)] and is a function of filler/binder interaction parameters, such as the interphase thickness, and individual filler/binder properties (i.e. yield stress of matrix and specific surface area of particles). Typically, as these properties are increased, then the yield stress is enlarged as well.

In addition to the linear extrapolation method, a procedure of nonlinear least squares regression analysis was performed, in order to fit the parameters of the Bingham model [Equation (2)] to the experimental data.

$$\tau = c_1 + c_2\dot{\gamma} \tag{2}$$

c_1 and c_2 are the parameters of the equation where c_1 is the yield stress and c_2 is the Newtonian viscosity. The Bingham model, as opposed to the Casson or Herschel-Bulkley

models, was selected because a more gradual transition from the Newtonian to the yield stress region is observed from our results. Since the experimental shear stress data in this low shear rate range is linear with $\dot{\gamma}$, an assumption of Bingham behavior was made. This analysis led to yield stress values of 0.024, 0.099, 3.14, and 71.5 Pa. Figure 6 shows the low shear data points and extrapolated lines corresponding to these points. These values are comparable in magnitude to the linear extrapolation values, however we can see a divergence between the values as the filler concentration increases. The previous analysis was utilized in order to investigate the possibility of the existence of yield behavior and not to specifically quantify it. Additional research is required through the use of controlled stress rheometry and other more accurate methods of determination.

4. CONCLUSIONS

The results of this work show the complex rheological information of various concentrations (0 - 50 vol% MQP) of PBM composites at a high processing temperature (320°C) under two deformation modes, steady shear and dynamic, over a broad range of shear rates and frequencies. Newtonian plateau regions, areas where viscosity is constant, at low shear rates/frequencies and high shear-thinning behavior at larger shear rates/frequencies was observed for these composites under both deformation types. Power law indices for the suspensions in order of increasing volume fraction (ϕ = 0.00, 0.05, 0.20, 0.35) were determined to be 0.726, 0.675, 0.603, and 0.577 for the parallel plate rheometry experiments and 0.406 and 0.364 for the capillary rheometry tests for 35% and 50% MQP in PPS. At higher shear rates/frequencies differences between the steady shear and complex viscosities were seen due to the heterogeneous, structured nature of the higher concentrates systems.

Capillary rheometry was utilized in order to explore the rheology of the more highly concentrated suspensions of which are too difficult to accurately measure flow properties and to analyze the behavior of these systems at higher shear rates of which cannot be attained with standard parallel plate and cone-and-plate rheometers. These measurements reinforced the notion that the suspensions continue to exhibit extreme shear-thinning behavior at higher shear rates ($\dot{\gamma} > 100\ s^{-1}$). ESEM micrographs confirmed this phenomenon through direct visualization of the particle alignment along the direction of shear.

Yield behavior was investigated and, its existence has been confirmed, through linear extrapolation and nonlinear least squares regression of Bingham model parameters. Yield stress values ranged from 0.027 to 26.1 Pa through linear extrapolation and 0.024 to 71.5 Pa for the 0 - 35% MQP suspensions from the Bingham model fitting. The yield stresses for each measurable suspension were evaluated, revealing an exponential growth with filler concentration. More accurate experiments, however, are necessary in order to obtain exact yield stress values of these PBM composites.

ACKNOWLEDGEMENTS

The financial support of the U. S. National Science Foundation through Grant No. DMR-9712688 is gratefully acknowledged. We are particularly grateful to Arnold Engineering Company, Phillips Petroleum Company, Ames Laboratory, and Dr. Christopher Macosko at the University of Minnesota without whose collaboration and support this work would have been impossible.

REFERENCES

1. Al-Hadithi TSR, Barnes HA, Walters K (1992) The relationship between the linear (oscillatory) and nonlinear (steady-state) flow properties of a series of polymer and colloidal systems. Coll. Polym. Sci., 270(1): 40-46.

2. Bullen S (1988), Engineering Materials & Design: 18.

3. Barnes HA (1989) Shear-thickening in suspensions of nonaggregating solid particles dispersed in Newtonian liquids. J. Rheol. 33: 329-366. See also Barnes HA (1999) Yield stress - a review or παντα ρει - everything flows? J. Non-Newt. Fluid Mech., 81: 133 – 178.

4. Beazley K (1980) Rheometry: Industrial Applications. K. Walters, Ed., Research Studies Press, Chichester.

5. Bhattacharya S (1999), Yield stress and time-dependent rheological properties of mango pulp. J. Food Sci., 64(6): 1029-1033.

6. Boersma WH, Laven J, Stein HN (1991), Time-dependent behavior and wall slip in concentrated shear thickening dispersions. J. Rheol., 35(6): 1093-1120.

7. Cheng DCH (1984) Further observations on the rheological behavior of dense suspensions. Powd. Tech., 37: 255-273.

8. Chong JS, Christiansen EB, Baer AD (1971) Rheology of concentrated suspensions. J. Appl. Polym. Sci., 15: 2007-2021.

9. Cohen Y, Metzner AB (1981) Wall effects in laminar flow of fluids through packed beds. AIChE J., 27(5): 705-715.

10. Crawford RJ (1981) Plastics Engineering, Butterworth-Heinemann, Boston.

11. Doraiswamy D, Mujumdar AN, Tsao I, Beris AN, Danforth SC, Metzner AB (1991) The Cox-Merz-rule extended: A rheological model for concentrated suspensions and other materials with a yield stress. J. Rheol. 35(4): 647-685.

12. Einstein A (1956), Investigations on the Theory of the Brownian Movement, edited by R. Furth, Dover, New York.

13. Fagan ME and Zukoski CF (1997) The rheology of charge stabilized silica suspensions. J. Rheol., 41(2): 373-397.

14. Farris RJ (1968) Prediction of the viscosity of multimodal suspensions from unimodal viscosity data. J. Rheol. 12(2): 281-301.

15. Gadala-Maria F and Acrivos A (1980) Shear-induced structure in a concentrated suspension of solid spheres. J. Rheol., 24(6): 799-814.

16. Guschl PC and Otaigbe JU (2000) Properties of blends of a thermotropic liquid crystalline polymer and poly (phenylene sulfide) filled with ferromagnetic powder of Nd-Fe-B alloys. submitted to Polymer Composites.

17. Husband DM, Asksel N, Gleissle W (1993) The existence of static yield stresses in suspensions containing noncolloidal particles. J. Rheol., 37(2): 215-235.

18. Jansma JB and Qutubuddin S (1995) Rheological behavior of concentrated calcium halophosphate suspensions. J. Rheol., 39(1): 161-178.

19. Krieger IM and Dougherty TJ (1959) A mechanism for non-Newtonian flow in suspensions of rigid spheres. J. Rheol., 3: 137-152.

20. Metzner AB (1985) Rheology of suspensions in polymeric liquids. J. Rheol., 29(6): 739-775.

21. Ormerod J and Constantinides S (1997) Bonded permanent magnets: Current status and future opportunities. J. Appl. Phys. 81: 4816-4820.

22. Otaigbe JU, Kim HS, Xiao J (1999a) Effect of coupling agent and filler particle size on melt rheology of polymer-bonded Nd-Fe-B magnets. Polym. Comp., 20(5): 697-704.

23. Otaigbe JU, Xiao J, Constantinides S (1999b) Influence of filler surface treatments on processability and properties of polymer bonded Nd-Fe-B magnets. J. Mat. Sci. Letters, 18(4): 329-332.

24. Rothon R (1995) Particulate-Filled Polymer Composites. Longman Scientific & Technical, Essex, UK.

25. Xiao J, Otaigbe JU, Jiles DC (2000) Modeling of magnetic properties of polymer bonded Nd-Fe-B magnets with surface modifications. J. Magn. Mag. Mater., 218: 60-66.

LIST OF FIGURES

Guschl and Otaigbe, Figure 1

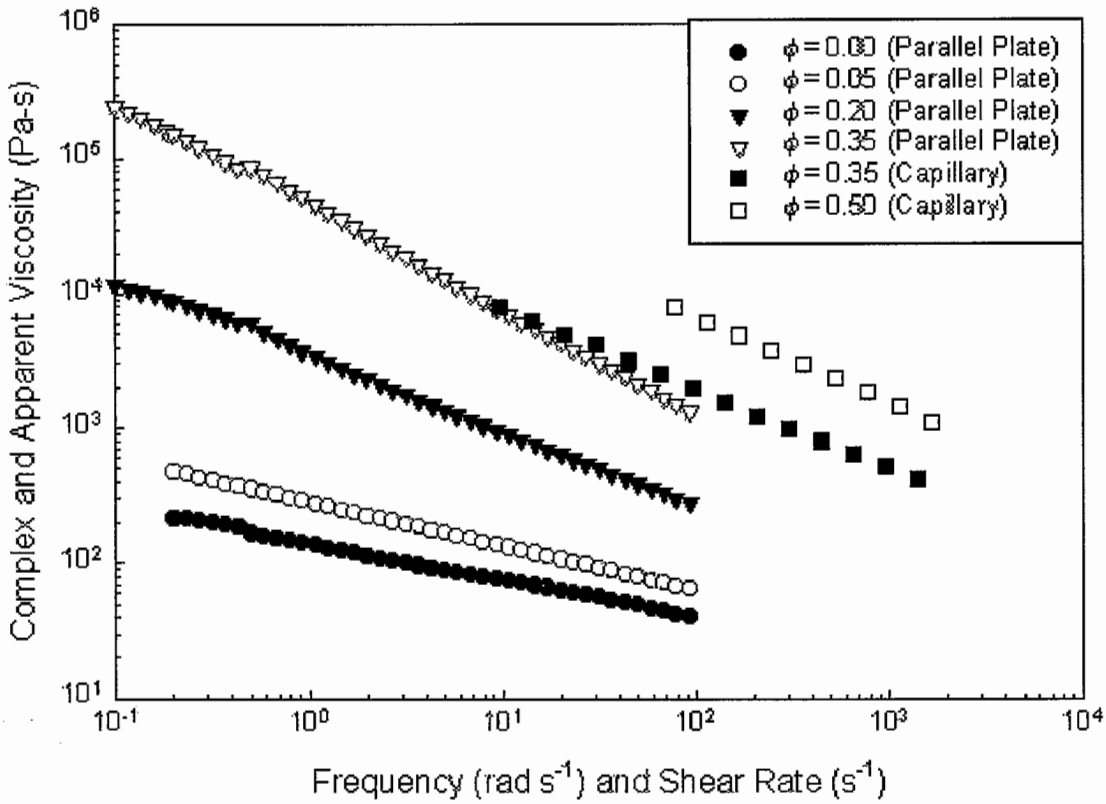

Guschl and Otaigbe, Figure 2

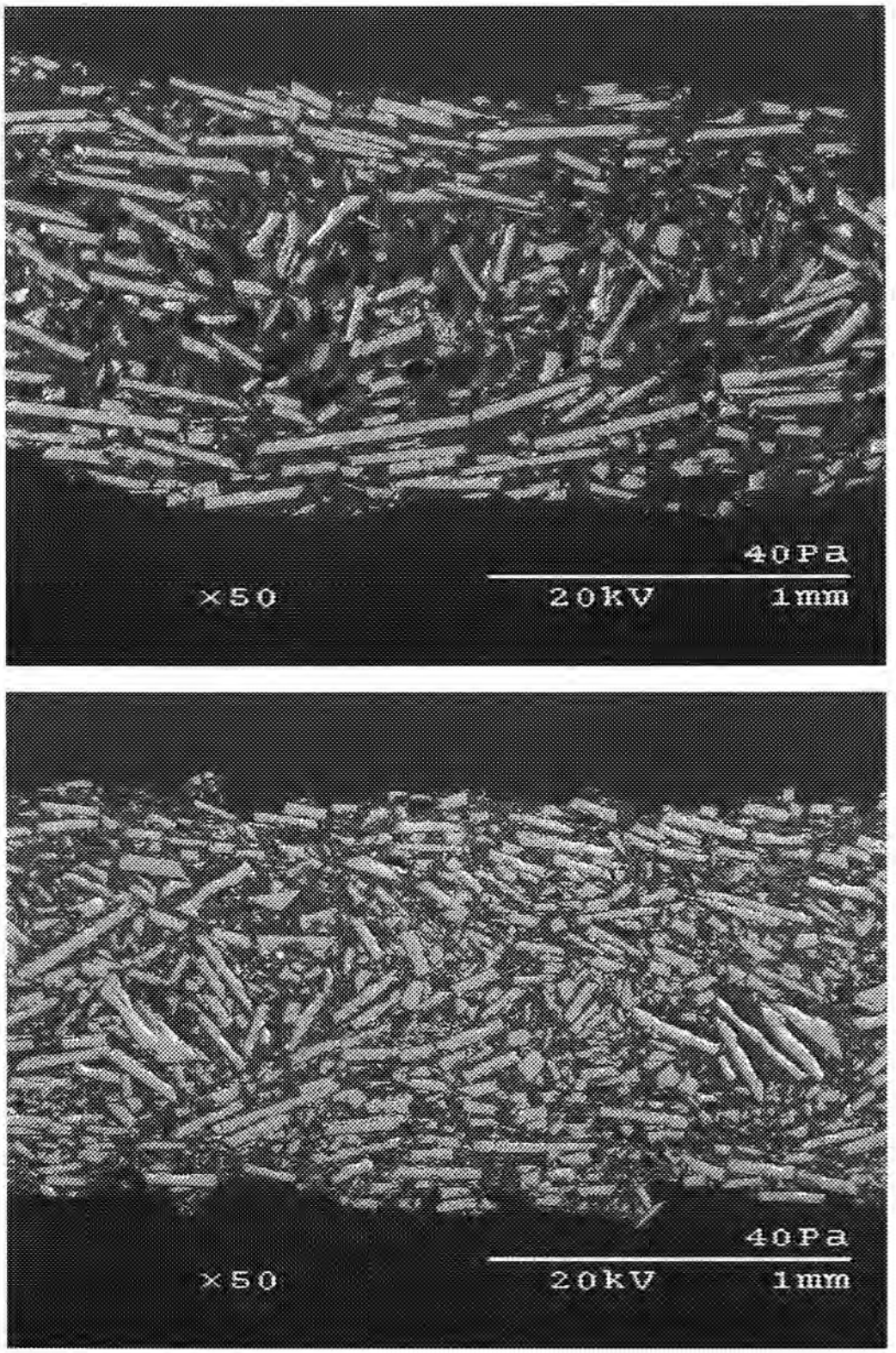

Guschl and Otaigbe, Figure 3

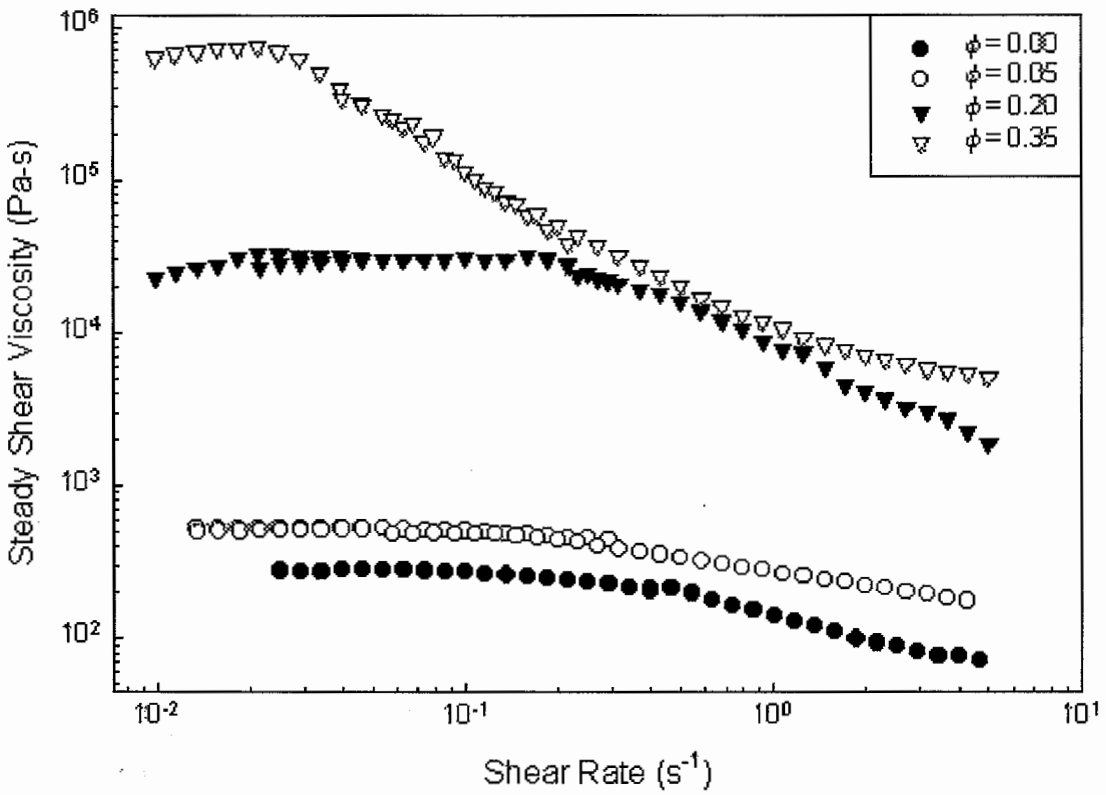

Guschl and Otaigbe, Figure 4

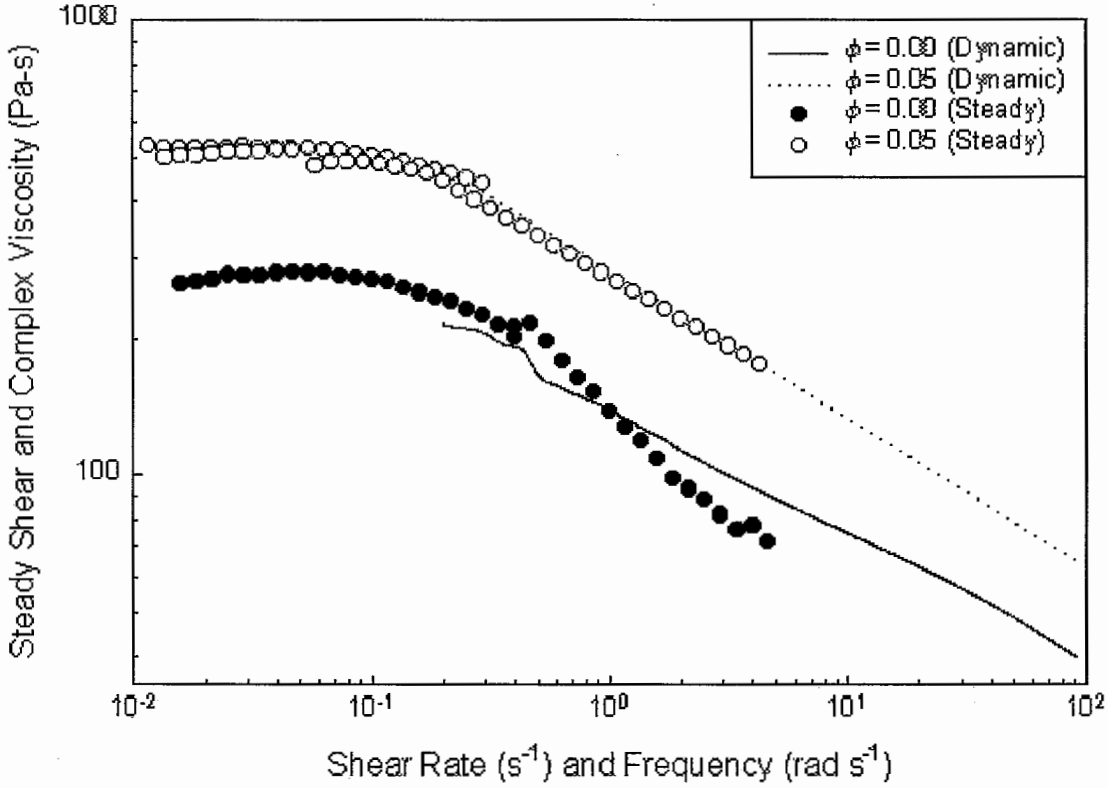

Guschl and Otaigbe, Figure 5

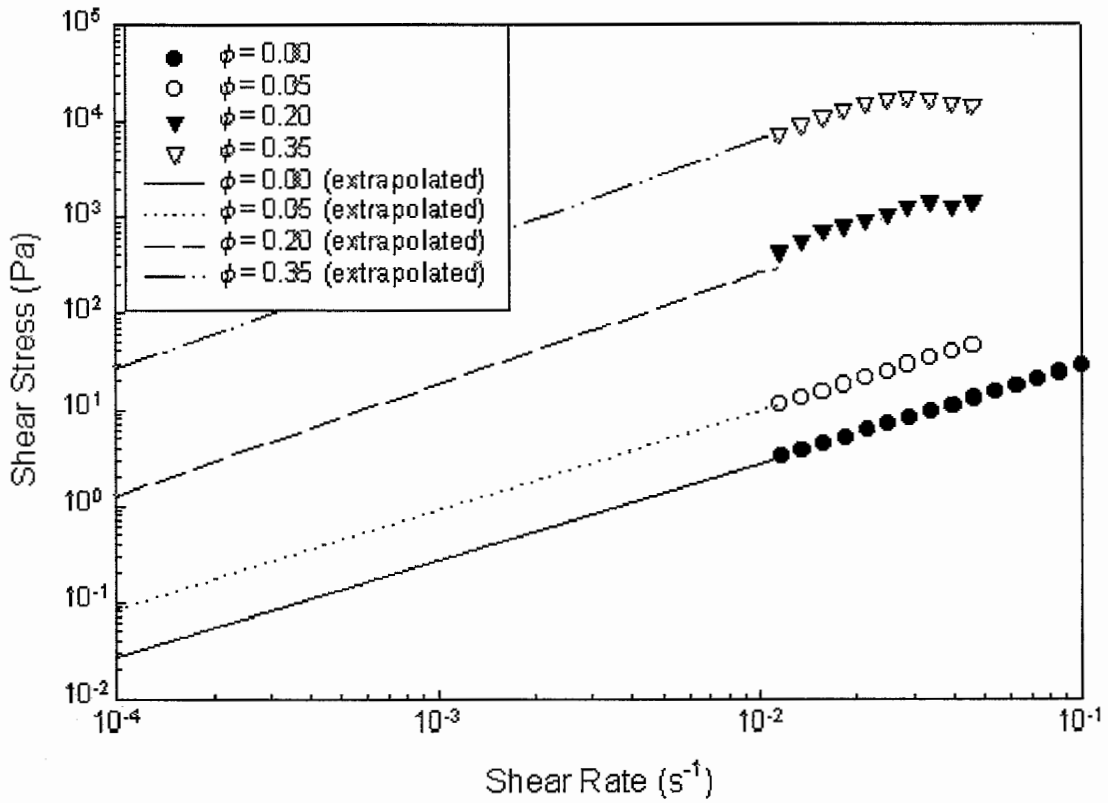

Guschl and Otaigbe, Figure 6

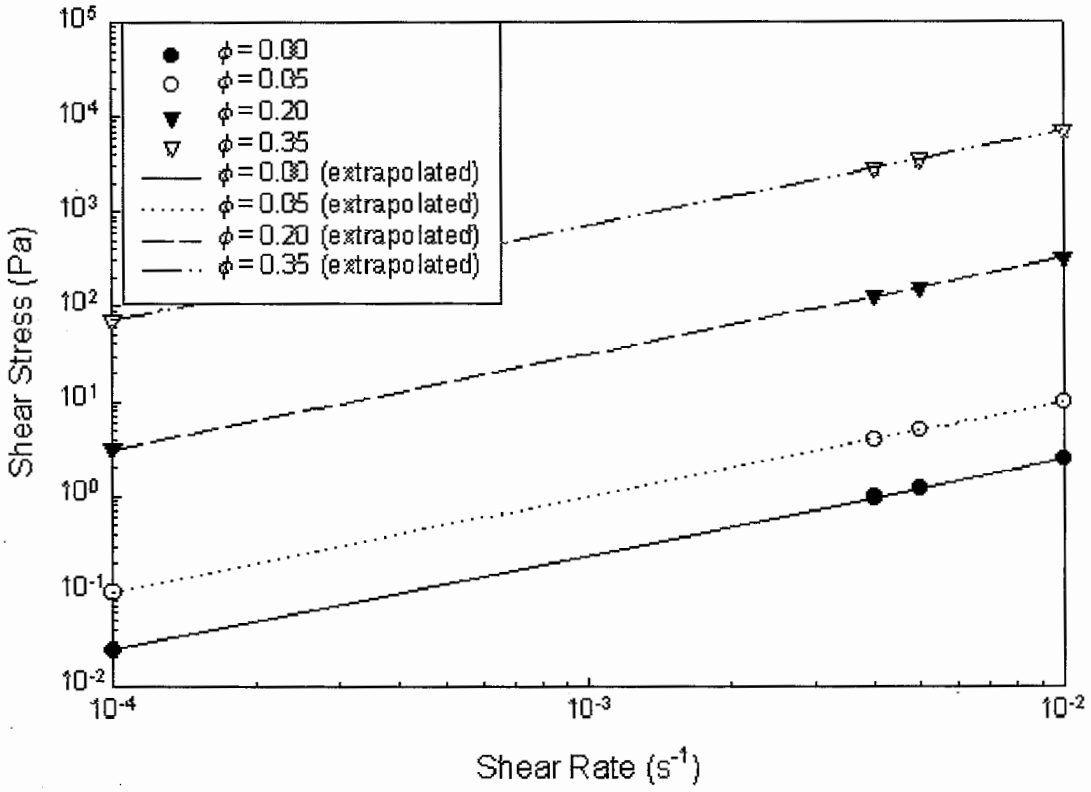

CHAPTER 5. GENERAL CONCLUSIONS

This thesis focuses on the development of composite materials called polymer bonded magnets, which are based on the suspension of a metallic, hard magnet (in this case Nd-Fe-B) filler in a high temperature organic, thermoplastic polymer, poly (phenylene sulfide) (PPS) binder. The advantages of PBM over their metallic and ceramic counterparts include low weight, resistance to corrosion, ease of machining and forming, and capability for high production rates. The rheology of the concentrated filler/polymer systems such as the PBMs is important because it underscores the processability of these materials under practical conditions. It is desirable to obtain a composite of polymer and filler that is not too viscous to be molded at an optimal magnetic powder concentration. Ideally, the addition of magnetic fillers to a polymer matrix results in a material with optimal mechanical properties, adequate magnetic properties (i.e. high coercivity, high remanence, and high energy product) and other beneficial properties such as stiffness and strength of the PBM composite. Unfortunately, the viscosity and ultimately the processability is adversely affected at these higher concentrations and particle shape.

The use of functional additives within a polyphenylene sulfide matrix has been previously reported to alleviate the aforementioned problems. The addition of a small amount of thermotropic liquid crystal polymer can lower the viscosity at low shear rates as well as enhance the modulus and strength of the PBM. The presence of Vectra A950, the liquid crystal polymer used during one of the studies included in this thesis, was found to reduce the melt PBM composite viscosity at small and moderate concentrations (1%-3%) and (10%-15%) concentrations. Higher LCP concentrations gave an unexpected increase in viscosity of

the blends possibly due to agglomerations of the LCP phase within the matrix. Coupling agent promotes a change of interfacial properties of the filler particles, giving rise to better wetting between the filler and binder and ultimately increased physical strength of the composite, as well. The coupling agent further enhanced the polymer crystallinity via improved wetting between the particle and polymer chains. The net effect of faster growth caused an internal strengthening to occur within the composite, giving rise to an increased storage modulus and improvement in mechanical properties.

Addition of the platelet-shaped Nd-Fe-B particles strongly affected the rheological and crystalline properties of the system. The distribution of these particles was found to be the critical factor that needs to be controlled to obtain high maximum packing densities at minimal viscosities for the composites. Specifically, the unimodal and bimodal system (1mod150 and 2mod150) gave rise to the system with the lowest viscosity at a volume fraction of 15% Nd-Fe-B. Particle size did not appear to affect the crystallinity of the composite significantly, but small particles did exhibit the longest crystallization times. The JMA index, n, seemed to be at a minimum for the 106-150 micron particle range and did not vary severely with crystallization temperature, much like the coated MQP particles. Higher Nd-Fe-B volume fractions (up to 75 vol. %) in the composites showed high viscosities that are melt-processible in conventional plastics processing equipment. However, it is believed that such high Nd-Fe-B volume fractions may compromise other properties such as the tensile strength and toughness of the materials for the targeted applications.

The complex rheological information of various concentrations (0 - 50 vol% MQP) of PBM composites at a high processing temperature (320°C) under two deformation modes, steady shear and dynamic, over a broad range of shear rates and frequencies was observed.

Newtonian plateau regions at low shear rates/frequencies and high shear-thinning behavior at large shear rates/frequencies was observed for these composites under both deformation types. At higher shear rates/frequencies differences between the steady shear and complex viscosities were seen due to the heterogeneous, structured nature of the higher concentrates systems. As the rates were lowered, the steady shear and complex viscosity values showed agreement. Capillary rheometry measurements reinforced the notion that the suspensions continue to exhibit extreme shear-thinning behavior at higher shear rates ($\dot{\gamma} > 100\ s^{-1}$). ESEM micrographs confirmed this phenomenon through direct visualization of the particle alignment along the direction of shear.

Yield behavior was investigated and confirmed to exist, through linear extrapolation and nonlinear least squares regression of Bingham model parameters. Yield stress values ranged from 0.027 to 26.1 Pa through linear extrapolation and 0.024 to 71.5 Pa from the Bingham model fitting for the 0 - 35% MQP suspensions. The yield stresses for each measurable suspension were evaluated, revealing an exponential growth with filler concentration.

This research aided in gaining a better understanding of the unique properties of PBM. The additives represent agents that can be combined into the composite in order to promote better interfacial characteristics of the filler and binder, reduce melt viscosity of suspension, and enhance crystallization and, ultimately, the mechanical properties of the composite below melt temperature. The use of these additives and the information gained from rheological measurements can allow industry to effectively manufacture and optimize a new material in the magnetic market for the future.

Future Directions

Since the majority of the original objectives of this research have been met, new problems and areas of interest have arisen within the boundaries of the PBM project. During the ongoing quest for filler concentration optimization, the analysis of highly concentrated systems ($\phi \geq 50$ vol%) has brought forth many issues experimentally and theoretically. These systems exhibit large resistances to flow and possible shear thickening behavior at higher rates of shear. Yield behavior has been observed to be an increasing function of particle volume fraction and may be dependent on particle modality as well. It is also believed that a yield stress will continue to be present even under a magnetic field. Information on the microstructures formed due to the field and how they affect the flow of the melt will be of great import to the project. Further and more accurate experiments involving this behavior are needed.

New experiments need to be undertaken so that one can obtain information in regard to the flow properties of the material in the presence of a magnetic field. It is believed that molding the PBMs while under a field can allow the magnetic particles to align both in the direction of the flow and the applied field. The product of this procedure should yield a higher magnetized PBM, due to anisotropy in the bulk. Optimal effects of this phenomenon would be noticed via use of anisotropic magnetic particles due to their preferred alignment in a particular direction. Unfortunately, melt PBMs under an applied field may actually exhibit a higher resistance to flow due to microstructural formation of the particles. Rheological testing under different deformation modes with the presence of an external magnetic field can shed further light on the subject.

Further alleviation of the processability issue may be instigated through incorporation of a method called vibrated gas assisted injection molding (Vibrogaim). The procedure shows how air or nitrogen can be used to impose vibrational pressure pulses to a polymer melt, inducing orientational benefits during filling. The main intent of using this method is to reduce the viscosity of melt PBMs during the filling without the integration of additives such as LCPs and/or coupling agents.

Future research will encompass investigations of the aforementioned problems in addition to other concerns. For instance, other polymer blends and subsequent composites of these immiscible/miscible blends will be researched, attempting to create a low viscosity matrix that can withstand high temperatures and efficiently shield the metallic particles from corrosion and oxidation. Magnetomechanical, as well as magnetorheological, information and their applications to the composites are equally important to the project and should be studied. Finally, in the interest of quantification of PBMs to characteristics beyond experiment and possible application to systems of similar makeup, mathematical models shall be developed. Through the use and availability of various computational fluid dynamics packages, one may be able to exhibit visual phenomena based on certain assumptions of certain suspensions as PBMs. For instance, the behavior of the particles under flow and applied field through a capillary is of interest. It is believed that nonspherical particles orient in the direction of shear in the outer regions, yet they misalign in the core regions at higher concentrations of filler. Furthermore many authors have published many models based on suspensions of spherical particles in simple fluids. It is of interest to us to attempt to model our system, which includes a more difficult particle geometry and suspending fluid, in the presence of an applied magnetic field.

ACKNOWLEDGEMENTS

I would like to thank my major professor, Prof. Joshua U. Otaigbe, for all his efforts in allowing me to become a better researcher. His encouragement, guidance, and infinite patience are thoroughly appreciated, and his enthusiasm for my research has encouraged my continuation with project.

The many group members in the Polymer and Composite Group have been my friends, colleagues and, for a few, my travel companions. They have all helped be become the researcher and professional that I am today.

Finally, a quick thank you to my friends and family outside of the research who patiently hear my problems and convince me to continue to attain all of my goals as a graduate student.